

AC losses in MgB₂ superconductors

Sigrid Anne Giljarhus

Master of Science in Energy and Environment

Submission date: June 2007

Supervisor: Magne Eystein Runde, ELKRAFT

Co-supervisor: Niklas Magnusson, Sintef

Problem Description

Superconductors will, when subjected to time varying magnetic fields, e.g. when carrying AC currents, have losses. These so-called "AC losses" are of obvious importance for many power applications of superconductors. MgB₂ was a few years ago found to be superconducting when cooled below 39 K. Up to now little experimental work is reported on AC losses in this material.

The student should:

- Look into relevant literature on superconductivity in general, and AC losses in particular.
- Perform AC loss measurements in the temperature range 25 - 45 K on received MgB₂ samples using an existing calorimetric setup.
- Compare the results with the Bean model for electromagnetic behaviour and AC losses, and also with results obtained by others.

Assignment given: 15. January 2007

Supervisor: Magne Eystein Runde, ELKRAFT

Abstract

This Master thesis studies losses in superconductors. Losses arise when the superconductor carries alternating current or is placed in an alternating magnetic field. As most power applications involve at least one of the two, loss mechanisms and magnitudes are important when examining the possibility of making superconductor systems competitive to conventional power systems.

There are two parts to the task at hand. The first part is a literature study on superconductivity and AC losses in superconductors. A division between two general types of superconductors is presented; type I and II. The Bean model for AC losses in type II superconductors is described, together with equations giving the power law between generated losses and applied magnetic field. In the Bean model, the losses are proportional to the applied field cubed below a limit called the penetration field. Above it, the exponent changes to one. Losses due to coupling of filaments are also treated. The measuring setup used in the AC loss experiments is calorimetric, and the principle behind the method is presented. The superconductor used, magnesium diboride (MgB_2), is introduced. The literature study is concluded with short résumés on other AC loss studies done on MgB_2 , and studies done on one type of high temperature superconductor.

The second part is measuring AC losses due to an applied alternating magnetic field in two superconductor samples from different manufacturers. Specific information on the two samples, details on the measuring system, preparations and the measuring procedure is described. The logged data and equations used when processing the results are also listed. Measurements have been performed at six different temperatures; 25, 28.5, 30, 31.5, 35 and 45 K. The magnitude of the applied magnetic field was varied between 3 and 150 mT. Both parallel and perpendicular field directions were applied. Generated losses lead to a temperature increase in the superconductor. The rise in temperature was detected as increased resistivity of a thin copper wire glued onto the sample, as the copper resistivity is temperature dependent.

The obtained results are examined in double logarithmic (loglog) and normal axis diagrams, where the main aim is to find loss slopes and penetration fields at the different temperature levels, and to compare these to the Bean model loss equations. In addition, the results are compared to theoretical loss equations for cylindrical conductor geometry. This is done in order to look at the accuracy of the fittings and to compare the penetration fields obtained here to the ones found in loglog diagrams. The results have also been compared to various studies on MgB_2 and other superconductor types.

The measured loss slopes at fields below the penetration field, found from loglog diagrams, do not fit the Bean model. The slopes are here lower than the applied field cubed. At fields greater than the penetration field, losses are proportional to the applied field, as in the Bean model. Two reasons for the deviations have been discussed; measuring errors and losses being coupling losses. Even if the measuring errors may be considerable due to human reading errors, they would have to be systematic for the losses to fit the Bean model. This is the reason why measuring errors are seen as unlikely to be the grounds for the non-fitting results. The results do also not fit the coupling loss slope and as only one field frequency has been used, the obtained results are not enough to support or reject this theory.

Due to the deviation from the Bean model loss slopes the curve fittings to the cylindrical conductor loss equations were mostly poor, as they have the same loss slopes as the Bean

model. The penetration fields found from loglog and normal axis diagrams and the curve fitting are not equal. It is establish that the ones found from loglog diagrams should be used.

Two of the other studies done on MgB_2 , which have been summarised in the thesis, fit the Bean model, and the last case did not. The authors found no explanation to the non-fitting results, and have ruled out coupling losses as a viable reason. Studies on the other type of superconductor also represented both cases. Here, some non-fitting results were explained by coupling losses. When comparing loss magnitudes, only one of the samples used in these experiments had as low results as found in two other studies.

Preface

The report 'AC losses in MgB₂ superconductors' is a Master thesis written at the Department of Electric Power Engineering, Norwegian University of Science and Technology (NTNU) during the spring semester of 2007. The aim of the thesis was to get familiar with superconductivity and AC losses in superconductors, and to perform AC loss measurements on MgB₂ superconductors.

The subject was suggested by Magne Runde and Niklas Magnusson at SINTEF Energy Research. The two have also been my supervisors and I wish to say Thank you for all your help and support. Others who have I owe thanks are the technical staff at the workshop, Ove Darell at SINTEF Materials and Chemistry and other members of the SINTEF Energy Research Current Applications group who have helped me along. Finally, I wish to thank Magrit Giljarhus.

Trondheim, 11.06.07

Sigrid Anne Giljarhus

Contents

1	Background	1
1.1	Aims and structure of the study.....	2
2	Superconductivity and AC losses.....	3
2.1	Behaviour in a magnetic field	3
2.2	Critical state model.....	4
2.3	AC losses.....	6
3	Filaments and coupling	8
4	Basis for calorimetric measuring system	10
5	Magnesium diboride.....	11
5.1	Results from various studies on MgB ₂	13
6	Results from various studies on Bi2223/BSCCO superconductors	16
7	Measuring losses due to applied alternating magnetic field	21
7.1	Superconductors used in these experiments.....	21
7.2	Measuring system.....	21
7.3	Preparations.....	23
7.4	Measuring procedure.....	25
7.5	Processing of data.....	25
8	Results	28
8.1	25 Kelvin.....	29
8.2	28.5 Kelvin.....	32
8.3	30 Kelvin.....	35
8.4	31.5 Kelvin.....	38
8.5	35 Kelvin.....	40
8.6	45 Kelvin.....	42
9	Discussion	44
9.1	Conductor temperatures	44
9.2	Uncertainty in calibration and AC loss measurements	45
9.3	Calibration measurements.....	46
9.4	Discussion of AC loss measuring results	46
9.4.1	Loss magnitudes.....	49
9.5	Penetration fields found from curve fitting.....	50
9.6	Comparison to other studies on MgB ₂	51
9.7	Comparison to studies on other superconductors.....	51
10	Conclusion.....	52
11	Future work	53
	References	54
	Bibliography.....	57
	Appendix	i

1 Background

A superconductor is, according to one source “an element, inter-metallic alloy, or compound that will conduct electricity without resistance below a certain temperature.” [1] This holds for direct current, but energy is dissipated when a superconductor is placed in an alternating magnetic field or is carrying alternating current. [2] Superconductors may be split into low temperature superconductors (LTS) which can be used around the boiling point of helium, 4.2 K, and high temperature superconductors (HTS) operating above the nitrogen boiling point of 77 K. Superconductivity in the form of LTS was discovered in 1911 and in 1987 HTS was discovered. [3]

When comparing superconducting systems to conventional systems it is important to consider electrical properties, mechanical strength, processibility, stability and price. [3] Chen et al. [4] have listed a number of power applications where HTS may be able to compete with conventional power systems if certain factors are improved;

- Cables: Superconductor cables may carry higher currents than conventional cables due to lower losses. The voltage levels can thus be reduced. Today, AC losses in superconducting cables are too high, and insulation, joints and terminations need to be improved. Developing the necessary cooling system is also a great challenge.
- Transformers and motors: Superconductor systems would reduce the losses, volume and weight compared to conventional systems. An over-loaded superconductor does not experience accelerated aging. The problems lay in the fact that the maximum current carrying capacity is reduced when the conductor is placed in a magnetic field. There are also high AC losses at coil ends.
- Fault current limiters. These components utilise the transition between the superconducting state and the normal conducting state; under normal conditions the superconductor has next to no resistance, but when a fault current arises, the resistance increases instantaneously. Conventional current relays have far longer time constants. Fault current limiters are the closest to reaching the market.

As superconductivity occurs at very low temperatures, a great deal of the cost of superconductor systems is the installation and running of the cooling system. The efficiency in these systems decreases with decreasing temperature. The superconductors operating at the highest temperatures (HTS) are thus preferred for use in power application as this reduces the power dissipated in the cooling system. [3]

Today, superconductors are used in magnets, magnetic resonance imaging (MRI) and nuclear magnetic resonance (NMR), all niche products. These are made of cylinder or tape shaped LTS with one or more filaments, mainly embedded in copper or silver. Scanlan et al. [5] claims that “as a whole, LTS conductors are used for applications where few or no conventional alternatives exist, while HTS materials must compete against copper in electric power technology, where cost pressures are almost always significant.”

1.1 Aims and structure of the study

There are two aims of this study. One is to, through a literature study, get familiar with superconductivity and losses in superconductors. The second is to perform measurements on a relatively new superconductor; magnesium diboride (MgB_2). MgB_2 is chosen as only a limited number of similar studies have been performed previously on this kind of superconductor. The measurements will be performed on samples from two different superconductor manufacturers. AC losses due to an alternating applied field are to be measured in a calorimetric setup. The field magnitude and direction will be varied and measurements will be performed at several temperature levels. The AC loss results are to be presented in loglog diagrams to search for penetration fields and power laws between the superconductor losses and applied field magnitude. These will be compared to conclusions on the same factors drawn from normal axis diagrams. The penetration field will be further discussed on the basis of the results being compared to AC loss equations for tape shaped and cylindrical conductor geometries.

The experimental part has several limitations. The range of temperatures is limited; measurements are done at six different temperatures ranging from 25 to 45 K. Two field directions are applied; parallel and perpendicular. The field magnitude is restricted by the current carrying capacity of the outer circuit cables and the temperature rise in the superconductors. The field frequency is given by the outer circuit current source.

The first section of the thesis describes superconductivity, and the background for splitting superconductors into two types. The Bean model for current density and magnetic field penetration in superconductors when in a time varying field is described. The section also includes AC loss equations. Coupling between superconductor filaments and the losses this generates follows. The focus is then moved to the basis for the experiments; the principle behind calorimetric measurements and some general information on the superconductor used, MgB_2 . Results from other AC loss studies done on this kind of superconductor are included, so are results on other types of superconductors as well, for the purpose of comparing to measured results.

The second part of the thesis first describes the superconductor samples used in the experiments. Then, the measuring system configuration, preparations that had to be made prior to the experiments and the procedure during measurements are presented. The logged data and the formulas used for their processing are also listed. The subsequent chapters are results and discussion.

2 Superconductivity and AC losses

The superconducting state is limited by critical temperature (T_c), critical current density (J_c) and critical magnetic flux density (B_c). B_c is called magnetic field in the remainder of the report, except for in Chapter 2.1 where the relation between magnetic flux density and magnetic field is used. If either one of the three factors is exceeded, the material is no longer superconducting. The sketch to the right in Figure 1 is a much used definition of critical current density. J_c is the current density when the voltage is $0.1 \mu\text{V}/\text{cm}$. To the left in Figure 1 is shown the superconducting surface for niobium-titanium. On the inside of the surface the conductivity is supra and on the outside it is normal. As is seen here, the three mentioned properties which limit the superconducting state influence each other. If, for instance, a superconductor is placed in a magnetic field, the critical current density decreases. [6]

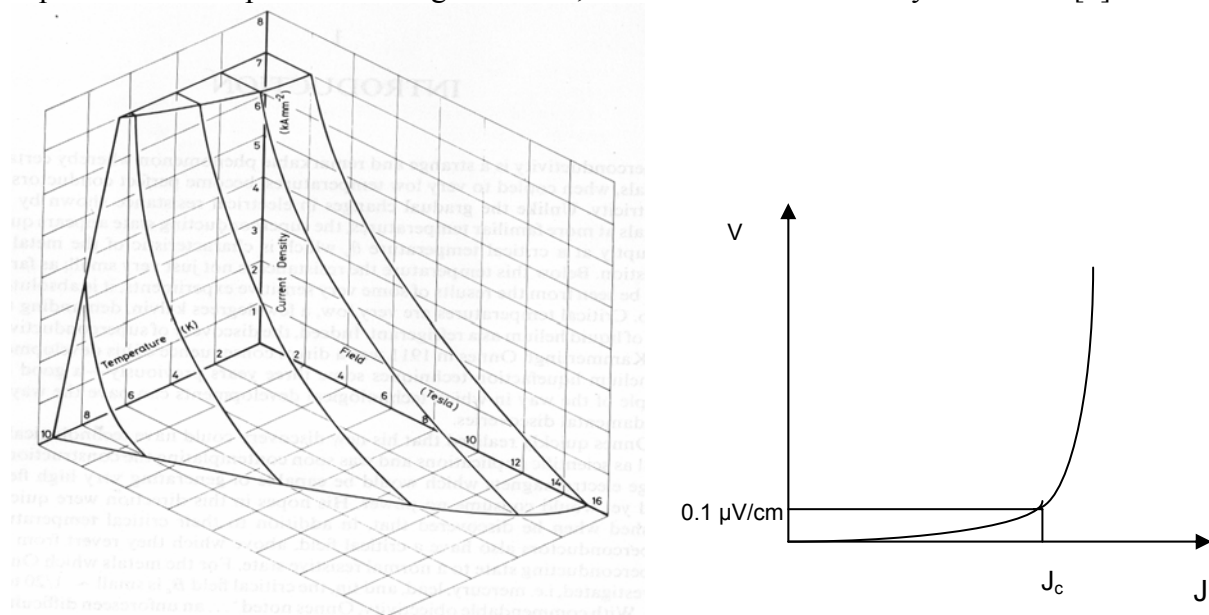


Figure 1 To the left: the three dimensional surface limiting the superconductive state for NbTi. [7, p 2] To the right: a much used definition of critical current density.

2.1 Behaviour in a magnetic field

Superconductors are split into type I and II, where the difference between them is their behaviour when placed in a magnetic field. This is sketched in Figure 2. In the figure, the solid lines correspond to type I superconductors, and the dotted lines to type II. When a low, constant magnetic field is applied to a superconductor of type I, complete Meissner effect occurs (Figure 2 a: the magnetization shows perfect diamagnetism). This means that eddy currents are generated in the surface. These expulse the magnetic field and it does not reach the interior of the conductor (Figure 2 b: the flux density is zero below H_c). If the critical magnetic field (H_c) is exceeded, the conductivity becomes normal (Figure 2 c: the resistivity goes from zero to a constant value). When a type II superconductor is placed in an external field there is an intermediate state in addition to the full Meissner effect and the normal conductivity states. If the applied field is low, the behaviour is as for type I, but in stronger fields ($H > H_{c1}$) flux lines penetrate the conductor (Figure 2 b). The sample is still superconductive when the field inside the conductor is greater than zero. When the applied field is increased further, more flux lines enter the sample. The conductor stays superconductive until the upper critical magnetic field (H_{c2}) is reached and its conductivity becomes normal (Figure 2 c). Type II superconductors can thus carry current inside the conductor when in the intermediate state. Type I only carry surface currents. [6]

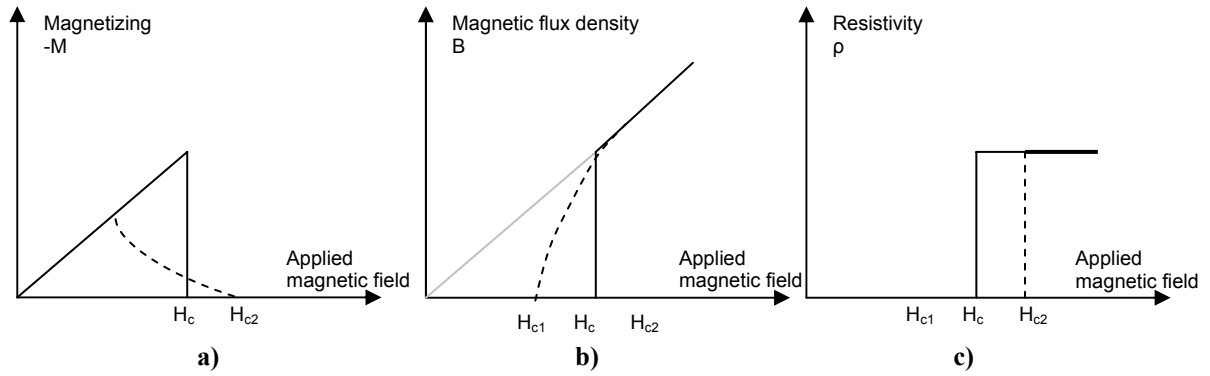


Figure 2 a) Magnetizing, b) magnetic flux density and c) resistivity in type I and II superconductors

When the flux density inside the conductor is greater than zero, flux lines, called vortices, have entered into the conductor. Each vortex carries a flux quantum (Φ_0) equal to

$$\Phi_0 = \frac{h}{2e} = 2.07 * 10^{-15} \text{ [Vs]} \quad (1)$$

where h is the Planck constant and e the electron charge. [2]

2.2 Critical state model

Superconductor AC losses and electromagnetic behaviour are described by the 'critical state model'. This is summarized here for a tape of thickness $2a$ along the x -axis and much larger dimensions along the y and z -axis. This is shown in Figure 3. An external field, B_y , is applied to the tape along the y -axis.

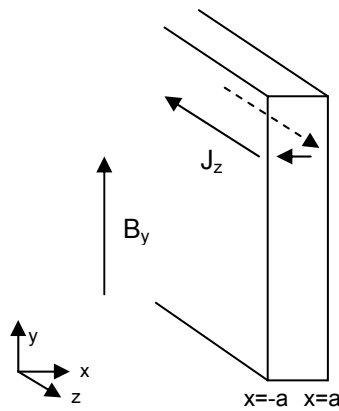


Figure 3 Tape of width $2a$ and far greater height and length. Applied field B_y and induced currents J_z

No magnetic field has been applied to the conductor, and the field inside the conductor is zero everywhere. The applied field is first ΔB . This induces current in the surface seeking to counteract changes in the magnetic field inside the conductor. The induced current has opposite flow directions on either side of the tape and creates a magnetic field of opposite direction of the applied field. [6] The current density in the conductor cross-section that carries current is equal to the critical current, see Figure 4 a). When the field is increased, the current density goes beyond J_c , but as the conductor then has normal conductivity, it decreases resistively back to J_c . [7] Current density equal to J_c also gives the least magnetic field penetration. [6] The flux density is higher closer to the surface, as seen in Figure 4 a). The current density in the conductor is given by Ampere's law:

$$\nabla \times \mathbf{B} = \mu_0 \mathbf{J}_c \text{ [T/m]} \quad (2)$$

where μ_0 is the permeability of free space. [2]

The applied field when the magnetic field reaches into the middle of the superconductor is called the penetration field,

$$B_p = \mu_0 J_c a \quad [T] \quad (3)$$

and is shown in Figure 4 b). At this point the entire cross-section is carrying critical current. [2] The same sketch illustrates that the current stays the same even if the applied field is increased above the penetration field (for $H < H_{c2}$). When the applied field is decreased, the field inside the conductor starts to change along the surface of the conductor, and this is also where the current flow changes direction first, see Figure 4 c). The situation in Figure 4 d) is when the current is completely reversed. Figure 4 d) also exemplifies that the field inside a superconductor is history dependent, and thus hysteresis losses. At this point, the entire cross-section carries current, but the applied field magnitude is not equal to the negative of the field in Figure 4 b). The reason for calling this the ‘critical state model’ is that the different tape sections either carry critical current or no current.

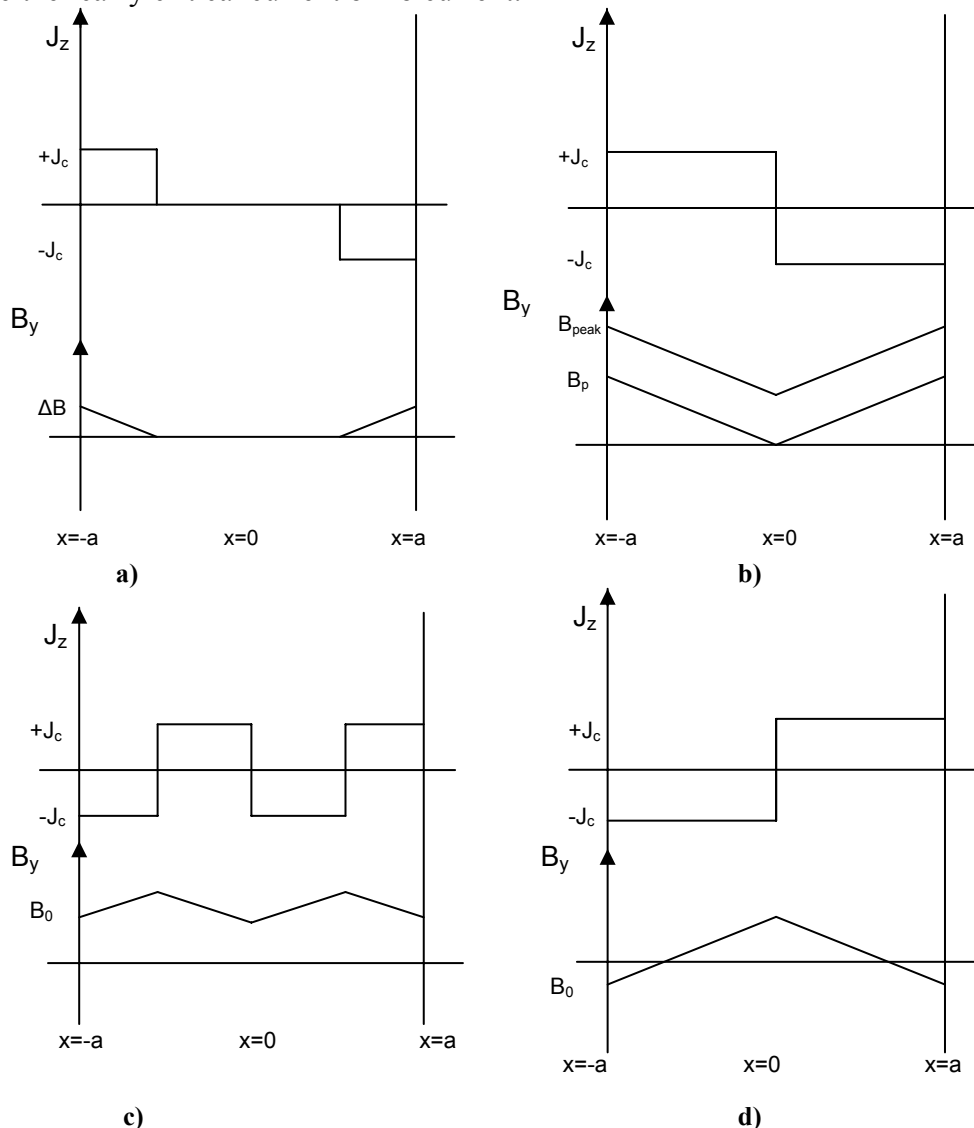


Figure 4 Magnetic flux density and current in the superconductor tape when a) the applied field is ΔB , starting with zero vortices inside the conductor b) the applied field equal to the penetration field (lower field graph) and applied field greater than the penetration field (upper field graph) c and d) the applied field is decreased

The situation where both current and magnetic field is applied to the superconductor is depicted with dotted lines in Figure 5. The applied current is called transport current and has

the same flow direction on either side of the superconductor. When this is increased to the degree that the entire cross-section carries critical current density in the same direction, the superconductor is saturated. If the transport current is further increased, the conductivity becomes normal.[6]

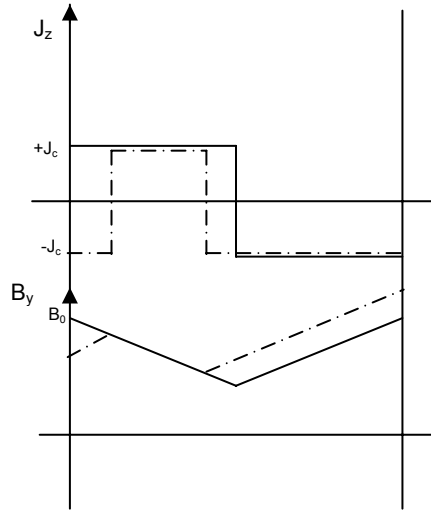


Figure 5 Magnetic flux density and current in the superconductor tape when it carries transport current

2.3 AC losses

Losses are generated in the superconductor when the conductor carries AC transport current or when the applied field varies with time, which includes both when changing from one DC level to another and applying an alternating field. [6] There are two ways of viewing the losses. One is based on vortex movement. Vortices in the superconductor are pinned with pinning forces to structural defects in the material. For instance do boundaries between metal and superconducting material exert such forces on the vortices. [8] When the applied field changes, Lorenz-forces act against the pinning-forces. If the Lorenz-force acting on a vortex is greater than its pinning force the vortex moves to a new equilibrium position. This movement is viscous and generates losses by generating heat. [6]

It is also possible to view the AC losses by considering the current in the superconductor. As mentioned in the previous section, the current density goes beyond the critical current density when the field is increased. It then decreases resistively back to the critical current density. AC losses are thus resistance losses. The resistivity is not linear and therefore not dependent on the cycle time. The losses are thus hysteresis losses. [7]

The hysteresis losses are influenced by the geometry of the superconductor, the direction of the applied magnetic field and the penetration depth. A smaller superconductor cross-section area gives less hysteresis losses. [3] The AC hysteresis losses were first calculated by Bean [9] for the geometry and applied magnetic field direction shown in Figure 3. The equations are

$$Q = \frac{2}{3\mu_0 B_p} B_0^3, \quad B_0 < B_p$$

$$Q = \frac{2B_p}{\mu_0} \left(B_0 - \frac{2}{3} B_p \right), \quad B_0 \geq B_p$$
(4)

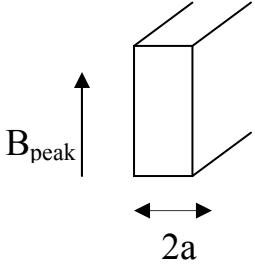
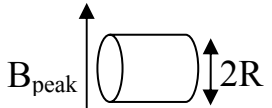
where B_p is the penetration field and B_0 is the maximum applied field (peak values). The losses are given in Joule per cycle and unit volume ($[J/(m^3 \cdot \text{cycle})]$). [10] In general, the losses may be rewritten to

$$Q = \frac{B_{peak}^2}{2\mu_0} \Gamma(\beta) \quad (5)$$

where $\Gamma(\beta)$ is the loss function and $\beta=B_{peak}/B_p$, where B_{peak} equals $2*B_0$ in equation (4). B_{peak} and B_p are thus peak-to-peak values. The greatest losses occur for $\beta=1$. When β is small there are losses in the surface of the superconductor, and when β is large the applied field is greater than the penetration field. The last case is more interesting as it is most useful in superconductor AC applications. [3]

In Table 1, equation (4) is rewritten to the form of equation (5). The loss equations for a cylinder shaped superconductor are also shown in the table. Both equations are valid for parallel applied magnetic fields.

Table 1 Loss equations for tape shaped and cylindrical superconductors in parallel field [11]

Sample geometry	Q [J/m ³]
	$\frac{B_{peak}^2}{2\mu_0} \frac{\beta}{3} \quad \beta < 1$ $\frac{B_{peak}^2}{2\mu_0} \left\{ \frac{1}{\beta} - \frac{2}{3\beta^2} \right\} \quad \beta > 1$ <p style="text-align: right;">(6)</p>
	$\frac{B_{peak}^2}{2\mu_0} 2 \left\{ \frac{2\beta}{3} - \frac{\beta^2}{3} \right\} \quad \beta < 1$ $\frac{B_{peak}^2}{2\mu_0} 2 \left\{ \frac{2}{3\beta} - \frac{1}{3\beta^2} \right\} \quad \beta > 1$ <p style="text-align: right;">(7)</p>

3 Filaments and coupling

A cross-sectional sketch of a superconductor tape is shown in Figure 6. The superconducting filaments are embedded in a matrix which is placed in a sheath. The matrix is included for improvement of the thermal stability and mechanical properties of the superconductor. [12]

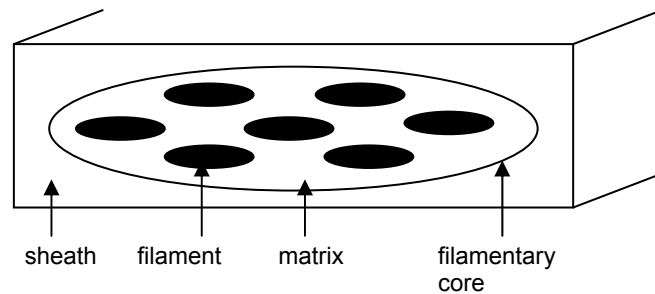


Figure 6 Cross-section sketch of a superconductor tape

When an alternating field of the direction depicted in Figure 7 is applied to a superconductor, currents are induced in the sheath, matrix and filaments. The induced currents in the filaments, as described in Chapter 2.2 are called screening currents. The currents in the sheath give eddy current losses and ohmic losses are generated by the induced coupling currents between the filaments. [13] These losses may greatly increase the total AC losses. [7]

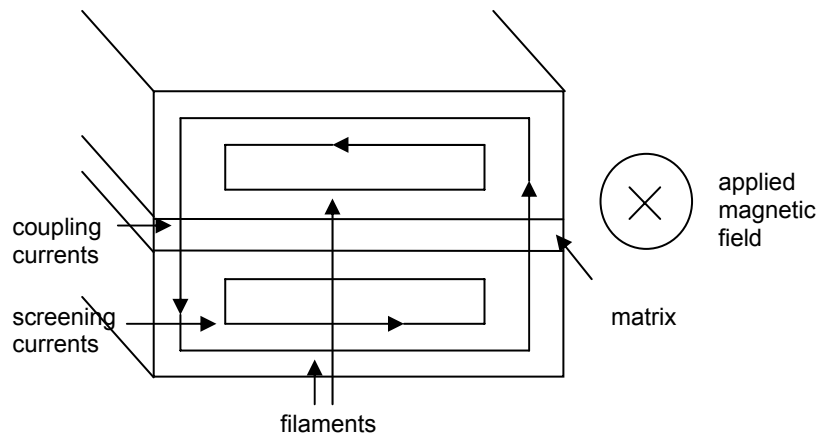


Figure 7 Sketch of two filaments and the coupling currents flowing between them

The coupling and screening currents seek to screen the superconductor from field changes. [7] The magnitude of the coupling current, among others depends on the length of the filaments. When the filament length is increased, the area enclosed by the coupling current becomes larger, which increases the coupling currents. If the length is greater than a certain limit, the coupling current magnitude equals the current carrying capacity of the conductor and the filaments are fully coupled. When the filaments are fully coupled, they all act together as one and there are no individual screening currents. Losses are decreased if there is less coupling. This may be achieved by twisting the filaments, which reduces the effective filament lengths. [13]

In the article ‘A general treatment of losses in multifilament superconductors’ A.M. Campbell has sought to find the factors that influence the AC losses by generalizing loss relations. The coupling losses described there are for copper. The main influence on these is the system time constant and the conductor geometry. The time constant is defined as

$$B = B_0 - \tau \dot{B} \quad (8)$$

where B_0 is the applied field, B the internal field, \dot{B} the rate of change of flux density and τ the time constant. The loss per unit volume and cycle is

$$Q = \frac{n\pi B_0^2 \omega \tau}{\mu_0(1 + \omega^2 \tau^2)} \quad [J/(m^3 * cycle)] \quad (9)$$

where n is the shape factor. The equation exhibits that the coupling current losses are proportional to the applied field squared and also depend on frequency. If $\omega \rightarrow \infty$ the coupling losses go to zero and the dominating losses are hysteresis losses. [14]

4 Basis for calorimetric measuring system

The general principle of the calorimetric measuring system used in the experiments reported here is comparing the temperature rise in the conductor when placed in an alternating magnetic field to a reference temperature rise given by a known heater power. The heater is in close proximity of the conductor. The dissipated power for small temperature variations [2]:

$$P_{AC} = \frac{c * m}{\Delta t_{AC}} \Delta T_{AC} \quad [W] \quad (10)$$

where c and m are the heat capacity and mass of the sample, respectively, Δt_{AC} is the measuring time interval and ΔT_{AC} is the temperature rise during this time. The equation is valid for small temperature changes. The temperature rise due to the heater is

$$\Delta T_{heater} = \frac{\Delta t_{heater} P_{heater}}{c * m} \quad [K] \quad (11)$$

where P_{heater} is the power dissipated in the heater. Combining these gives

$$P_{AC} = \frac{\Delta T_{AC} \Delta t_{heater}}{\Delta T_{heater} \Delta t_{AC}} P_{heater} \quad [W] \quad (12)$$

The temperature rise in the conductor is measured by measuring the change in resistance in a thin copper wire glued to the sample.

Above a certain temperature there is a linear dependence between resistivity and temperature:

$$\rho_{\Theta} = \rho_{20^{\circ}} (1 + \alpha(\Theta - 20^{\circ})) \quad [\Omega m] \quad (13)$$

where ρ_{Θ} is the resistivity at temperature Θ and α is a constant which depends on the material and is in the region $4 * 10^{-3} \text{ K}^{-1}$. [15] Tables of resistivity versus temperature exist (Appendix 1), and by comparing these values to the equation above it is found that the linear expression is not valid below about 150 K. Graphs showing this are found in Appendix 2. A comparison of the real resistivity versus temperature dependency compared to an adopted linear relationship of the 25 K resistivity rate of change is in the same appendix.

5 Magnesium diboride

Magnesium diboride (MgB_2) is the superconducting material used in the experimental studies. In 2001 it was discovered that this compound is superconducting below 39 K. [16] It is thus a type II, intermediate temperature superconductor. The molecular structure of MgB_2 is as in Figure 8. The most common way of producing MgB_2 superconductors is the powder-in-tube method. An example is Columbus Superconductors' ex situ (pre-reacted Mg and B to MgB_2) method. They use MgB_2 powder in nickel tubes. These are cold-worked into long wires. Several of these wires are placed together inside another nickel tube, again cold-worked and end up as tape for DC use. Ending the process is a heat treatment. This is necessary to obtain a high critical current density.[17] In DC MgB_2 superconductors the sheath in Figure 6 is typically a ferromagnetic material such as nickel or iron. When these are placed in an alternating magnetic field, hysteresis losses are generated. Other sheath and matrix materials must thus be used for AC applications.

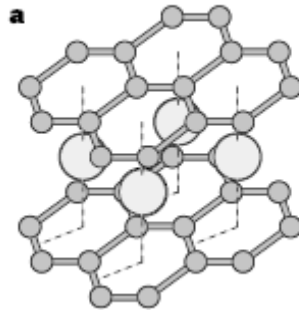


Figure 8 The MgB_2 molecular structure; the larger spheres are magnesium atoms [18]

Various studies have been performed on magnesium diboride in order to enhance the superconductor properties. Results from a few of them are cited here. Flükiger et al. [19] have compared different production methods and found that the critical current density is influenced by aspects such as “the details of the deformation process, the quality and size of the powder particles and the annealing temperature and time”. Pinning may be improved by making modifications to the structure or microstructure. The best sheath material for MgB_2 is iron as the MgB_2 and iron hardly react. Nickel and nickel alloys react more with magnesium diboride. Rowell [20] has studied the resistivity of various MgB_2 samples and has found that it varies greatly, which is very unusual at such low temperatures. Yang et al. [21] states that many studies have been performed in trying to develop MgB_2 bulk materials and conductors for practical use, and this has led to a “significant improvement” in MgB_2 .

A paper from the round table discussion at the 19th International Conference on Magnet Technology states that three aspects of MgB_2 needs improvement before it might replace Nb_3Sn in high field magnets. These are: increased H_{c2} , the quality and price of conductors must be improved and J_c needs to be higher than for competing superconductors. The first point (H_{c2}) is already accomplished. The last (improved J_c) seems possible from present studies. The article claims it is likely MgB_2 may be used in niche products, e.g. “NMR/MRI; high-energy physics; high-field research; semiconductor material processing (...) fusion and MAGLEV”. With much improvement it can possibly also enter a wider market. Table 2 lists the necessary improvements needed for various applications. The numbers in parenthesis are today's values, F_{OP} the frequency of operation, B the operating field strength and J_E the engineering current density. Figure 9 shows an MgB_2 superconductor manufacturer roadmap

for future development and aims. [22] As is seen from the figure, prospective mass production still lays a few years ahead.

Table 2 Frequency, magnetic field and engineering current density needed for MgB₂ to compete in the markets listed. [22]

	F_{OP} [Hz]	B [T]	J_E [kA/cm ²]
Motor/Generator Rotor	50-500	1	100 (35)
Motor/Generator Stator	50-500	0.002	100 (35)
Transformer (military; @20 K)	50-500	0.15	50 (60)
Transformer (utilities; @30 K)	50-60	0.15	50 (20)
Adiabatic demagnetization	2 T/min	3	100 (20)
Open MRI	DC	0.5	20 (50)
Close MRI	DC	2-3	20 (10)
Muon collider	DC	5-20	? ?
Wiggler/Undulator	DC	3-5	10-20 (100)
Proton Collider	DC	15	120

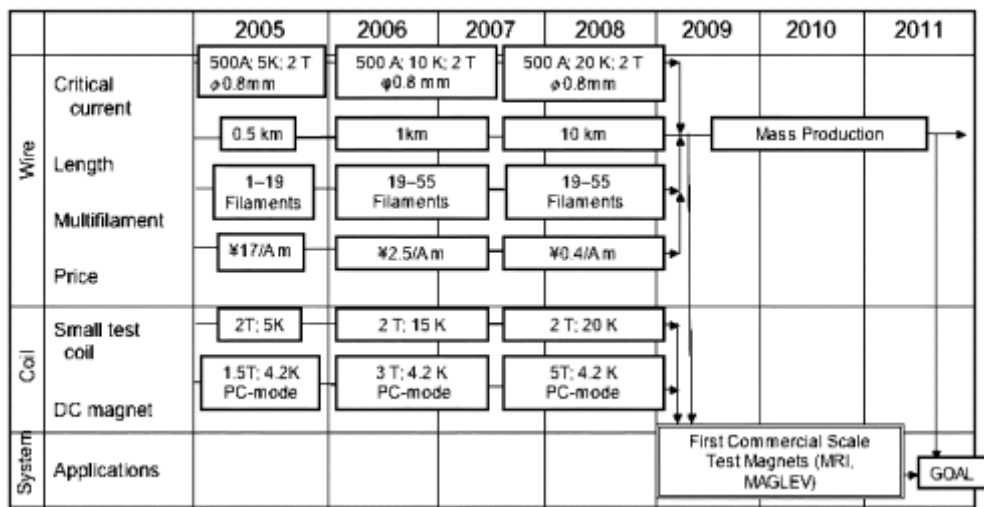


Figure 9 A Hitachi roadmap for MgB₂ development [22]

Various other articles have views on the potential applications at which magnesium diboride may be used:

- superconducting fault current limiters [21]
- electric motors, magnetic field screening apparatus and variable inductor/resistor [23]
- may be able to compete with LTS wires. The main advantage is the low price on magnesium and boron. [5]

5.1 Results from various studies on MgB₂

In this section, various studies on MgB₂ are cited, and the emphasis is put on AC losses and the power law between loss and applied field, i.e. the n in $Q \propto B^n$.

Lou et al. [24]

The experiments are performed in order to find what influence temperature, frequency and AC and DC magnetic field magnitudes have on the bulk sample losses. The results are compared to HTS and LTS studies and the AC loss mechanisms in MgB₂ are discussed. The superconductor matrix is tantalum and the sheath quartz. The AC field equation is $B(t)=B_d+B_{ac}*\cos(2\pi ft)$, where B_d is varied up to 7 T and B_{ac} between 6.5 and 91 μ T. The frequency is 80 Hz to 9 kHz.

The AC loss results drawn in Figure 10 show that the loss slope goes from B^2 via $B^{1.8}$ to $B^{1.2}$. The authors do not know why the results do not follow the B^3 to B slope given by the Bean equations. Their conclusions are that the AC losses depended on the applied field frequency. This is the same conclusion as studies done on HTS (Ag-Bi2223) and LTS (NbTi). The dependence between AC losses and applied field amplitude is also similar to those of HTS and LTS.

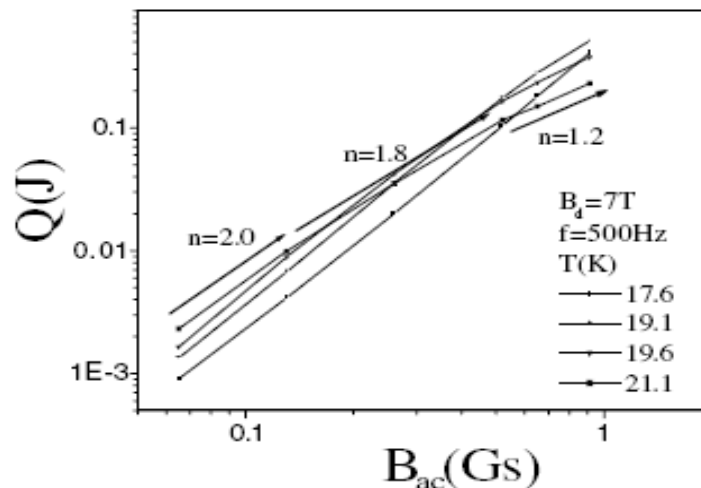


Figure 10 Magnetizing losses in bulk MgB₂ samples. Loss slopes are written in the diagram. [24]

Yang et al. [21]

The article presents measurements done on MgB₂ wire and bulk samples at temperatures between 25 and 40 K and applied field up to 0.2 T. Figure 11 displays AC losses in different geometries. The upper left graph shows the losses in a flat plate in a perpendicular field of frequency 59 Hz. The solid lines are H^4 , and the results were expected to follow this field power. The constant results at high fields were not expected. The upper right graph is for a bar and shows a different loss slope. The solid lines are H^3 , which is the loss' field dependence in a cylindrical conductor, and it seems likely it may be used on a square-shaped sample as the height-to-width ratio is 1.5. Their overall conclusion is that the losses depend on geometry.

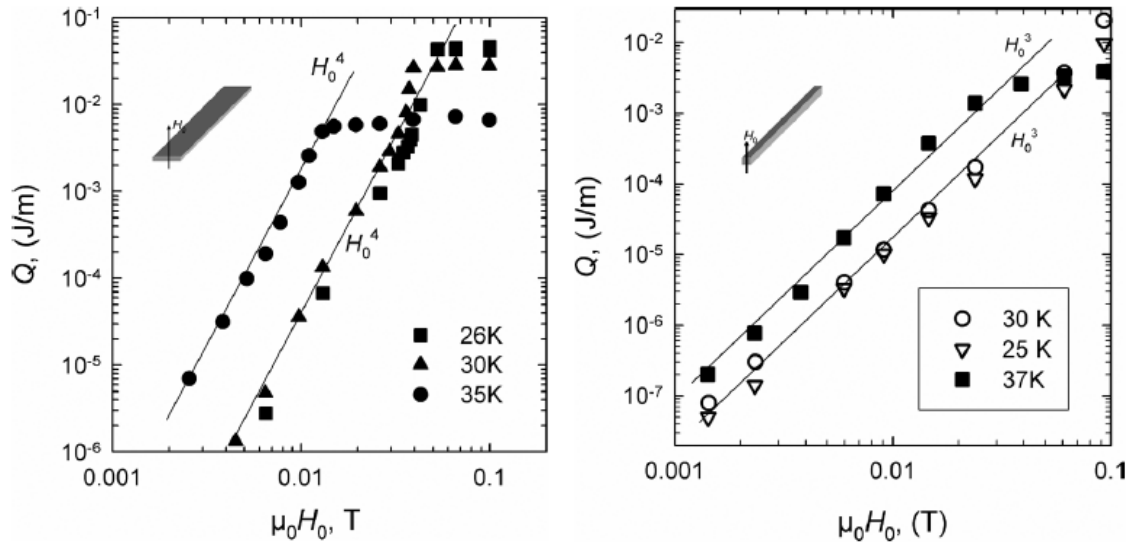


Figure 11 AC losses in different geometries [21]

Ginuchi et al.[23]

The study is performed in order to find the dependence between MgB₂ grain size in bulk materials and AC susceptibility, magnetic cycles and magnetic screening. The authors claim the grain boundaries do not influence the critical current in MgB₂, but the grain dimensions may. In Figure 12 it is seen that two of the samples have penetration fields greater than 1 T, while the others have B_p at far lower fields, out of bounds of the measurements. One of the grain sizes showed a B³ slope; see Figure 13. This figure also shows good agreement with another study, shown in the figure. The authors' conclusions are that different boron powder starting points give similar results.

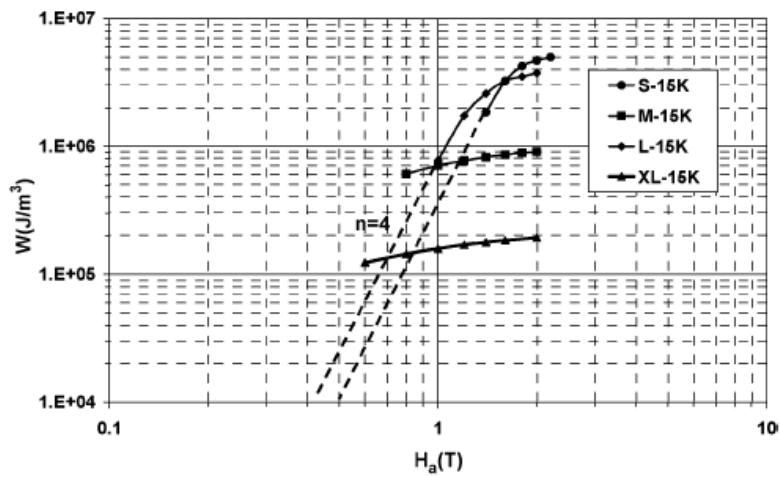


Figure 12 Losses for four different MgB₂ grain sizes [23]

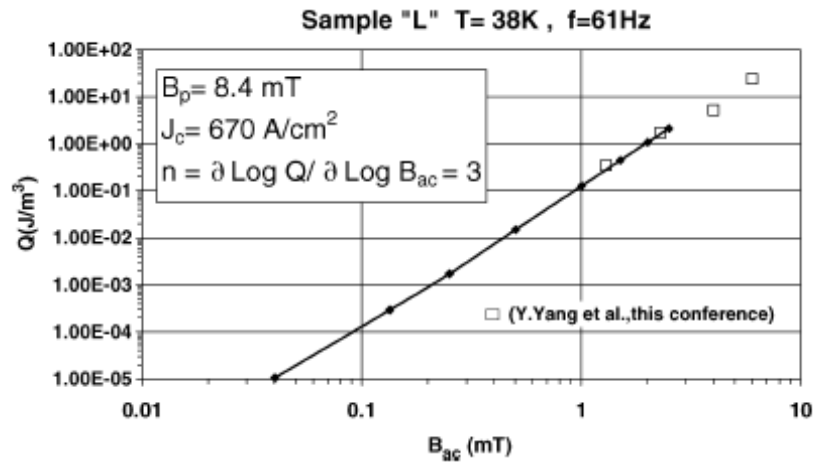


Figure 13 Losses in one grain size compared to results from another study [23]

6 Results from various studies on Bi2223/BSCCO superconductors

The results from studies on other types of superconductors may be used to compare the loss magnitudes and power law dependence between applied field and AC losses to MgB₂.

Magnusson[2]

The doctoral thesis describes an AC loss measurement setup, measurements and a model for AC losses, partly with basis in the measured results. The setup is the same as the one used in this study. Results from magnetizing measurements on two different BSCCO/Ag tapes are shown in Figure 14. As is seen from the diagrams, low field losses are measured at a high frequency: 507 Hz, and high field losses at a lower frequency: 47 Hz. Losses in both tapes follow the Bean equation power law well.

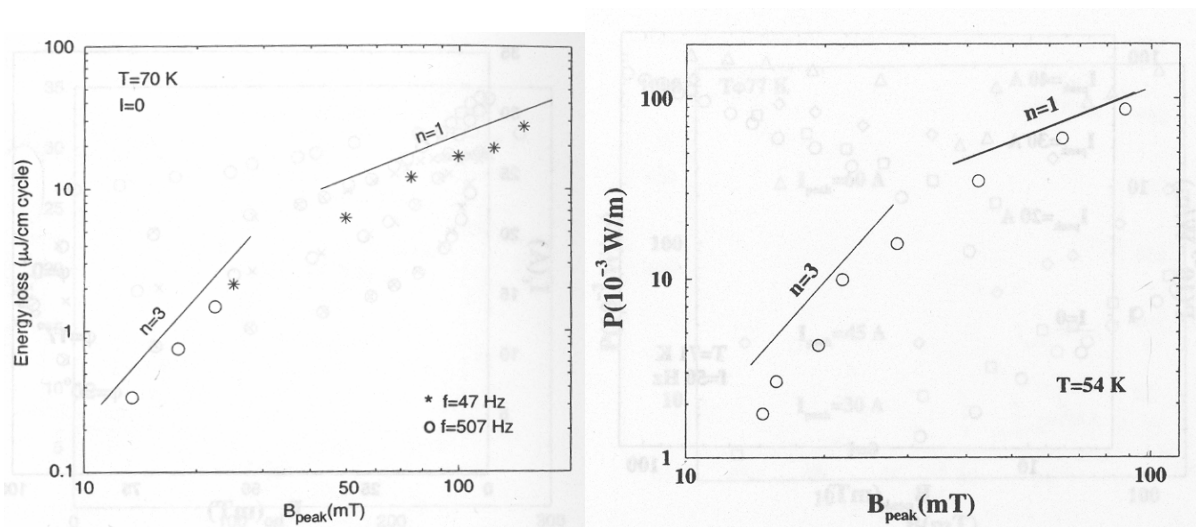


Figure 14 Magnetizing AC loss results in two different BSCCO/Ag tapes at different temperatures [2]

Rabbers [13]

The doctoral thesis studies analytical models and looks at which models may be used for Bi-2223/Ag. In Figure 15, AC magnetizing losses are compared to calculations and a model. As can be seen, losses are about one order of magnitude greater in a perpendicular field, but the general behaviour is similar for the two field directions. At low fields with perpendicular direction the slope is close to $B^{3.2}$, and in parallel field B^3 . At high fields the loss slope is B . The results follow the model reasonably well.

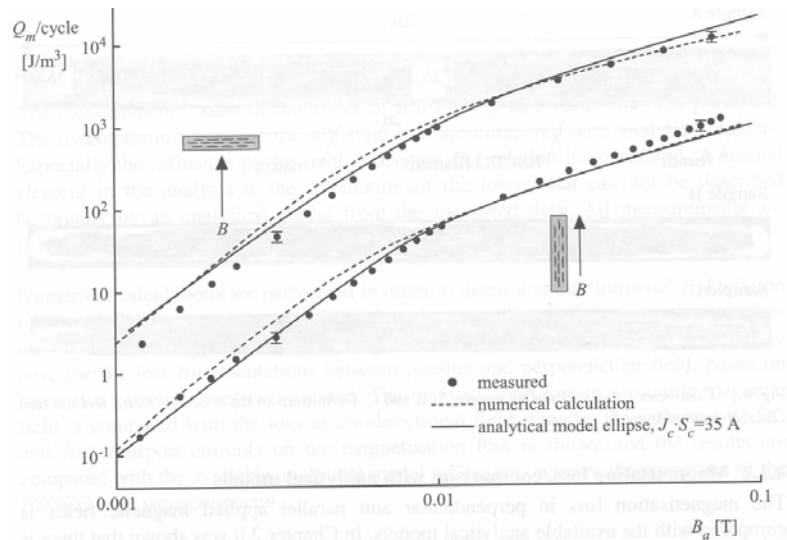


Figure 15 Magnetizing losses in Bi-2223 tapes [13]

Inada et al. [25]

The study is done on Bi2223 Ag sheathed tapes with resistive barriers (Ca_2CuO_3). The aim is to examine their AC magnetizing losses. Each sample is 10 mm long, the applied field is varied between 1 and 50 mT, and the frequency between 40 and 125 Hz. The Bean model equations for a slab are used for comparison. The results are shown in Figure 16. The authors' conclusions are that the losses depend on frequency and that the decoupled filament samples almost follow the theoretical equations. The barrier free samples have far higher losses.

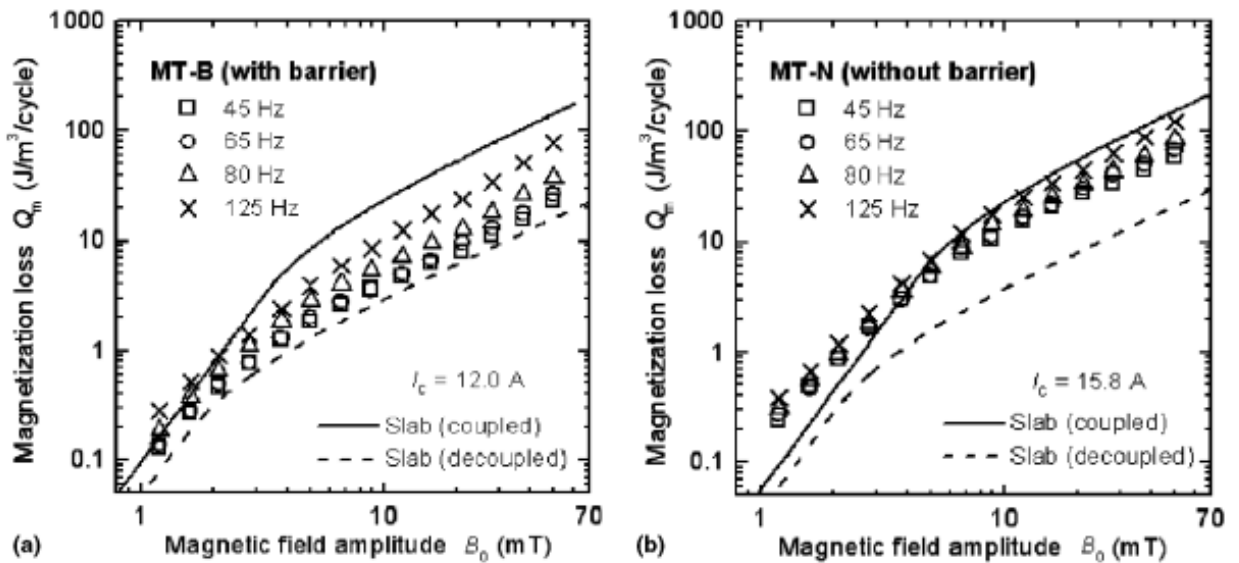


Figure 16 Magnetizing losses found in the study [25]

Polak et al [26]

The study treats Bi-2223/Ag tapes and filaments. Magnetization losses for three single filaments are shown in Figure 17. The rate of change of magnetic field is 0.75 mT/s. The results at low fields are proportional to B^3 and high fields B . The authors claim the high field dependence should have been B^0 .

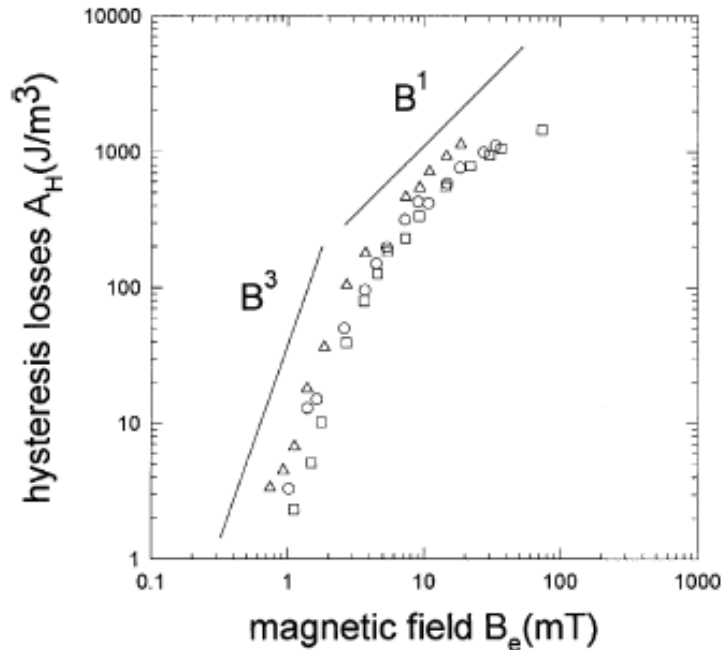


Figure 17 Magnetization losses for three single filaments [26]

Su et al. [27]

Several square and round Bi(2223)/Ag wires with different twist pitches were prepared, and it is sought to find the geometry and twist length influence on the AC losses. Figure 18 presents AC magnetizing losses for a flat tape and two square conductors. The loss slope is written in the figure. As can be seen, the tape has the highest losses. The authors claim that round and square configurations and twisting all have positive influence on the losses.

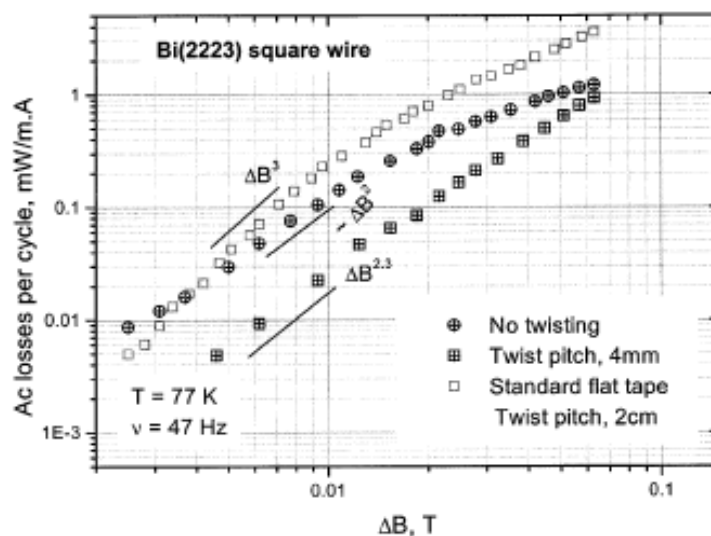


Figure 18 Magnetizing losses in square Bi(2223)/Ag wires [27]

Fang et al. [28]

The article presents measurements done in a perpendicular field on Bi-2223/Ag tapes of different aspect ratios to find the geometry influence on AC losses. The various sample results at two different frequencies are shown in Figure 19. The left graph shows the losses at frequency 30 Hz are proportional to B^2 for low fields and B for higher fields. The low field B^2 slope is explained as coupling losses. The graph to the right for frequency 270 Hz has Q proportional to B^3 and B for high fields. The authors claim the frequency used here does not give coupling losses and the measured losses are thus hysteresis losses. It is the conductor with the smallest aspect ratio which has lowest losses.

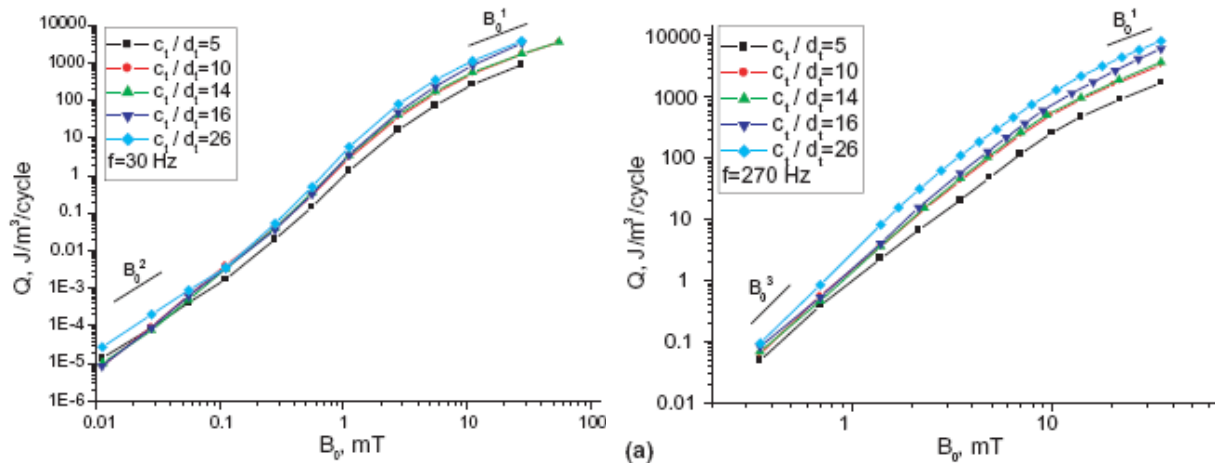


Figure 19 Aspect ratio and the influence on hysteresis losses [28]

Witz et al. [29]

The authors have measured on square Bi,Pb(2223) /Ag superconductors, looking at AC losses and comparing them to theoretical equations. The results for two conductors are presented in Figure 20. The left graph is for perpendicular field and the authors claim the conductor is saturated or close to saturation from coupling currents at low fields. The graph to the right is also for perpendicular field. Here, various twisting pitches lower the losses, compared to the untwisted case. This conductor is not saturated. The overall conclusion is that square and round superconductors may be interesting to use in fields where a perpendicular field component is present.

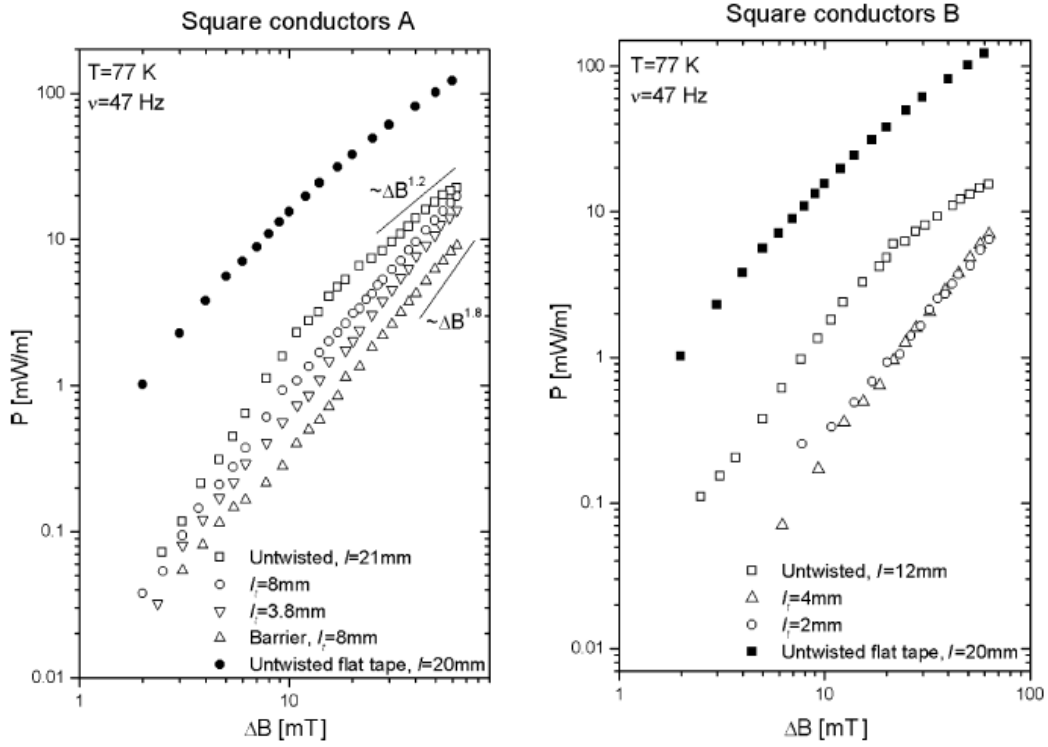


Figure 20 Square conductor AC losses in perpendicular field [29]

7 Measuring losses due to applied alternating magnetic field

The chapter starts with a summary on the data on the two samples used. Following this is a description of the measuring system, preparations necessary prior to performing measurements and the measuring procedure. The chapter is concluded with a presentation on the logged data and the performed calculations.

7.1 Superconductors used in these experiments

Superconductors from two manufacturers – the Italian Columbus Superconductors Spa and the American Hyper Tech Research, Inc – were used in the experiments. Superconductor data are listed in Table 3 . Appendix 3 is critical current versus field in the Columbus conductor at 20 K. An analogous graph for a sister conductor of the Hyper Tech superconductor is also included. The Hyper Tech sample went through a heat treatment after being received, and the recommended and performed heat treatment profiles are shown in Appendix 4.

Table 3 Superconductor data

Manufacturer	Number of filaments	Twisted	Barrier material	Matrix/ Sheath	Cross-section dimensions	Length
Columbus	7	No	Nb	60%Cu,40%Ni	1.74*1.76 mm → 3.06 mm ²	44 cm
Hyper Tech	7	No	Nb	Cu30Ni/ Cu30Ni	Ø 0.83 mm → 0.54 mm ²	48.5 cm

7.2 Measuring system

Figure 21 is a cross-sectional sketch of the system used for measuring losses due to an applied alternating magnetic field. The figure is not to scale. The outer barrier of the system was the cryostat, made of fibre-glass reinforced epoxy. The superconductor holder was fastened to the cold head of the cold pump and the superconductors were glued onto the holder. In order to achieve good thermal connection between the cold head and the samples, there were copper tapes in the holder. The samples were placed in vacuum. To radiation shields, one horizontal under the holder and one vertical were included to minimise the heat penetration from the surroundings towards the sample. Super insulation was glued onto these. The upper cryostat half was mounted onto the lower before the measurements could start. The magnetizing coils were placed inside the vessel created by the upper half of the cryostat. This was also where liquid nitrogen was poured when the experiments were running.

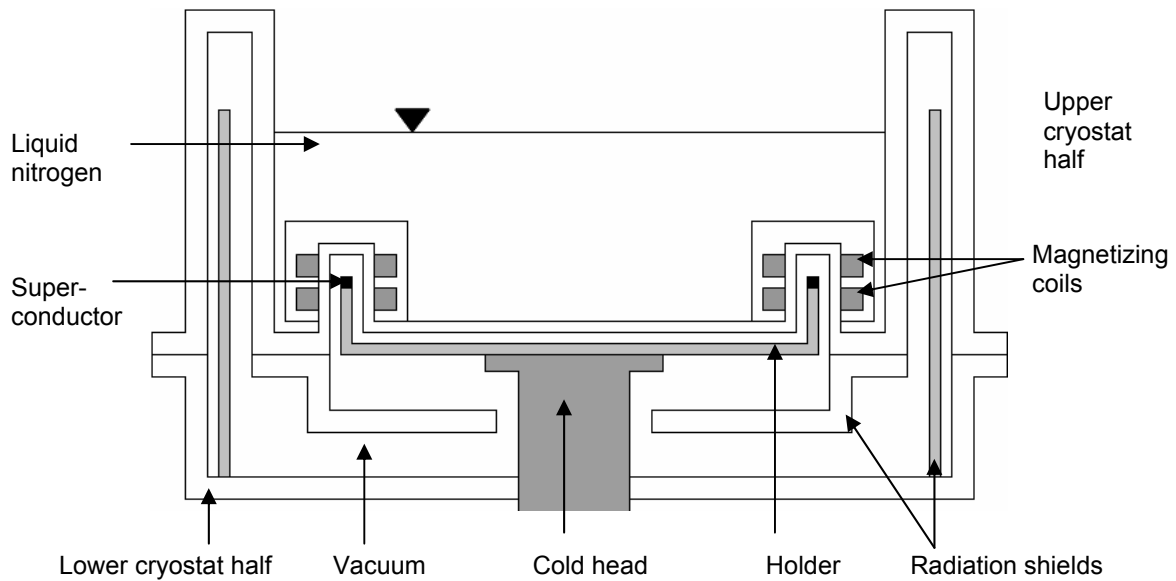


Figure 21 Cross-section sketch of cryostat, magnetizing coils and superconductors

Figure 22 is a sketch of the current in the magnetizing coils and the corresponding field configurations. Each field direction was made by three series connected coils. Changing from one field configuration to the other was done by interchanging between the main connections. The applied field was a sine of frequency 50 Hz and the magnitude was varied in the range of 3 to 150 mT. When 'low' and 'high' fields are mentioned in the remainder of the chapter it is meant within the applied field range.

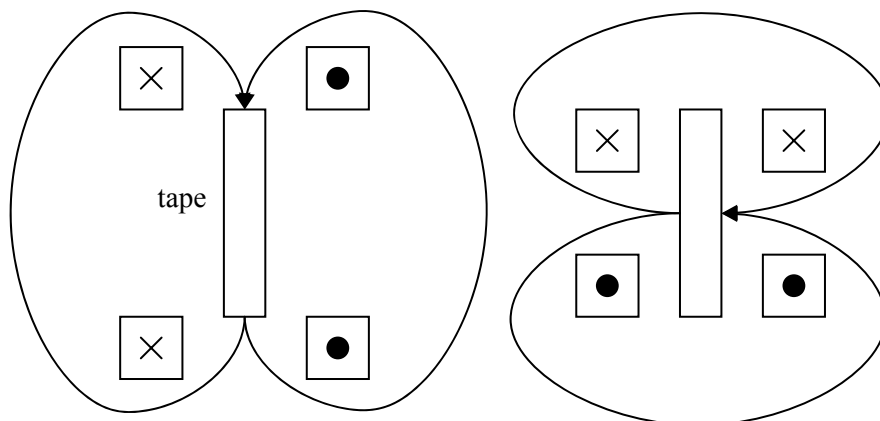


Figure 22 Parallel and perpendicular fields. Dots means current coming out of the paper, crosses is current going into the paper.

The outer circuit connected to the magnetizing coils is drawn in Figure 23. As the magnetizing coils were mainly inductive, partly cancelling this out was done by placing a capacitor bank in parallel with the coils.

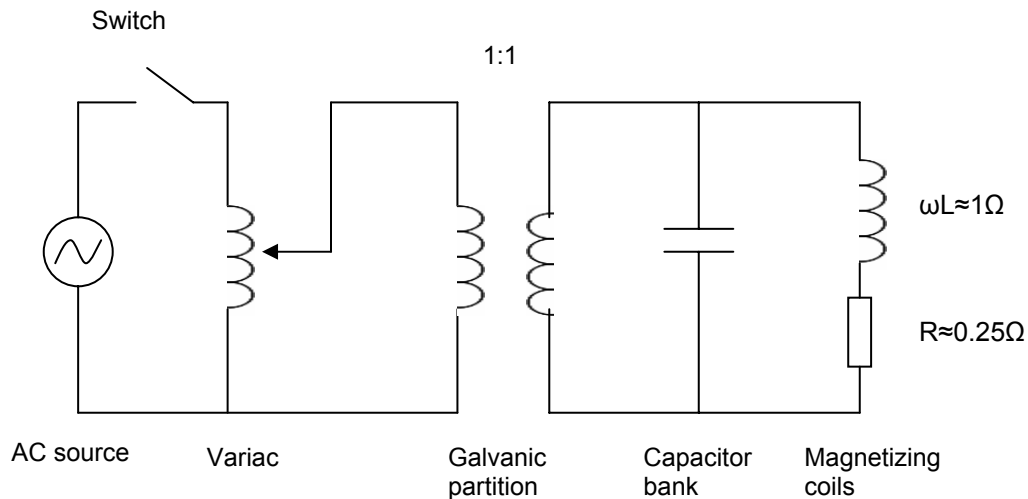


Figure 23 The circuit connected to the magnetizing coils

An equipment list is found in Appendix 5

7.3 Preparations

The following section describes what was done before the measurements could start.

- Old glue on the superconductor holder was sanded away. New superconductors were then glued to the holder using epoxy glue (a mixture of STYCAST 2850 and CATALYST 24 LV, with ratio 100 gram to 7 gram). The lengths of each of the superconductors were somewhat less than half the holder circumference.
- Copper wire of diameter 0.1 mm was glued (GLV Cryoengineering, IMI 7031 Varnish, Low temperature adhesive) onto the conductors, each back and fourth two times. As the Hyper Tech conductor was cylindrical, the copper wire was wound around it. A heater was also glued onto the conductors. This is a resistance alloy (Manganin®) of diameter 0.05 mm. A sketch of the Columbus conductor on the holder with wires glued onto it is shown in Figure 24.

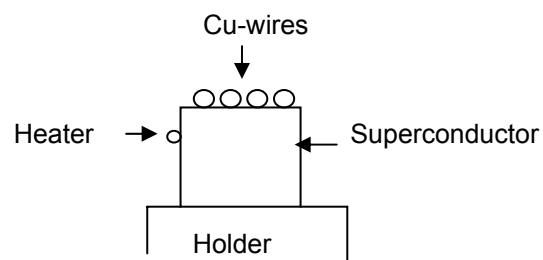


Figure 24 Columbus superconductor, copper wires and heater

- The holder was then screwed to the cold head (as shown in Figure 21) and current and voltage connections were soldered to the heater and copper wires.
- One of the current wires soldered to the heater was connected to a switch where the three possible positions were: calibration settings, base settings and open switch. The ‘calibration and base settings’ outputs were connected to individual power supplies.
- Voltage, current and thermo element wires were connected to 20 channel multiplexers that went into a data acquisition unit connected to a pc with data logger software. The user interface is called virtual oscilloscope for the remainder of the report.
- Thicker copper wires marked H1+, H1- ... H4+ and H4- were soldered to each of the four copper quarters on the underside of the holder, shown in Figure 25. By applying

voltage to one of these, the temperature at this quarter was increased (when necessary). As is also seen in Figure 25, numbered thermo elements were glued to the two conductors. The positions of the numbers indicate whether they were glued on the side facing in or out of the holder. As the thermo element wires were not long enough to reach across, fewer thermo elements were connected to the Hyper Tech conductor. Figure 26 is a close-up sketch of how most of the thermo elements were placed. It is showed that they were placed in between ‘holder fingers’.

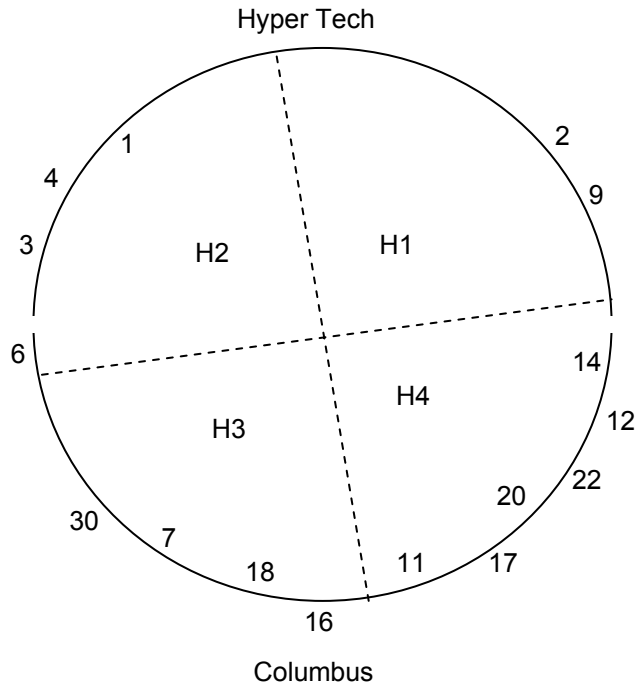


Figure 25 Placing of thermo elements onto the two superconductors

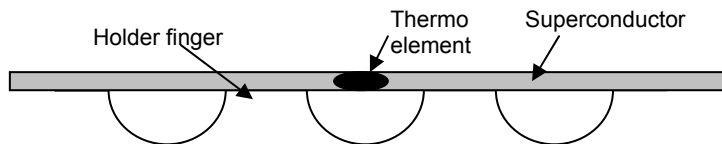


Figure 26 Close-up sketch of placing of thermo elements on the superconductors

Figure 27 is a picture of the holder with the superconductors glued to it, and copper wires, heater and thermo elements glued onto them. The red wires are thermo elements.



Figure 27 Picture of the holder and superconductors with copper wires and thermo elements glued onto them

7.4 Measuring procedure

Before the two cryostat halves were put together, all wiring resistance values were measured. These were controlled regularly during the assemblage to discover any open circuits. The measuring procedure for this particular setup, Figure 21, was as follows.

- After the cryostat was assembled, the vacuum pump connected to the cryostat was turned on. A low pressure of less than 0.1 mbar was sought. If the system cannot reach this low pressure, a leak is present, must be found and removed. When the system was cooled the pressure should be below the manometer scale.
- Before cooling the system, calibration measurements of the copper wires were taken. A desired copper wire base power was set.
- The cooling pump was then turned on and liquid nitrogen was poured into the vessel created by the cryostat. The system was left to cool and the thermo element readings were logged. If the difference between them is large when they stabilized, i.e. several degrees, power may be supplied to one or more of the copper quadrants, leading to a local temperature increase. When a satisfactory temperature difference was attained experiments could be performed.
- A particular copper wire temperature could be set by adjusting the heater power. The copper wire resistance had been found at room temperature (293 K), and by using tables of resistance ratio versus temperature, the resistance at the desired temperature was calculated. (A more detailed description is found in the next section.) This was obtained by adjusting the heater power.
- Before the AC loss measurements could be performed, a series of calibration measurements were done. The power source connected to the ‘calibration settings’ position of the heater switch was set to a desired calibration heater power. When the system again was stabilized at the base level, a series of measurements were done. The heater switch was turned to ‘calibration’ for a specific time period (10, 20...60 seconds). During the measuring, the voltage and current in the heater were logged. Right after a measurement the voltage rises in the copper wires were recorded. Prior to the next measurement voltages in the copper wires were attempted returned to their base levels.
- The AC loss measurements were then done. The desired field configuration main wires were connected to the outer circuit shown in Figure 23. The current in the coils was changed by adjusting the output from the variac. The current was turned on and off by a manual switch. The time period the current was flowing was measured by using a stop watch, and for short time intervals also by reading off an oscilloscope. The voltage rises in the copper wires were logged. After each measurement, the copper wire voltages were attempted returned to their base levels.

7.5 Processing of data

The data collected, the calculations needed and the corresponding equations are listed below. All data processing was done in Matlab.

Before cooling:

- Copper wire voltages ($U_{cu,293K}$) and current ($I_{cu,293K}$) were logged. These were used to calculate the reference resistance ($R_{0,293K}$) at room temperature (293 K).

$$R_{0,293K} = \frac{U_{cu,293K}}{I_{cu,293K}} \quad [\Omega] \quad (14)$$

During cooling:

- Thermo element voltage levels were registered. Interpolating in tables of voltage – temperature coherence (Appendix 6) gave the individual temperatures.

When cooled:

- Initial voltage (U) and current (I) values for the copper wires were noted. Together with $R_{0,293K}$ and resistance ratio – temperature tables (Appendix 1) the copper wire temperature (T_0) was found.

$$U = I * \frac{R}{R_0}(T_0) * \frac{R_{0,293K}}{R/R_0(293K)} \Rightarrow \frac{R}{R_0}(T_0) = \frac{U}{I} * \frac{R/R_0(293K)}{R_{0,293K}} \quad (15)$$

$$\text{where } \frac{R_{293K}}{R/R_0(293K)} = R_{0,273K}$$

By reversing the calculation the system could be set at a desired temperature. Then, the temperature had to be decided, its corresponding resistance value was found and the needed copper wire voltage was calculated.

During calibration measurements:

- Copper wire and heater voltages and currents were logged both with the heater switch set to ‘base settings’ (I_{cu} , $U_{heater,basis}$ and $I_{heater,basis}$) and to ‘calibration settings’ (ΔU_{cu} , $U_{heater,calibration}$ and $I_{heater,calibration}$). The time Δt was also noted. These were used to calculate the resistance rise in the copper wire and the heater energy input.

$$\Delta E_{heater} = (U_{heater,calibration} * I_{heater,calibration} - U_{heater,basis} * I_{heater,basis}) * \Delta t \quad [J]$$

$$\Delta R_{cu} = \frac{\Delta U_{cu}}{I_{cu}} \quad [\Omega] \quad (16)$$

$$\frac{\Delta E}{\Delta R} = \frac{\Delta E_{heater}}{\Delta R_{cu}} \quad [J / \Omega]$$

The heater input powers used in the first calibration series were attempted used in all calibration series.

During AC loss measurements:

- Logged data were copper wire voltages and current, rms current in the magnetizing coils (I_{rms}), time interval (Δt_n) and voltage increases in the copper wires.

$$B_{peak} = I_{rms} * \frac{B(1A)}{1A} \quad [T] \quad (17)$$

The peak field magnitudes for 1 A current are: for parallel field 1.37 mT and perpendicular field 1.16 mT. From the calibration results, regression lines for the various power inputs were drawn.

$$y_i = a_i t_i + b_i \quad [J / \Omega] \quad (18)$$

Where y_i is the regression function, t_i the time and a_i and b_i are constants. The power (ΔP_n) dissipated during the time interval (Δt_n) was found using the regression lines and the resistance increases in the copper wires (ΔR_{cu}) derived from the measured voltage increases.

$$\Delta P_n = \frac{(a_i * \Delta t_n + b_i) * \Delta R_{cu}}{\text{wire length} * \Delta t_n} \quad [W / m] \quad (19)$$

At each temperature level, three calibration series were run. As the highest calibration powers were closer to the AC losses, the regression lines corresponding to the highest calibration powers were used in the above calculation.

- The results have been studied in both double logarithmic (loglog) diagrams and graphs with normal axes. From these it was sought to find penetration fields and loss slopes.
- The results were also attempted fitted to the tape and cylindrical AC loss equations (6) and (7) to examine if the losses fit the equations and find whether tape shape or cylindrical conductor equations fit the data best. The graphs were also used in trying to determine the penetration field. In order to for the graphs and the measured results to have the same denomination (W/m), the equations (6) and (7) were multiplied with CAf , where f is the frequency, A is the cross-section area and multiplying it with C (C is between 0 and 1) gives the 'efficient area'.

8 Results

The section headings in this part are named after the temperatures sought to achieve in the Columbus superconductor, and not the actual temperatures measured. Where abbreviations have been used, HT is Hyper Tech, C is Columbus, || is parallel field and T is perpendicular field. The order of the measurements was:

- first series: 25, 30, 35 and 45 K. Both parallel and perpendicular fields were used.
- The results lead to a second series: further measurements at 30 K, mainly at low fields, but also a few at higher fields to compare to the first results. Series at 28.5 and 31.5 K were also performed.

Some results have been included for all temperature levels. This includes conductor temperatures measured by thermo elements and copper wires, AC loss results plotted in loglog diagrams and normal axis diagrams and curve fitting to cylindrical conductor equations. The loglog diagrams also contain lines of various slopes between B and B^3 . Curve fitting is shown in both normal axis and loglog diagrams. Correlating between measured results and theoretical curves is for low fields better in loglog diagrams and for high field in normal axis diagrams.

Other results have only been shown as an example for one temperature. The calibration graph at 25 K is shown in the report, the rest are found in Appendix 7. The different thermo element readings and temperature increases during AC measurements are listed for 28.5 K, the rest are shown in Appendix 8 and Appendix 9. As it turned out that cylindrical loss equations fit better to the measured results than the tape shape equations, only diagrams based on cylindrical conductor equations are included in the results, however, an example of curve fitting to tape shape equations at 30 K is in Appendix 10.

Thermo element state after measurements had been performed

The state of the thermo elements glued onto the two conductors after having performed experiments and opening the cryostat is summarised in Table 4. Their placing on the two conductors is in Figure 25. As thermo elements 1 and 4 had fallen off during experiments, their readings are not included in the calculated averages.

Table 4 State of thermo elements when opening the cryostat after running the experiments

Thermo element Columbus	State	Thermo element Hyper Tech	State
6	Glued onto heater	9	Ok
30	Had almost fallen off	2	Ok
7	The end was sticking out	1	Had fallen off
18	Ok	4	Had almost fallen off
16	Glued onto heater	3	Ok
11	Ok		
17	Close to heater		
20	Ok		
22	Ok		
12	Ok		
14	Ok		

8.1 25 Kelvin

The temperatures in the two superconductors given by the thermo elements and the resistance in the copper wires were as listed in Table 5. The first two rows show the results measured prior to the calibration measurements. The temperature was adjusted prior to the measurements and as no thermo element readings were done at this temperature, only copper wire temperatures are given.

Table 5 Thermo element and copper wire temperatures

Temperature [K]	Columbus	Hyper Tech
Average, thermo elements	28.64	29.24
Copper wire	22.49	24.90
Copper wire during measurements	25.20	27.31

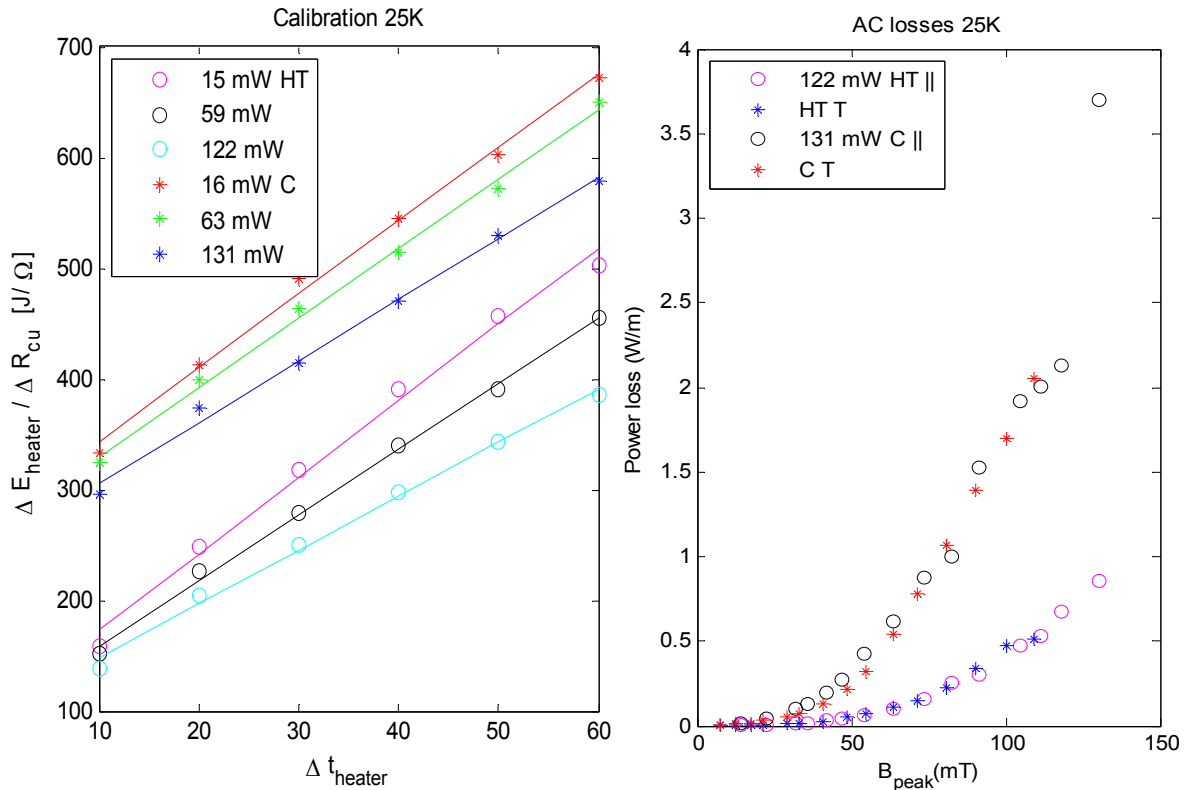


Figure 28 To the left: results from calibration measurements at 25 K. The lines are regression lines based on the calibration results. The powers listed in the legend are the heater powers in the Hyper Tech and Columbus conductors. To the right: AC losses at 25 K plotted in a diagram with normal axes.

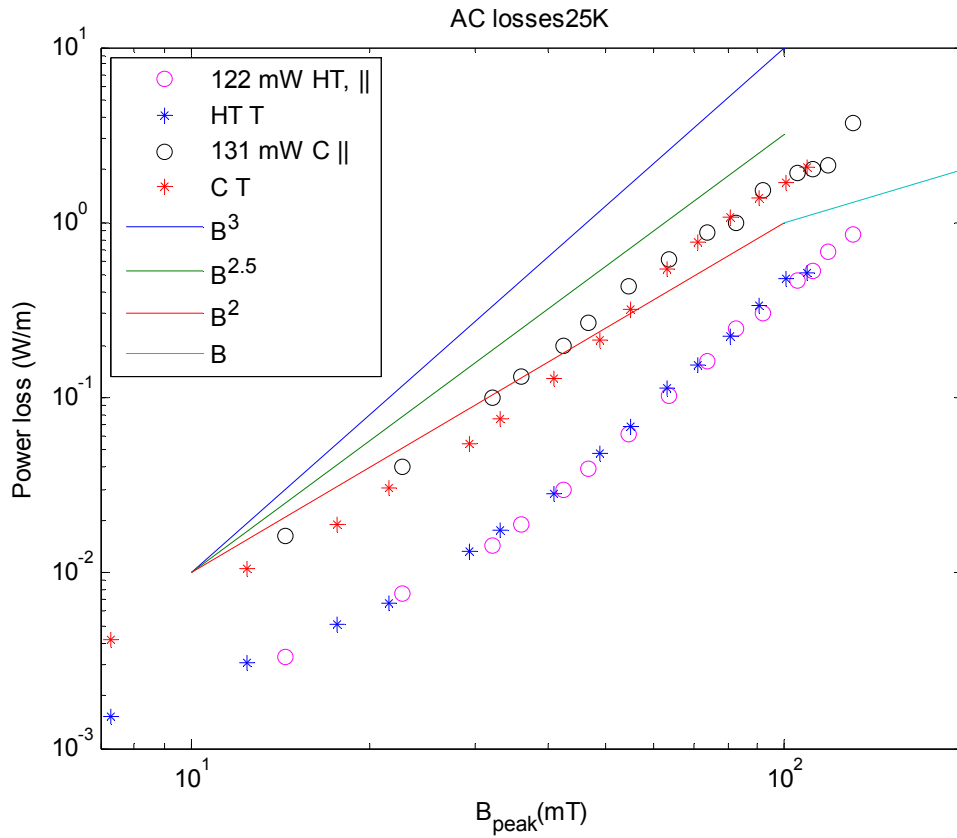


Figure 29 AC losses in both superconductors and both field configurations at 25 K. The results are plotted in a loglog diagram, and B , B^2 , $B^{2.5}$ and B^3 lines are also included.

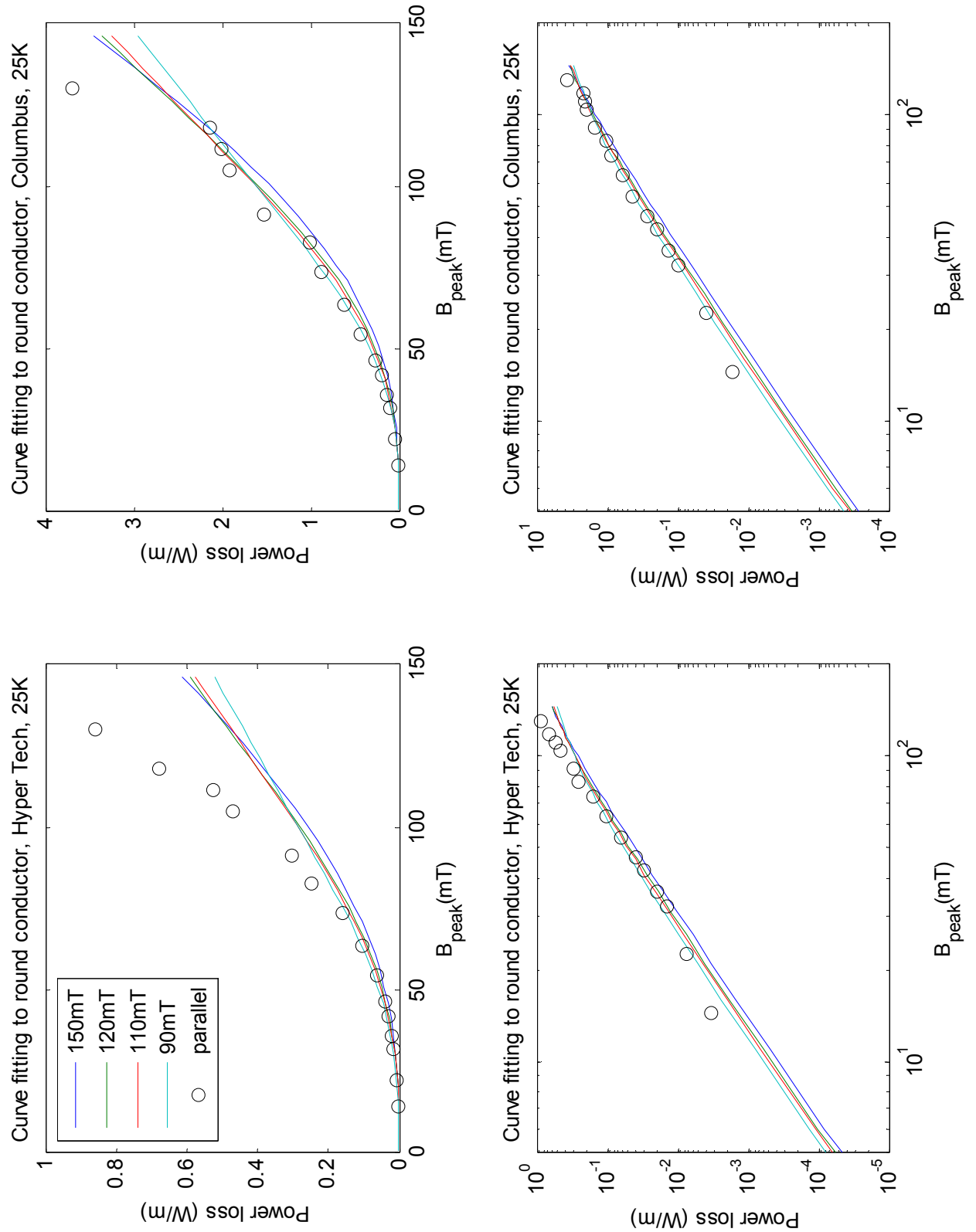


Figure 30 The AC losses in parallel field and cylindrical conductor loss equations are plotted in the same diagrams, both normal axes and loglog diagrams. In the legend are listed the penetration fields used when drawing the equations.

8.2 28.5 Kelvin

At this temperature, only parallel field was applied. Table 6 is the individual thermo element temperature readings, the average and copper wire temperature. In Table 7 are gathered the temperature rises (ΔT) in the copper wire at each magnetizing measurements. The values correspond to increasing magnitude of the applied field.

Table 6 Initial thermo element and copper wire readings

Thermo element, Columbus	Temperature [K]	Thermo element, Hyper Tech	Temperature [K]
6	32.6477	9	33.1192
30	31.2953	2	33.6943
7	33.3758	3	28.2752
18	31.2349	<i>Average</i>	<i>31.70</i>
11	30.0336	<i>Copper wire</i>	<i>31.11</i>
17	34.3691		
20	32.9060		
22	30.9933		
12	32.8054		
14	30.9195		
<i>Average</i>	<i>32.06</i>		
<i>Copper wire</i>	<i>28.46</i>		

Table 7 Copper wire temperature increase in each alternating field measurement, rising applied field magnitude order

T Columbus [K]	ΔT [K]	T Hyper Tech [K]	ΔT [K]
28.4551	0	31.1132	0
28.4729	0.0177	31.1187	0.0056
28.4943	0.0392	31.1243	0.0112
28.5177	0.0625	31.1280	0.0149
28.5695	0.1143	31.1429	0.0298
28.6325	0.1773	31.1615	0.0484
28.6838	0.2287	31.1783	0.0651
28.8752	0.4200	31.2359	0.1228
29.6387	1.1835	31.4480	0.3348
30.7001	2.2450	31.6712	0.5580
31.7603	3.3052	31.8944	0.7812
31.7603	3.3052	31.9874	0.8742
31.7603	3.3052	32.0885	0.9753
31.8290	3.3738	32.3380	1.2248
32.2154	3.7602	32.7371	1.6239
31.5887	3.1335	32.3213	1.2082
31.6230	3.1679	32.5375	1.4244
31.8290	3.3738	32.7371	1.6239
31.6230	3.1679	33.0651	1.9520
31.7603	3.3052	32.8701	1.7570
32.3381	3.8830	33.2826	2.1694
31.6917	3.2365	32.8369	1.7237
31.0738	2.6186	32.7704	1.6572

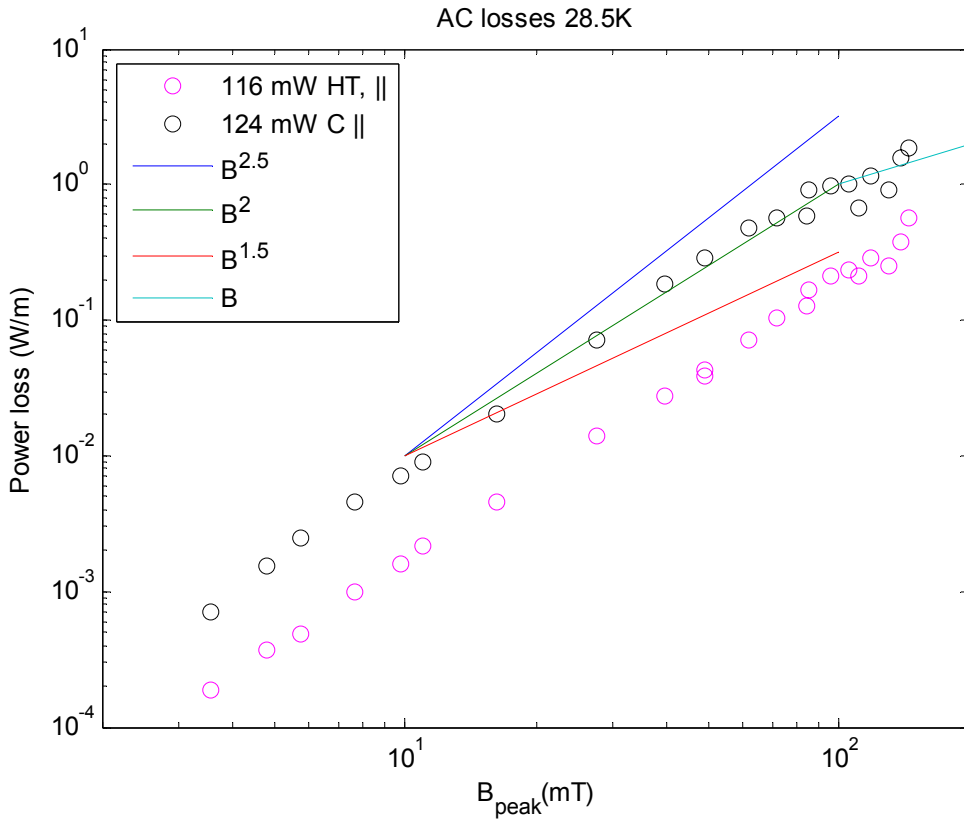


Figure 31 AC losses in both superconductors at 28.5 K. B , $B^{1.5}$, B^2 and $B^{2.5}$ lines are also included.

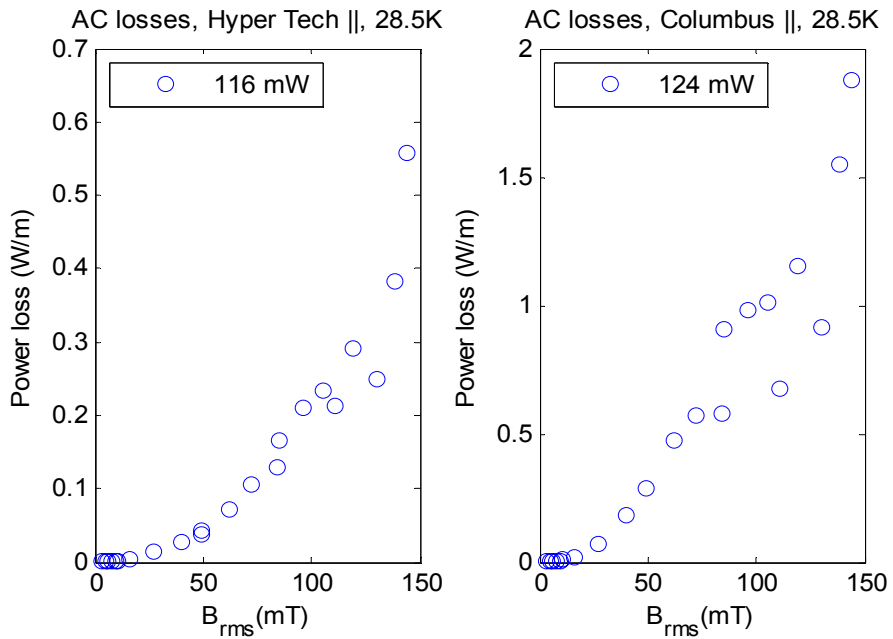


Figure 32 AC losses at 28.5 K

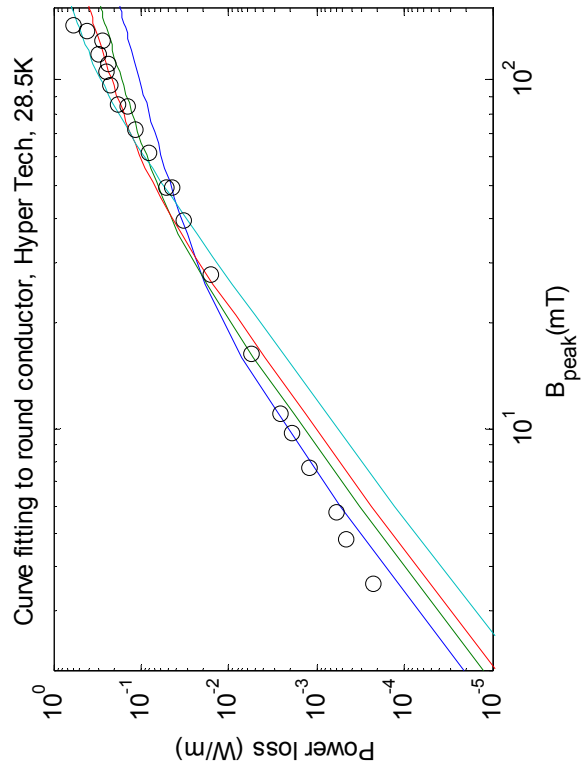
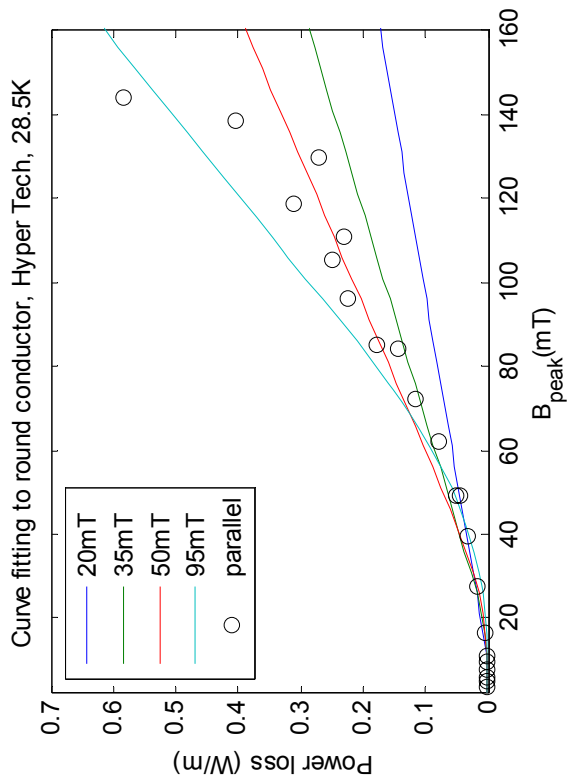
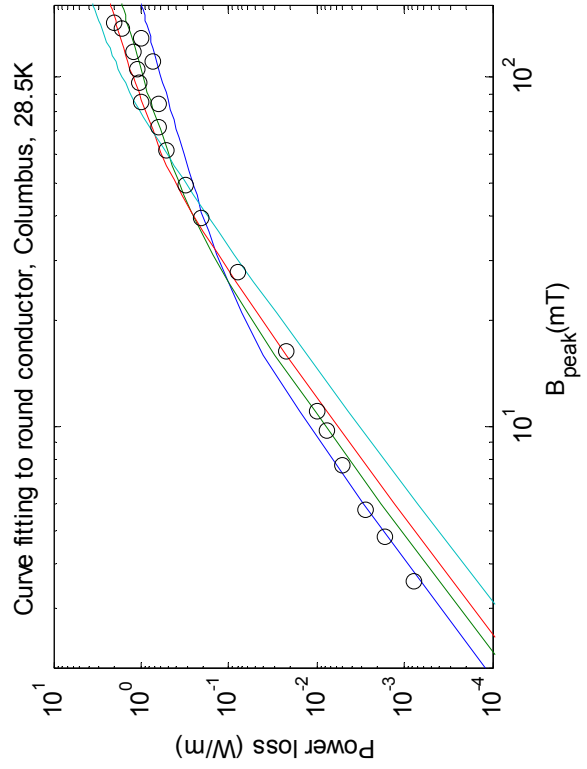
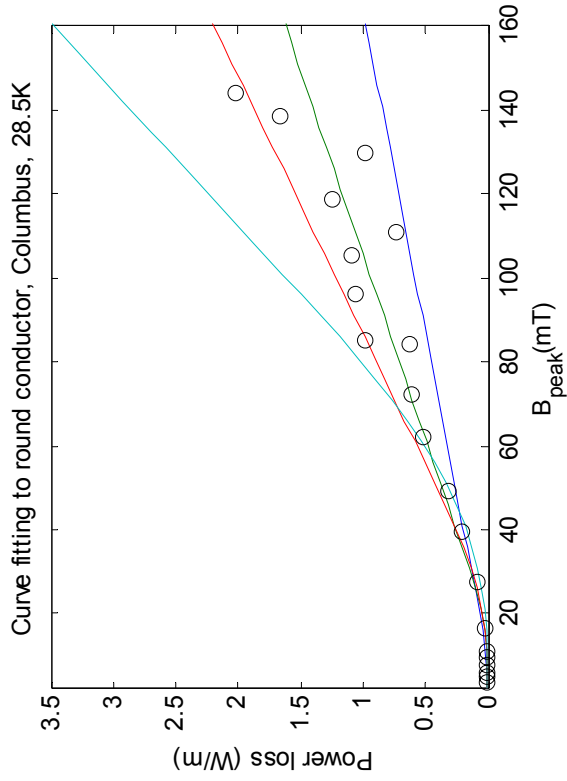


Figure 33 Measured AC losses and cylindrical conductor equations plotted in the same diagrams. In the legend are listed the penetration fields used when drawing the equations.

8.3 30 Kelvin

Both the two series at 30 K have been included in the same graphs. The first series results have been calculated from the first series calibration and the second results from the second calibration (found in Appendix 7, Figure A 12 and Figure A 13).

Table 8 Thermo element and copper wire temperatures, both series

Temperature [K]	Columbus	Hyper Tech
Average, thermo elements first series	33.00	34.13
Copper wire first series	30.68	32.54
Average, thermo elements second series	30.75	30.14
Copper wire second series	30.26	32.91

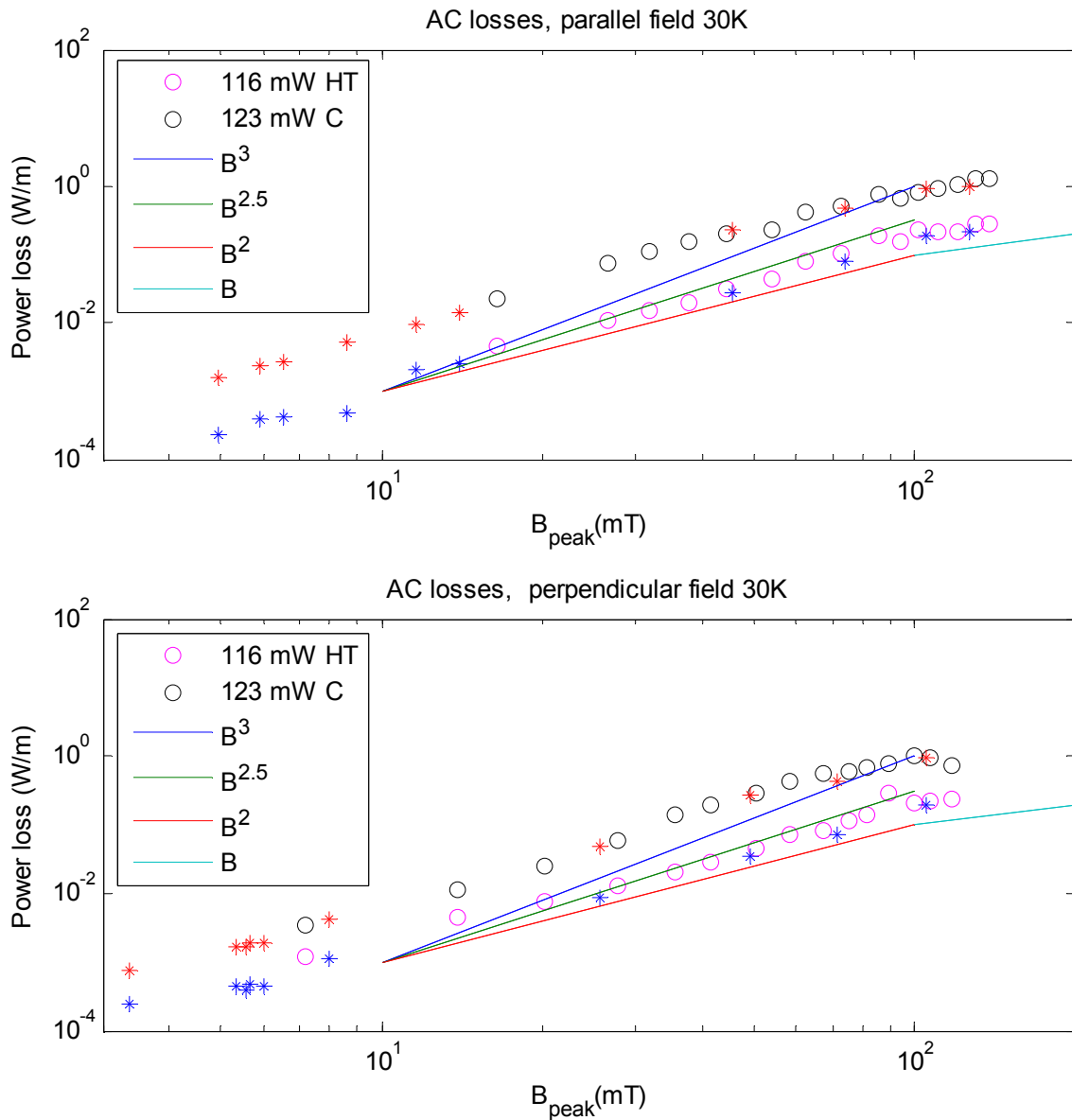


Figure 34 AC losses at 30 K. The first series are the circles, while the second series are stars, red stars are Columbus and blue Hyper Tech.

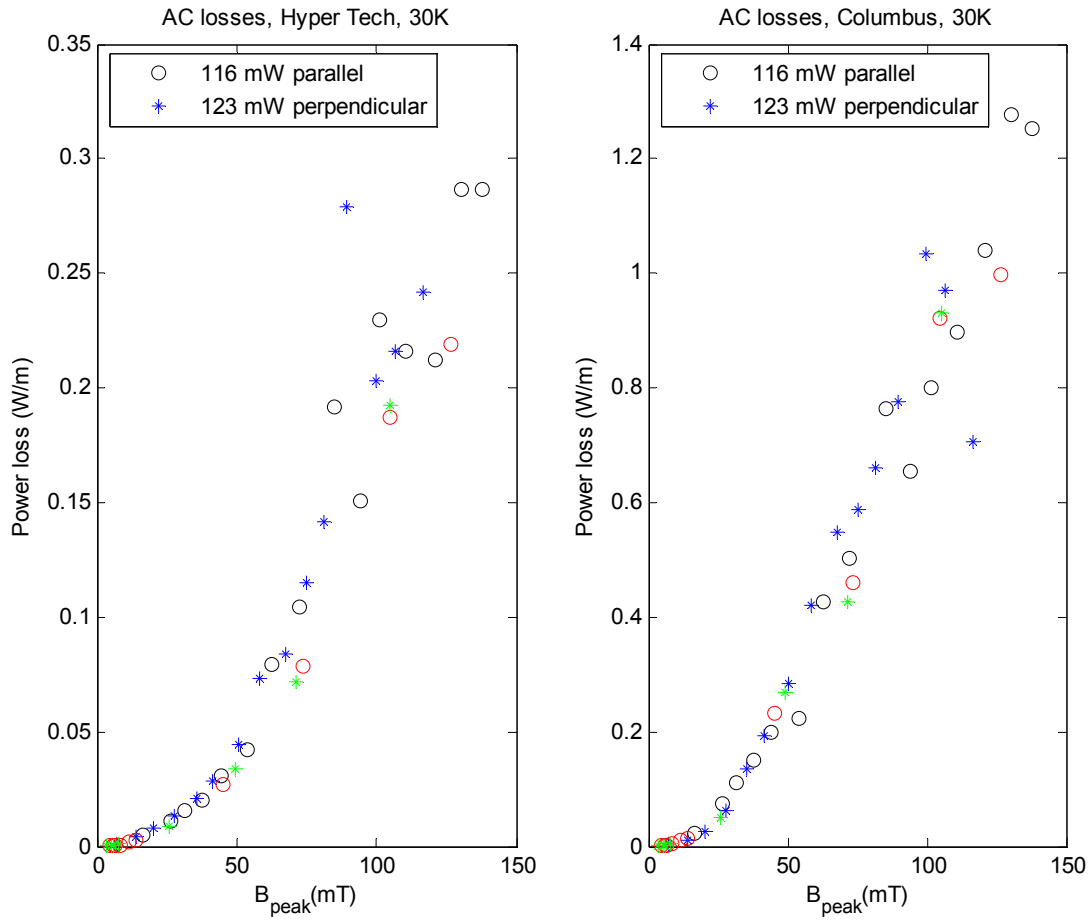


Figure 35 AC losses at 30 K. The Hyper Tech and Columbus results are split in different graphs. The black circles correspond to the first series and the green stars to the second series parallel applied field results. The blue stars correspond to the first series and the red circles the second series perpendicular applied field results.

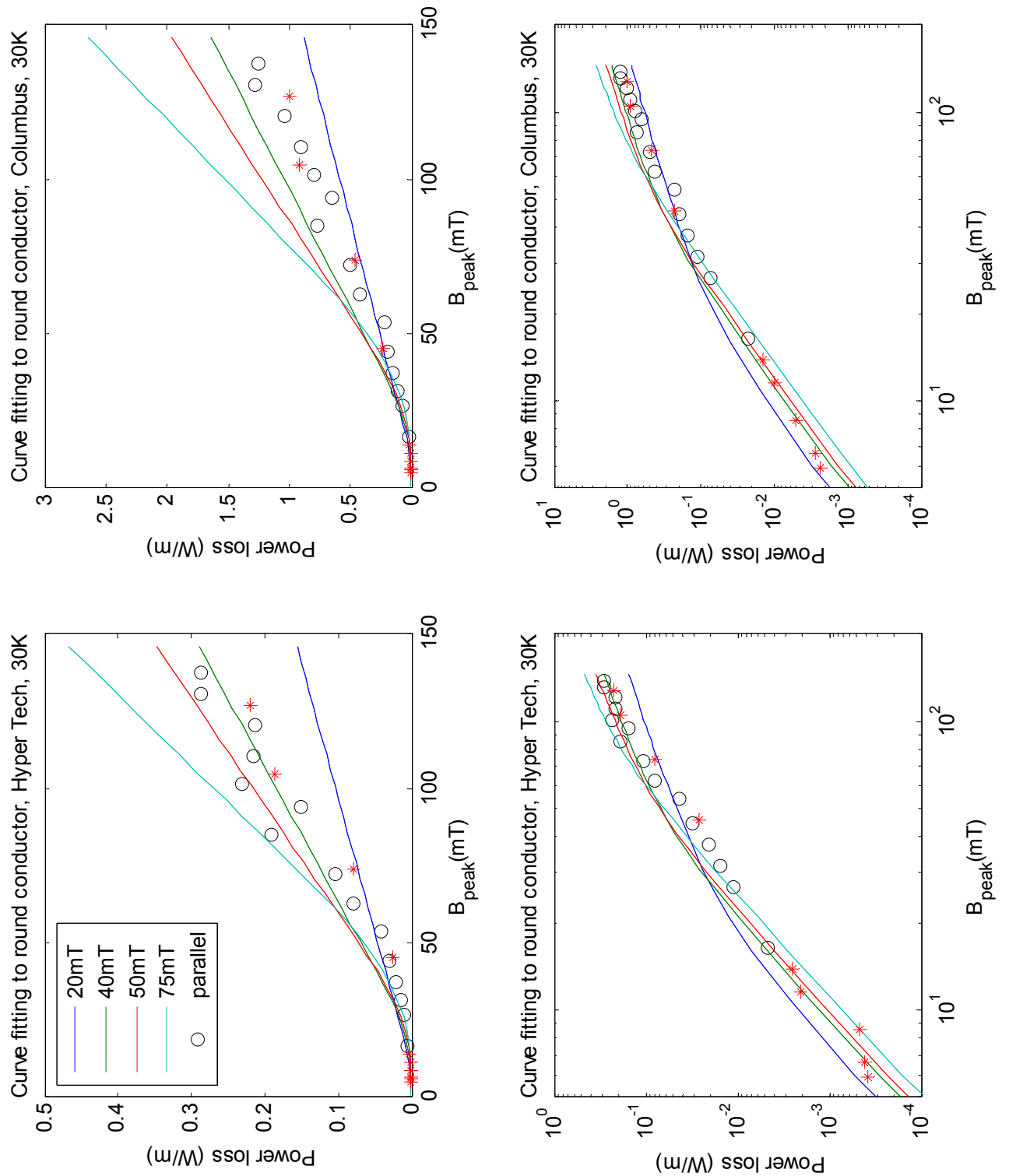


Figure 36 AC loss results and cylindrical loss equations for parallel field plotted in the same diagrams. The red stars are the second series results. In the legend are listed the penetration fields used when drawing the equations.

8.4 31.5 Kelvin

At this temperature, only parallel field was applied.

Table 9 Thermo element and copper wire temperatures

Temperature [K]	Columbus	Hyper Tech
Average, thermo elements	33.93	35.32
Copper wire	31.86	34.61

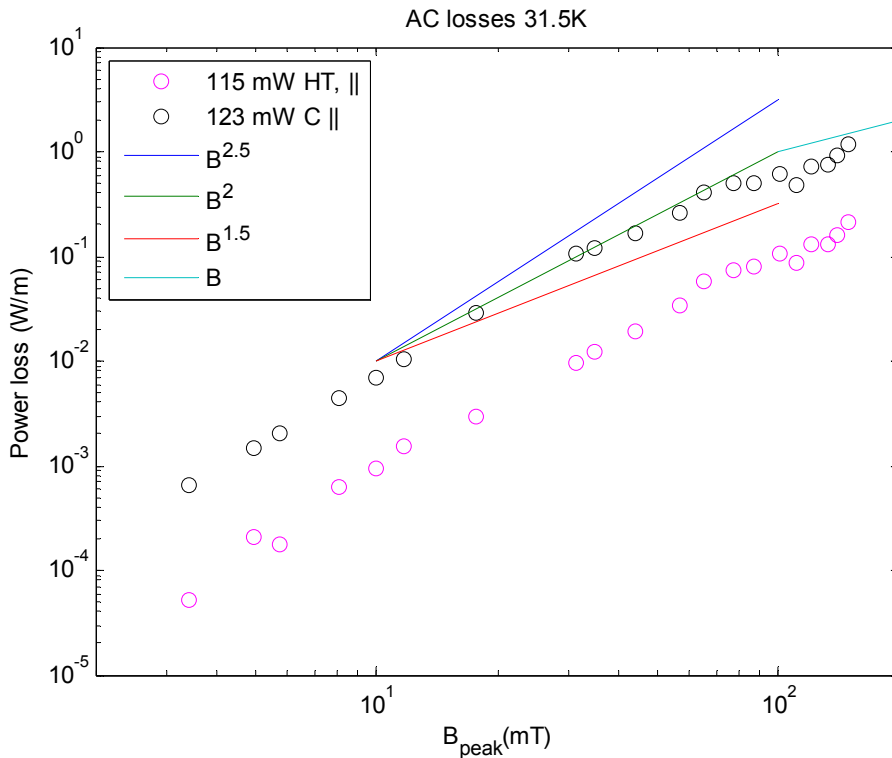


Figure 37 AC losses at 31.5 K, plotted in loglog diagram together with various loss slopes between B and $B^{2.5}$

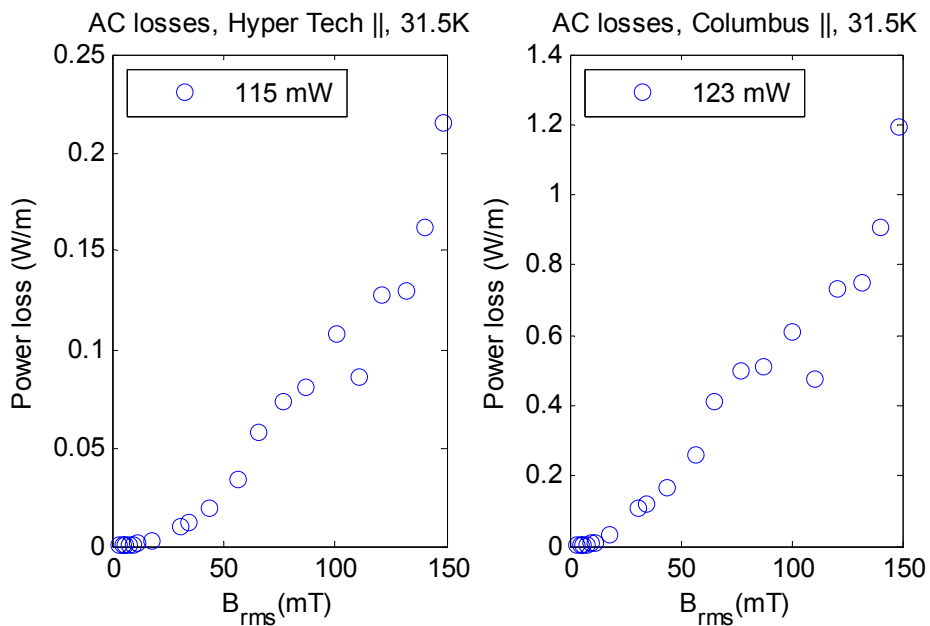


Figure 38 AC losses at 31.5 K

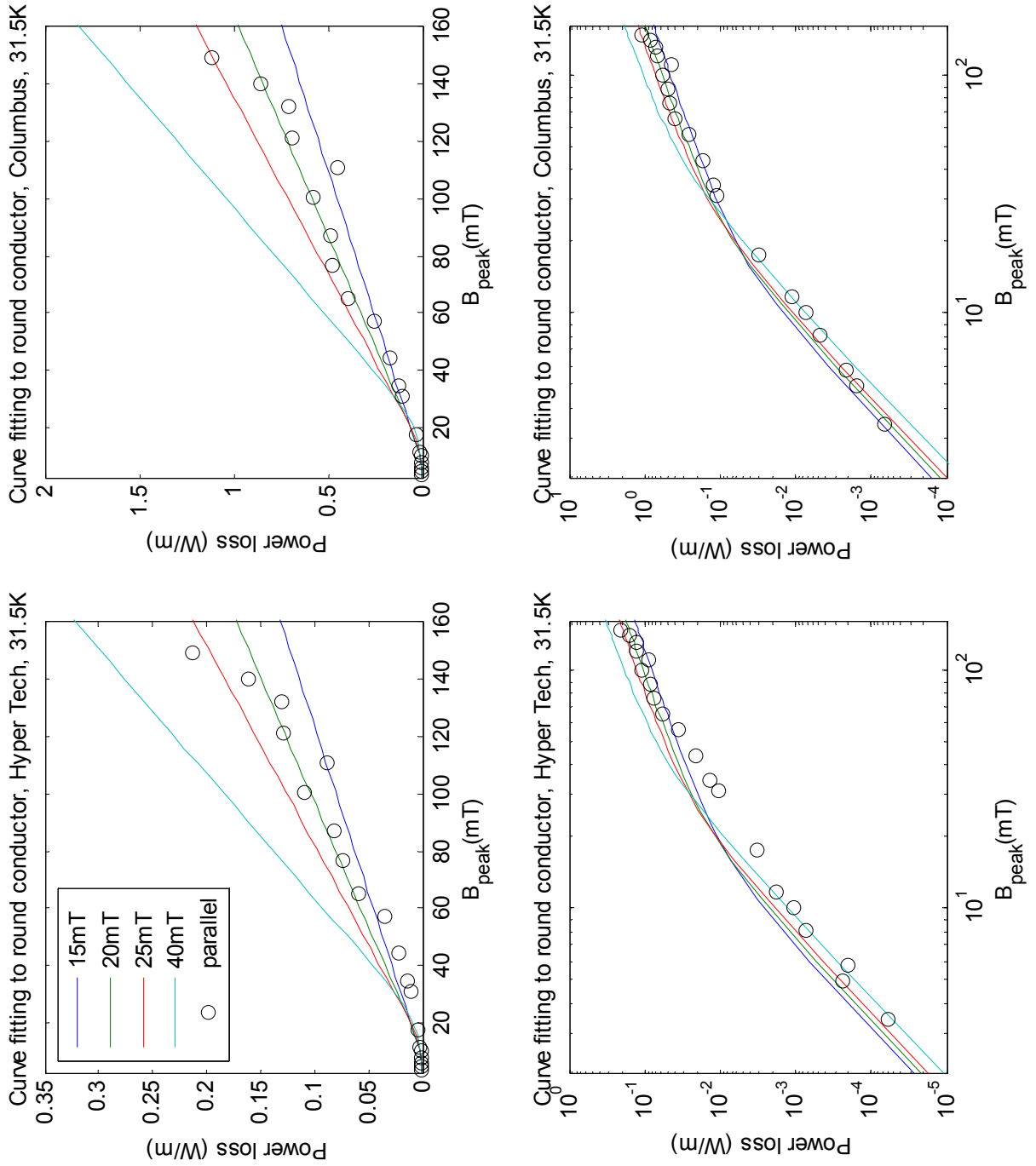


Figure 39 Measured AC losses and cylindrical conductor loss equations plotted in the same diagrams. In the legend are listed the penetration fields used when drawing the equations.

8.5 35 Kelvin

Table 10 Thermo element and copper wire temperatures

Temperature [K]	Columbus	Hyper Tech
Average, thermo elements	36.89	39.26
Copper wire	35.01	37.98

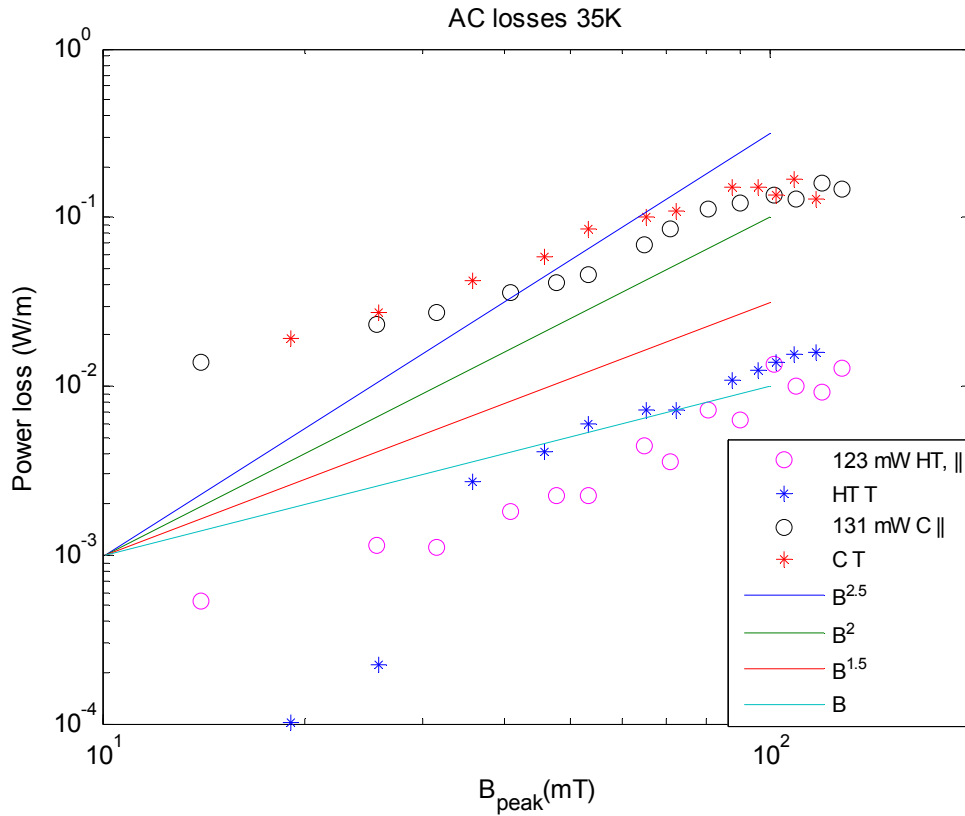


Figure 40 Measured AC losses and different loss slopes between B and B^{2.5}

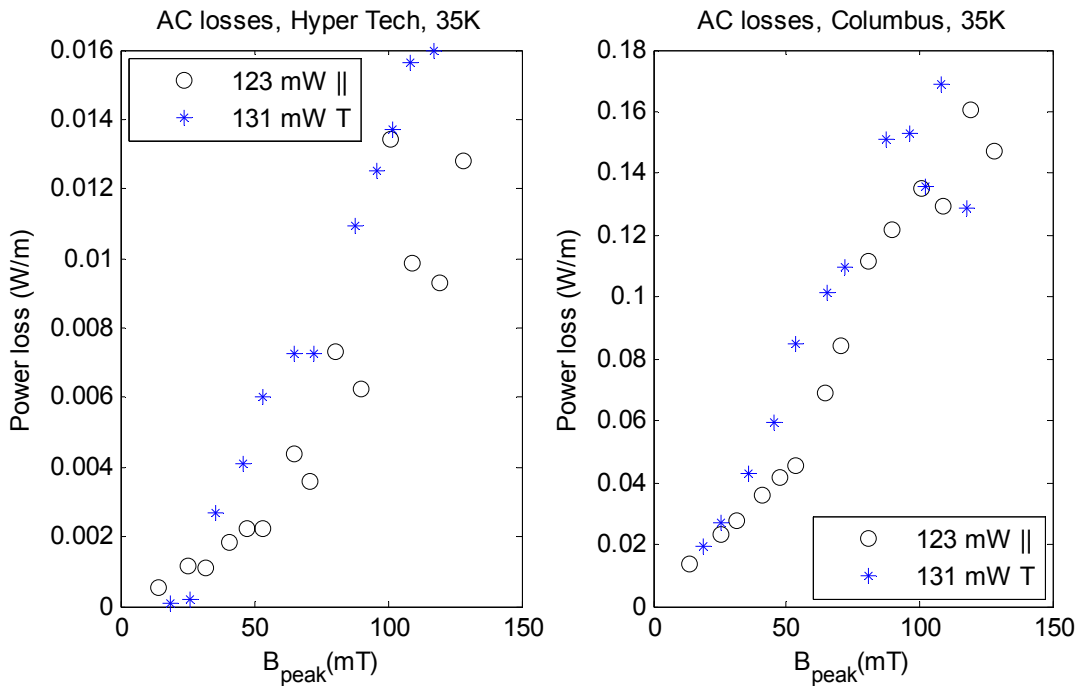


Figure 41 AC losses at 35 K

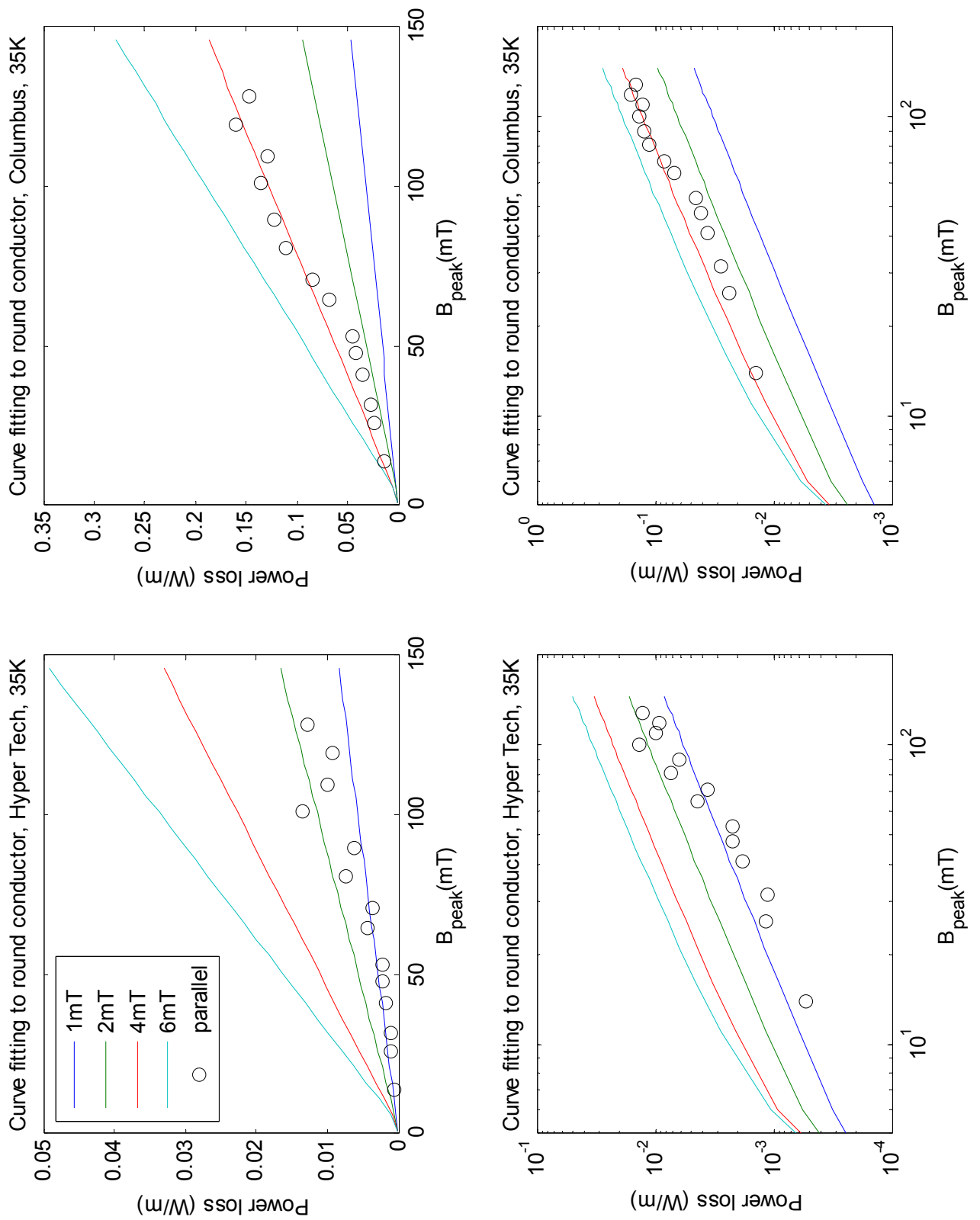


Figure 42 Measured AC losses and cylindrical conductor loss equations plotted in the same diagram. In the legend are listed the penetration fields used when drawing the equations.

8.6 45 Kelvin

As this temperature is above the critical temperature of MgB₂, only a few measuring points in parallel applied field were taken. No thermo element readings were done.

Table 11 Thermo element and copper wire temperatures

Temperature [K]	Columbus	Hyper Tech
Copper wire	45.06	47.74

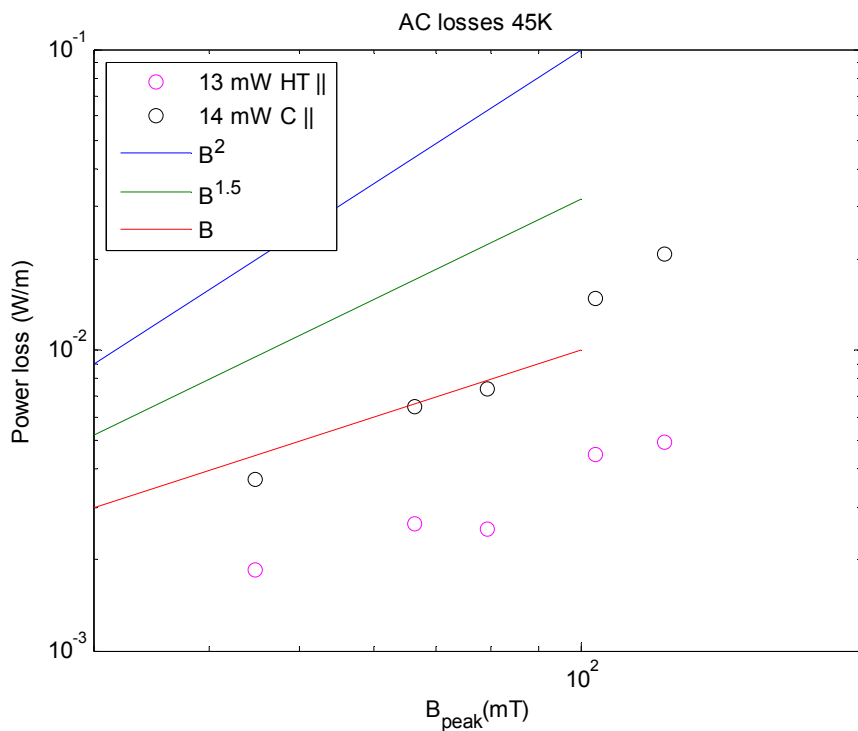


Figure 43 Measured AC losses and loss slopes

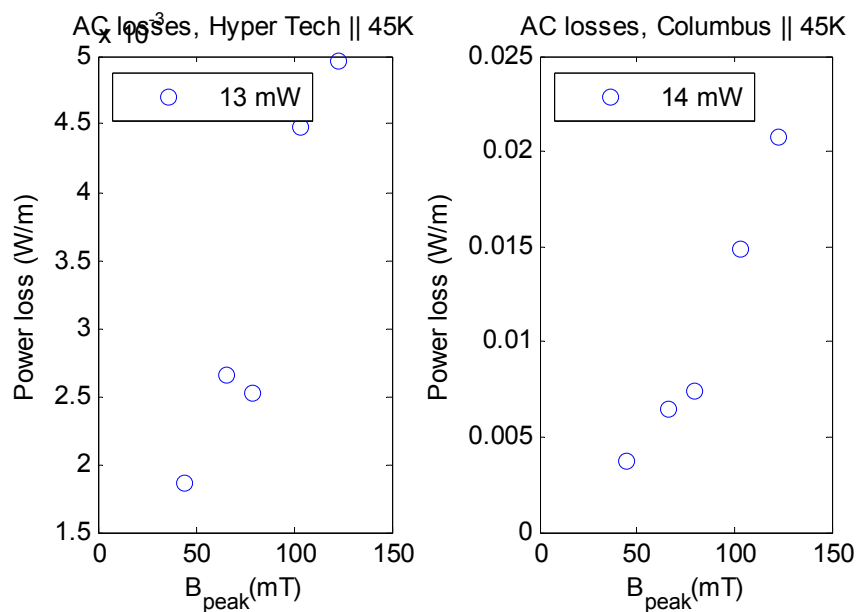


Figure 44 AC losses at 45 K

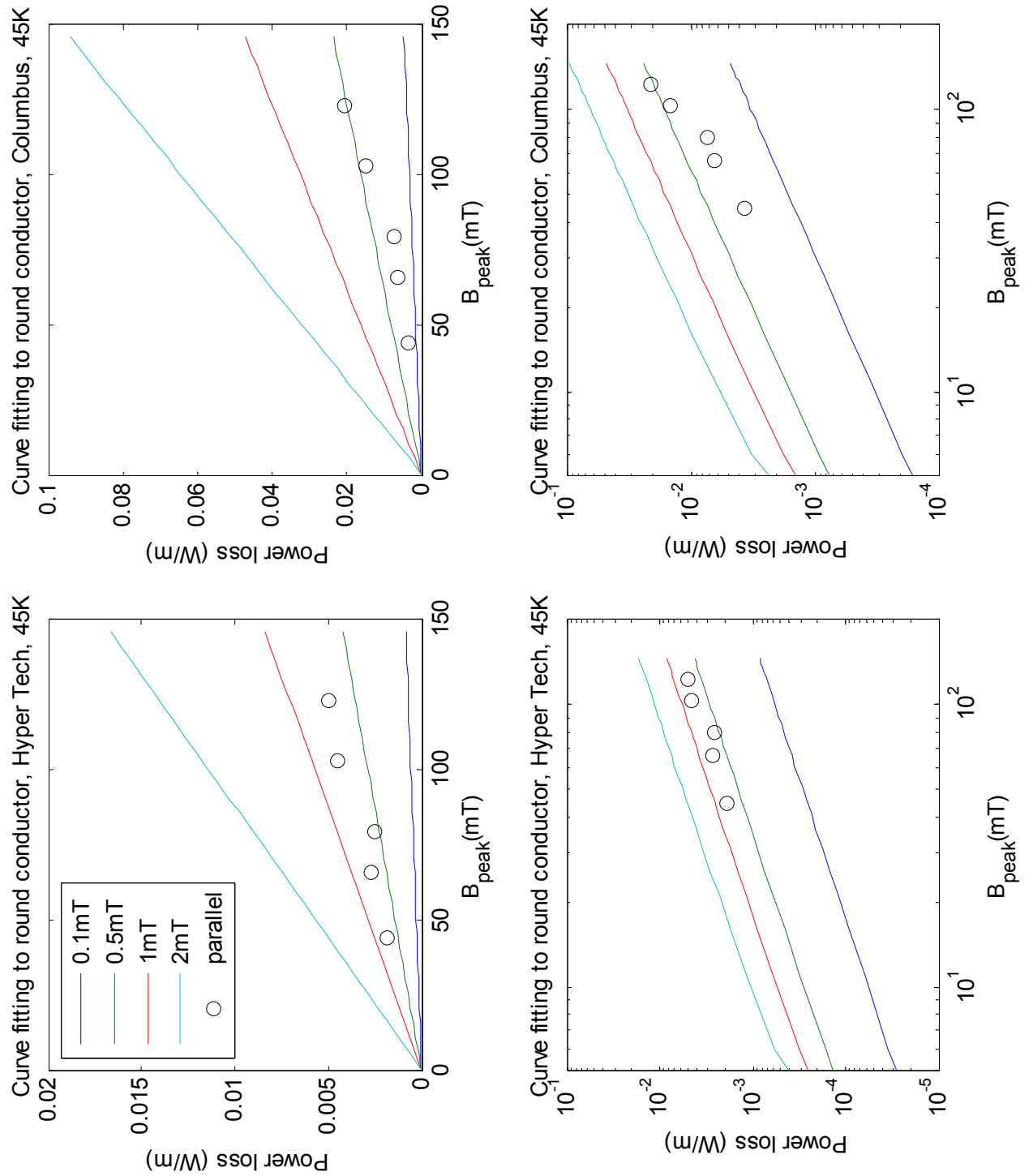


Figure 45 AC losses and cylindrical conductor equations plotted in the same diagrams. In the legend are listed the penetration fields used when drawing the equations.

9 Discussion

The first paragraph of this section discusses conductor temperatures, including possible sources of error. The second paragraph is on error sources in the calibration and AC loss measurements. Following that is a paragraph on calibration results. A discussion based on the loglog and normal axis diagrams, including loss magnitudes is the subsequent part. The chapter is concluded with discussions on curve fitting results and comparison against other MgB₂ measurements and studies on other types of superconductors. The magnetic field is in the reminder of the thesis called B

9.1 Conductor temperatures

As shown in Tables 5, 6, 8, 9, and 10 the thermo element readings indicate higher temperatures in the superconductors than the copper wire resistance increase does. The average superconductor temperature is supposed to be reflected in the copper wire temperature, while the thermo elements measure the temperature at some single points.

The individual thermo element readings are found in Table 6 and Appendix 8, and it is seen that the variations are quite large; up to 7 degrees. When comparing the mentioned tables, it is found that temperature variations among the thermo elements are similar at different temperatures; e.g. the same thermo elements measure the highest temperatures at each temperature level. The variations could be due to the proximity between conductor and holder and thus the cooling of the samples. This may vary along the sample, leading to different temperatures at different points along the conductors. Another possible reason is variations in the thermo elements proximity to the heater. If an element is fastened close to the heater, it may experience higher temperature than the other elements.

The difference between the thermo elements and copper wire is for Columbus between 3.5 and 1.9 degrees, and for Hyper Tech between 2.9 and 0.6 degrees (this is without the 25 K readings as the thermo element temperatures were logged for the wrong heater power). A possible reason for the differences is that the copper wire surface is in closer proximity of the superconductor surface. In addition, the thermo elements are placed between ‘holder fingers’, see Figure 26, and a temperature gradient is present between two such ‘fingers’. The lowest temperature is at the middle of a ‘finger’ and the highest between two ‘fingers’. It is therefore possible the thermo elements are correct when measuring a higher temperature than the average, given by the copper wire temperature.

By comparing the values for Columbus and Hyper Tech at different temperature levels, it is seen that the Hyper Tech superconductor has the higher temperature. Approximately the same power is dissipated in the heater glued to the Hyper Tech and Columbus conductors, and as the Columbus cross-section area is 5.7 times the Hyper Tech area, it seems likely the Hyper Tech conductor obtains a greater temperature rise. The smaller cross-section area also means the temperature changes far quicker in the Hyper Tech conductor.

To sum up, there exists a degree of uncertainty in the accuracy of the temperature readings based on the copper wires and thermo elements. However, the actual readings are based on numbered values and minimal uncertainty is connected to them. The conclusion is that the copper wire temperature is assumed representative for both conductors, with the possibility that thermo elements give correct point readings. The degree of uncertainty is low.

9.2 Uncertainty in calibration and AC loss measurements

The main source of error in calibration and AC loss measurements is believed to be measuring errors, made up of the reading of the voltage increase across the copper wires (ΔU) on the virtual oscilloscope and the time period the heater and applied field are on. The time is measured with a stop watch and also with an oscilloscope at short time intervals and the longer time measurements thus have a medium degree of uncertainty. The reason behind the ΔU measuring errors is for low fields a bias on the signal and for high fields peaks on top of the signal. This makes it harder to decide the correct start and end –points of the voltage increases. In Table 12 are listed general comments on which field magnitudes were harder to read at the different temperature levels, and thus have a higher degree of uncertainty connected to them.

Table 12 General comments on what applied field magnitudes gave higher degree of uncertainty in reading the graphs

Temperature [K]	Hyper Tech, parallel field	Columbus, parallel field	Hyper Tech, perpendicular field	Columbus, perpendicular field
25	Low fields	Low fields	Low fields	Low fields
28.5	Low and high fields	Low fields	-	-
30	First series: high fields, second series: low fields	First series: high fields, second series: low fields	First series: high fields, second series: low fields	First series: high fields, second series: low fields
31.5	All	Low fields	-	-
35	Low and high fields	High fields	All	All
45	All	All	All	All

The field amplitude is derived from the current flowing in the magnetizing coils. This is measured by a multimeter and minimum uncertainty is thus connected to this. The voltage increases are found from manual reading of graphs on the virtual oscilloscope, and the measuring error may be considerable due to the mentioned bias. The error magnitude is different for high and low fields as the resolution of the virtual oscilloscope varies greatly. At low voltage increases, i.e. from 2 to 30 μV , the resolution is in the 10^0 - 10^1 $\mu\text{V}/\text{division}$ range, and the assumed error range is $\pm 2 \cdot 10^{-1}$ to $\pm 2 \cdot 10^0$ μV . At high voltage increases, i.e. up to 2000 μV , the resolution is in the 10^2 - 10^3 $\mu\text{V}/\text{division}$ range, and error range: $\pm 2 \cdot 10^1$ to $\pm 2 \cdot 10^2$ μV . A reading error will influence the results differently according to what kind of diagram is used when studying the results. In loglog diagrams the magnitude of the various errors are evened out due to the logarithmic scale. However, the individual low field losses are likely to be of greater importance when it comes to finding loss slopes as they become more spread (along the x-axis) and each is taken more notice of. In normal axis diagrams high field errors have larger influence when evaluating the results.

Another source of error is the fact that the three critical parameters (T_c , J_c and B_c) influence each other. When the temperature increases during a measurement, the critical current density decreases and the losses also decrease. The impact magnitude on the obtained results is not known as the MgB_2 superconducting surface (cf. Figure 1, left) is not drawn. However, looking at Table 7 and the tables in Appendix 9, showing the temperature increases during measurements, it is seen that the temperature increase varies both with the magnitude of the

applied field and the initial temperature. The greatest temperature increase is at high fields at the initial temperature of 25 K, while the smallest are for low fields at the highest temperatures. The effect of reduced losses at increased temperatures should therefore be taken into consideration for the high field, low temperature results, and less so for the highest temperatures.

A last issue is that the AC losses in the superconductor are measured via a temperature rise. The superconductor is in thermal contact with the cold head, which reduces some of the temperature rise. This is shown by the voltage increase across the copper wire not being linear, but rather has a bow shape. The rate of change in voltage across the copper wires is greatest right after turning on the outer field, and reduced not long after. The influence from this has larger impact when the voltage rise is greatest.

Summing up the above discussion; a bias on the signal leads to a measuring error which is more prominent at the lowest and highest field magnitudes. At low temperature, high field measurements the temperature increase during measurements might reduce the losses. The cooling of the samples also leads to lower results at high fields.

9.3 Calibration measurements

By looking at the calibration graphs in Figure 28 and Appendix 7, a tendency is found in next to all regression lines; the change in energy per change in copper wire resistance ($\Delta E_{\text{heater}}/\Delta R_{\text{cu}}$) is greater for smaller heater powers. When inverting the results to study changed resistance due to changed energy input ($\Delta R_{\text{cu}}/\Delta E_{\text{heater}}$), greater heater powers give greater increase in resistance. By examining Figure A 3 in Appendix 2, it is seen that the copper wire resistivity dependence is non-linear at low temperatures. When comparing the real $R-T$ dependence to a linear one, as in the example at 25 K, (Appendix 2, Figure A 4) it is seen that the real resistivity increase is greater than the linear. If two given temperature increases are applied to the conductor, one twice the magnitude of the other, the higher gives more than twice the resistivity increase. The higher heater powers should thus give greater resistance increase.

9.4 Discussion of AC loss measuring results

In the two following tables, the low and high field loss slopes and penetration fields found from the AC loss loglog diagrams are listed. Table 13 is for Hyper Tech and Table 14 for Columbus. Both are based on Figures 29, 31, 34, 37, 40 and 44. Low field loss slopes are named B_l^n , high field loss slopes B_h^n , penetration fields B_p and ‘-’ means non-existing. Where two loss slopes are mentioned, the results lay between them. Comments on loss slopes and penetration fields that arise when studying the normal axis graphs (Figures 28, 32, 35, 38, 41 and 43) are also listed in the tables. As it is difficult to tell what loss power law is present in these diagrams, B^n in the ‘Comments on normal axis’ column is used for all power laws greater than B^1 . It may thus mean B^3 , B^2 and so on.

Table 13 Listing of loss slopes and penetration fields at different temperatures for the Hyper Tech superconductor

Temp- erature [K]	Hyper Tech parallel field				Hyper Tech perpendicular field			
	B_l^n	B_p [mT]	B_h^n	Comments on normal axis graph	B_l^n	B_p [mT]	B_h^n	Comments on normal axis graph
25	$B^3-B^{2.5}$	-	-	Shows B^n shape	$B^{2.5}$	-	-	Shows B^n shape
28.5	$B^2-B^{2.5}$	-	-	Low fields B^n shape, spread results at high fields	-	-	-	-
30	$B^2-B^{2.5}$	90	B	Low fields B^n shape, spread results at high fields, could be a shift at $B>75$ mT	B^2	100	B	Low fields B^n shape, spread results at high fields
31.5	$B^2-B^{2.5}$	80	B	Low fields B^n shape, shift to lower power present at $B>50$ mT	-	-	-	-
35	-	-	$B-B^{1.5}$	Spread results, but possibly B or low power B^n shape	?	-	$B-B^{1.5}$	Shows B shape
45	-	-	B	Shows B shape	-	-	-	-

The question mark indicates that it has not been possible to decide on a slope.

Table 14 Listing of loss slopes and penetration fields at different temperatures for the Columbus superconductor

Temp- erature [K]	Columbus parallel field				Columbus perpendicular field			
	B_l^n	B_p [mT]	B_h^n	Comments on normal axis graph	B_l^n	B_p [mT]	B_h^n	Comments on normal axis graph
25	$B^{2.5}$	100	B	Shows B^n shape, no clear shift to B	$B^{2.5}-B^3$	-	-	Shows B^n shape
28.5	$B^2-B^{2.5}$	90	B	Shows B^n shape, no clear shift to B	-	-	-	-
30	$B^2-B^{2.5}$	90	B	Low fields B^n shape, possibly a shift to lower power present at $B>75$ mT	$B^2-B^{2.5}$	90	B	Low fields B^n shape, possibly a shift present at $B>70$ mT. Spread results at high fields.
31.5	$B^2-B^{2.5}$	80	B	Low fields B^n shape, shift to lower power present at $B>50$ mT	-	-	-	-
35			B	Shows B shape	-	-	$B-B^0$	B shape at low fields, spread results at high fields
45	-	-	$B^{1.5}$	Shows B shape	-	-	-	-

Whether or not penetration fields and high field loss slopes are present in the Columbus conductor at 25 and 28.5 K is very uncertain. In addition to being difficult to decide this from the graphs, the high field, low temperature losses are possibly larger than what is measured, as the critical current density and losses decrease when the temperature increases (described in paragraph 9.2.)

Tendencies drawn from Table 13 and Table 14 are listed here, and subsequently discussed.

- The Bean model assumes B^3 below B_p and B above. In the loglog diagrams, only B above B_p and not B^3 below is found. The power laws seen at low fields are less than B^3 . Great uncertainty is connected to the various loss slopes and penetration fields as it is difficult to find uniform B^n and B_p values from the graphs.
- When determining penetration fields, the normal axis graphs indicate lower B_p than the ones found from loglog diagrams
- The loss power law is decreasing when the temperature increases. The penetration field also decreases.
- There are only small differences between parallel and perpendicular field losses for the individual superconductors.
- At 45 K, which is greater than the critical temperature, the loss slope is B .

Bean model loss slopes and uncertainty

As mentioned, the various loss graphs do not give uniform answers as to what the slopes or penetration fields are. It is also seen that the found results do not fit the Bean model loss slopes B^3 below the penetration field. A possible reason is measurement errors, including reduced loss due to increased temperature. Another is measured losses being coupling losses.

To look at the last first; the power law between coupling current losses and applied field is B^2 , see equation (9). Several of the low field loss powers found in these studies are B^2 - $B^{2.5}$, showing that it is also not a perfect match to the coupling current losses. As mentioned in Chapter 3, it is when the frequency is high that coupling losses may be neglected. The applied field frequency in the experiments done here was 50 Hz and is possibly too low to measure AC losses at low fields. Measurements at higher frequencies would have to be performed in order to determine if the losses are coupling losses.

If, on the other hand, measuring errors are the reason for not getting Bean model loss slopes, the measuring error must be too high results at low fields and too low at medium to high fields. As next to all graphs differ from the model, the error must be systematic. An example is the graph showing the closest proximity to the Bean model: the Columbus conductor in parallel field at 25 K, Figure 29. Here, it is seen that if removing the highest and lowest field results (as these were harder to read) a better fit to the Bean model equations are found. Contradicting the removal of low field results due to possible measuring errors are the two measuring series at 30 K, where the second series is focused at low fields. When looking at Figure 34, the two series are well correlated and have approximately the same slopes.

Summing up this point; due to a measuring error having to be systematic it does not seem likely this is the reason for the poor fitting to the Bean model equations. As the measurements were only done at one frequency it is not possible to draw any conclusions as to whether or not the measured losses are coupling losses.

Loglog versus normal axis results

When comparing the normal axis graphs to the loglog graphs, several of the same tendencies are found, except the penetration field may seem to be somewhat lower when studying normal axis graphs, and high field loss slopes are in some cases undefined. It is uncertain why the penetration fields are lower, but could be due to the difficulty in finding uniform power law dependencies in both types of diagrams. A reason for undefined loss slopes is measuring errors being more prominent at high fields in normal axis graphs and high field results are in several cases too spread to find a uniform loss slope.

Decreasing B_p and loss slope power with increasing temperature

Both superconductors' losses when in a parallel field have decreasing penetration fields when increasing the temperature. As described before, increasing temperature means decreased critical current density. Equation (3) shows that the penetration field is proportional to the critical current density, and as this falls, the penetration field does as well. A question that may arise when seeing that the loss slopes decrease with increasing temperature and are not equal to the Bean model, is if the measurements are done in the transition area between B^3 and B . The probable answer is that the field range this concerns is too large for this to be likely. The reason for the falling loss slopes is thus unknown.

Parallel and perpendicular applied fields

The behaviour of the Hyper Tech sample in parallel field is similar to its behaviour in perpendicular field, except from at 35 K. The same applies for the Columbus sample. As the Hyper Tech superconductor is cylindrical and the Columbus is almost square, the two field directions were expected to give comparable results between themselves. At 35 K the Hyper Tech conductor shows a deviance between parallel and perpendicular fields. Looking at Table A 8, Appendix 8, showing the initial temperatures measured, and Table A 13, Appendix 9, showing the temperature increase during AC measurements, it is found that two of the thermo elements measured temperatures above T_c . The spread results may therefore be due to some measurements being above the critical temperature. In addition, the voltage increase graphs were difficult to read and there is a high degree of uncertainty connected to these series.

Losses at the temperature greater than T_c

A surprising result for the conductor temperature above the critical temperature is that the losses were proportional to the applied field. They were expected to be constant as normal conductivity gives resistive losses, independent of applied field. The voltage increases across the copper wires at 45 K were very low, and the measuring errors may therefore be great.

9.4.1 Loss magnitudes

In Table 15 are listed approximate loss magnitudes for the two conductors and field directions for applied field equal to 10 and 100 mT. The table shows that the loss magnitudes for the Columbus superconductor, independent of field direction, are in the 8 – 10 mW/m range for field strength 10 mT and 700 – 2000 mW/m for 100 mT. The Hyper Tech loss magnitudes are 0.3 – 2 mW/m for 10 mT and 10 – 500 mW/m for 100 mT. The filament sizes in the two superconductors are unknown, but as they both have seven, it is supposed the Hyper Tech superconductor has thinner filaments, as thinner filaments give lower losses (as mentioned in Chapter 2.3)

Table 15 Loss magnitudes found from loglog diagrams

Temp-erature [K]	Columbus, parallel field [W/m]		Columbus, perpendicular field [W/m]		Hyper tech, parallel field [W/m]		Hyper Tech, perpendicular field [W/m]	
	10 mT	100 mT	10 mT	100 mT	10 mT	100 mT	10 mT	100 mT
25	$8 \cdot 10^{-3}$	$2 \cdot 10^0$	$8 \cdot 10^{-3}$	$2 \cdot 10^0$	$2 \cdot 10^{-3}$	$5 \cdot 10^{-1}$	$2 \cdot 10^{-3}$	$5 \cdot 10^{-1}$
28.5	$8 \cdot 10^{-3}$	$1 \cdot 10^0$			$2 \cdot 10^{-3}$	$2 \cdot 10^{-1}$		
30	$\sim 8 \cdot 10^{-3}$	$1 \cdot 10^0$	$\sim 7 \cdot 10^{-3}$	$1 \cdot 10^0$	$\sim 1 \cdot 10^{-3}$	$\sim 2 \cdot 10^{-1}$	$\sim 3 \cdot 10^{-3}$	$\sim 2 \cdot 10^{-1}$
31.5	$9 \cdot 10^{-3}$	$7 \cdot 10^{-1}$			$1 \cdot 10^{-3}$	$1 \cdot 10^{-1}$		
35	$1 \cdot 10^{-2}$	$2 \cdot 10^0$	$1 \cdot 10^{-2}$	$2 \cdot 10^0$	$\sim 3 \cdot 10^{-4}$	$\sim 1 \cdot 10^{-2}$?	$\sim 1 \cdot 10^{-2}$
45	?	$\sim 1 \cdot 10^{-2}$?	$\sim 3 \cdot 10^{-2}$		

9.5 Penetration fields found from curve fitting

When the curve fittings to cylindrical and tape shaped loss equations (6) and (7) were compared, it was found that the cylindrical equations gave the best fit to the measured results. Curve fitting to tape shaped conductor equations are only given as an example for the results at 30 K, see Appendix 10. Even if the Hyper Tech conductor is cylindrical, the measured results show deviance from cylindrical conductor equations. As the Columbus conductor is close to square, the cylindrical conductor equations were expected to fit rather well. These results also show deviance from the equations.

Each curve in the curve fitting diagrams is given by the penetration field. The penetration fields that gave the best fit to low and high field results are summarised in Table 16. These are based on Figures 30, 33, 36, 39, 42 and 45. Short comments on which results that did not fit the chosen curves are included in the table with italic style. Penetration fields at low field are found from the curve fitting loglog diagrams, while the penetration fields at high fields were found from curve fitting normal axis diagrams. Question mark means no curves fit the results. The C values used are all equal to 1 (C being the 'efficient area' factor). Curve fitting with different C values have been performed, but are not shown. At 25 K, decreasing C led to less fitted results. For the rest of the temperatures, the difference between fitting at low and high fields were too great for C to make much difference.

Table 16 Comparison of penetration fields at different temperatures from the curve fitting diagrams

Temperature [K]	Hyper Tech		Columbus	
	B_p low fields [mT]	B_p high fields [mT]	B_p low fields [mT]	B_p high fields [mT]
25	110-120 <i>except for the two lowest results</i>	? <i>out of bounds</i>	90-110 <i>except for the lowest results</i>	? <i>partly out of bounds</i>
28.5	Around 20 <i>except for the two lowest results</i>	Around 50 <i>except for the highest results</i>	20-35 <i>the middle results do not fit</i>	Around 35 <i>except for the highest results</i>
30	40-50 <i>the middle results do not fit</i>	40-50	40-50 <i>the middle results do not fit</i>	20-40
31.5	Around 40 <i>middle results do not fit</i>	Around 20	<i>Varies, but the lowest results are around 20-25</i>	Around 20
35	1-2	1-2	4	4
45	0.5-1	0.5-1	0.1-0.5	0.1-0.5

When summarising the table, the only rather well fitted results are Hyper Tech at 30, 35 and 45 K and Columbus at 35 and 45 K. Except for the Hyper Tech at 30 K, the others are above the penetration field. As found in Table 13 and Table 14, the measured results do not follow the B^3 to B slope dependence given by both the Bean model and the cylindrical conductor equations. This seems to be the most likely reason for the mainly poor fitting. An alternative explanation is the possibility of having two penetration fields present in the same diagram. Again the temperature increase during a measurement is brought out, where J_c and B_p decreases. If this is considerable, there could be different penetration fields for low and high applied fields, where high fields should give lower B_p , which is the case in some of the fittings. The question is what magnitude the temperature rise must reach in order for B_p to change considerably. To find this, the superconducting surface must be drawn (cf. Figure 1, superconducting surface for NbTi).

If comparing Table 16 to Table 13 and Table 15, it is seen that both low and high field penetration fields are mainly higher when studying the loglog diagrams. As the fittings to the cylindrical conductor equations are not better, it gives reason to trust the loglog diagrams penetration fields. However, since both AC loss normal axis diagrams and curve fitting indicates lower penetration fields than what is found there, the penetration fields may be somewhat lower than the ones found in loglog diagrams.

9.6 Comparison to other studies on MgB2

When comparing the results from this study with other studies on AC losses in magnesium diboride, the power law and magnitude of losses is the main focus. The articles mentioned in Chapter 5.1 are the ones used for comparison. Lou et al. [24] have found loss slopes that do not fit the Bean equations, see Figure 10. Their results go from B^2 via $B^{1.8}$ to $B^{1.2}$, and as mentioned earlier, they do not have an explanation to these unexpected results. The measurements were done at 500 Hz and should rule out coupling current losses. As the losses are measured in Joule, their magnitude cannot be compared to the results achieved here. The geometry best suited to compare to the results found in the Yang et al. article, [21] is the bar (the right hand graph in Figure 11). These loss slopes go from H^3 to H^0 when placed in an alternating field. They thus follow the Bean model at low fields, but not at high fields. The losses are measured in Joule/meter and may not be compared to the loss magnitudes achieved here. The last study for comparison is Ginuchi et al. [23] The results show that one grain size does follow the Bean model. The results are presented as Joule/meter³ and may also not be compared to the results in this report. From the mentioned studies it is seen that the loss slopes vary, and no explanations have been suggested for the ones deviating from the Bean model.

9.7 Comparison to studies on other superconductors

As in the previous section, when using results from articles and doctoral thesis for comparison to the measured results, the power law and magnitude of losses is the main focus. Some of the studies mentioned in Chapter 6 had results fitting the Bean model loss slopes: Magnusson [2], Rabbers [13] and Inada et al. [25]. Other articles mentioned in the same paragraph did not or did not quite fit the Bean equation loss slopes: Rabbers found one too steep slope [13] and Su et al. [27] have also found non-fitting results. Fang et al. [28] found non-fitting results at frequency 30 Hz and fitting results at 270 Hz and claimed the non-fitting losses were coupling losses. Witz et al. [29] have come to the same conclusion as their results do not fit the Bean model. Three of these articles: Su et al., Fang et al. and Witz et al. have all performed measurements on various geometries and found that in perpendicular field the round or square geometries give lower losses than tape shaped superconductors.

There are only two studies using the same denomination as in this report. Magnusson has found a loss magnitude of about 0.1 W/m at an applied field of 100 mT in BSCCO tape, and Witz et al. have found a loss magnitude of about 1-2 mW/m at 10 mT in square BSCCO conductors. In section 9.4.1 is found loss magnitudes for Columbus superconductor; 8 – 10 mW/m at 10 mT and 700 – 2000 mW/m at 100 mT. The Hyper Tech loss magnitudes are 0.3 – 2 mW/m at 10 mT and 10 – 500 mW/m at 100 mT. It is thus only the Hyper Tech loss magnitudes that can compete with the loss magnitudes in both the two mentioned BSCCO superconductors.

10 Conclusion

Alternating magnetic field loss measurements have been performed on two superconductor samples of magnesium diboride. A calorimetric setup has been used and the losses were found from the change in resistance of a copper wire glued onto the conductor. The resistivity changed due to the changed temperature, which originates in the AC losses in the superconductor. The sample temperature was varied between 25 and 45 K and the field amplitude between 3 and 150 mT. Both parallel and perpendicular field was applied. The most important conclusions drawn from the results are:

- The temperatures in the superconductors were measured by two methods: thermo elements and resistance increase in a thin copper wire in close proximity to the superconductors. The conclusion is that the superconductor temperatures equal the copper wire temperatures, with the possibility that thermo elements are correct when measuring higher point temperatures.
- The main source of error in calibration and AC loss measurements is measuring errors following from reading off graphs giving the voltage increase across the copper wires. The error magnitude varies with the resolution of the virtual oscilloscope. The greatest uncertainty is mainly at the lowest and highest field magnitudes as their voltage increases start and end points were harder to establish.
- The AC losses did not follow the theoretical Bean model. The power laws at fields below the penetration field were less than B^3 . Two possible reasons have been discussed for the deviations; measuring errors and the losses being coupling losses. The conclusion is that none of these seem likely; the measuring error would have to be systematic as the obtained results at all temperature levels indicate a too low loss slope. At the same time the loss slope is steeper than for coupling losses.
- Penetration fields were found from curve fitting, loglog and normal axis diagrams. Loglog diagrams gave higher penetration fields than the two other. Due to poor fitting and difficulty in determining B_p from normal axis graphs leads to choosing the loglog diagram B_p , or possibly somewhat lower as both the other diagrams indicate this.
- Tendencies that agrees with theory and expected results:
 - As the temperature is increased, the penetration field decreases. This is due to the penetration field being proportional to the critical current density, which falls with rising temperature.
 - Parallel and perpendicular fields applied to the individual conductors give similar results. Due to the cylindrical and square geometry of the samples, this was as expected.
- The two samples had different loss magnitudes, where it was assumed the lower losses were due to thinner superconductor filaments.
- Studies on MgB_2 done by others have obtained various results; some have not followed the Bean model slopes, others have. The same holds for studies on BSCCO superconductors. When comparing loss magnitudes, the Hyper Tech conductor used here is the only showing the same loss magnitudes as two studies on BSCCO.

11 Future work

In order to find if the measured losses were coupling losses, high frequency measurements should be performed. It is also possible to examine this by measuring on similar conductors with twisted filaments.

The critical current density should also be measured. Drawing the superconducting surface for MgB_2 would establish the magnitude of the impact high temperature increases has on the losses.

In Appendix 11 is given a description on a method on soldering of BSCCO tapes. The method was not used here, but established as a part of preparations for measuring critical current.

References

- [1] Image window at superconductors.org. [online] Available from <http://superconductors.org/INdex.htm>, accessed 12 May 2007
- [2] N. Magnusson, AC Losses in High-temperature Superconducting Tapes: Calorimetric Measurement System and Semi-empirical Modelling. (Doctoral dissertation, Kungl Tekniska Högskolan, Stockholm, 2000)
- [3] M. Runde, K. Gamlesæter, J.O. Skarpmes, E. Styrken, *Superledende materialer i elkraftteknikken*. (Teknisk rapport nr TR 3521, 1988, EFI AS)
- [4] M. Chen, L. Donzel, M. Lakner, W. Paul, High temperature superconductors for power applications, *Journal of the European Ceramic Society*, Vol. 24, 2004, pp 1815-1822
- [5] R.M Scanlan, A.P. Malozemoff, D.C. Larbalestier, Superconducting Materials for Large Scale Applications, *Proceedings of the IEEE*, Vol. 92, no 10, 2004
- [6] M. Runde, Superledning og elkraftteknikk, Fag 41115 Elektrotekniske materialer, extract from textbook received from the author 9 Jan 2007
- [7] M.N. Wilson, *Superconducting Magnets*, Oxford Science Publications, 1983
- [8] T. Orlando, K. Delin, *Foundations of Applied Superconductivity*, Massachusetts, 1991, pp 368 - 383
- [9] C.P. Bean, Magnetization of High-Field Superconductors, *Review of modern physics*, Jan 1964
- [10] N. Magnusson, S. Hörnfeldt, Losses in HTS Carrying AC transport currents in AC external magnetic fields, *IEEE Transactions on applied superconductivity*, Vol. 9, June 1999, pp 785-788
- [11] M. Ciszek, A.M. Campbell, S.P Ashworth and B.A Glowacki, Energy dissipation in high temperature ceramic superconductors, *Applied Superconductivity*, Vol. 3, No 7-10, 1995, pp. 509-520
- [12] D. Zola, F. Gömöry, M. Polichetti, F. Strycek, J. Souc, P. Kovac, S. Pace, Analysis of Coupling Losses in Multifilamentary Untwisted BSCCO/Ag Tapes Trough a.c. Susceptibility Measurements, *IEEE transactions on applied superconductivity*, Vol.15, no 2, 2005
- [13] AC loss in superconducting tapes and coils , J.J. Rabbers, (Proefschrift Universitet Twente, Enschede (thesis) 2001)
- [14] A.M Campbell, A general treatment of losses in mulifilamentary superconductors, *Cryogenics*, Vol. 22, Jan 1982, pp 3-16
- [15] E.H. Hansen, *Elektroinstallasjoner*, Classica forlag AS 2003 p 67-68

- [16] J. Nagamatsu, N. Nakagawa, T. Muranaka, Y. Zenitani, J. Akimitsu, Superconductivity at 39 K in magnesium diboride, *Nature*, Vol. 410, march 2001
- [17] G. Grasso, An Overview of Fundamental and Applied Aspects of Magnesium Diboride Superconductors, *IUMRS Facets* Vol. 5, no 3, July 2006
- [18] H.J Choi, D. Roundy, H. Sun, M.L. Cohen, S.G. Louie, The origin of the anomalous superconducting properties of MgB₂, *Nature*, Vol. 418, 15 Aug 2002
- [19] R. Flükiger, H.L. Suo, N. Musolino, C. Beneduce, P. Toulemonde, P. Lezza, Superconducting properties of MgB₂ tapes and wires, *Physica C* Vol. 385, 2003, pp 286-305
- [20] J.M. Rowell, The widely variable resistivity of MgB₂ samples, *Supercond. Sci. Technol*, Vol. 16, 2003, pp. R17-R27
- [21] Y. Yang, E.A. Young, M. Bianchetti, C. Beduz, E. Martinez, G. Giunchi Measurement of AC losses in MgB₂ wire and bulk conductors at different temperatures, *IEEE transactions on applied superconductivity* Vol. 15, no 2, 2005
- [22] Y. Iwasa, D.C. Larbalestier, M. Okada, R. Penco, M.D. Sumption, X. Xi A Round Table Discussion on MgB₂ Toward a Wide Market or a Niche Production? – A Summary, *IEEE transactions on applied superconductivity* Vol. 16, no 2, 2006
- [23] G. Giunchi, S. Ginocchio, S. Raineri, D. Botta, R. Gerbaldo, B. Minetti, R. Quarantiello, A. Matrone, High density MgB₂ bulk materials of different grains size: supercurrents instability and losses in variable magnetic fields, *IEEE transactions on applied superconductivity*, Vol. 15, no 2, 2005
- [24] H. Lou, X.F Wu, C.M. Lee, T. Yang, X. Leng, Y. Liu, L. Qiu, H.M. Luo, Z.H. Wang, S.Y. Ding, AC losses of superconductor MgB₂, *Supercond. Sci. Technol.* Vol. 15, 2002, pp. 370 - 374
- [25] Inada, R., Iwata, Y. Tatemaya, K., Nakamura Y., Oota, A., Zhang P.X, AC losses in Ag-sheathed Bi₂₂₂₃ tapes with Ca₂CuO₃ as interfilamentary resistive barriers, *Physica C*, Vol. 445-448, 2006, pp 762-767
- [26] M. Polak, L. Krempasky Study of important factors affecting AC losses of multifilamentary Bi-2223 tapes, *Physica C* Vol. 357-360, 2001, pp 1144-1152
- [27] Su, X., Witz, G., Passerini, R., Kwasnitza, K., Flükiger, R., Square and round Bi(2 2 2 3) wire configurations and their AC losses, *Physica C*, Vol. 372-376, 2002, pp 942-944
- [28] J. Fang, X.M. Luo, D.X. Chen, E.W. Collings, E. Lee, M.D. Sumption, A.K.M. Alamgir, H.P. Yi, J.G. Fang, C. Gu, S.Q. Guo, M.L. Liu, Y. Xin, Z. Han, AC magnetic losses in Bi-2223/Ag tapes with different aspect ratios, *Physica C*, Vol. 412-414, 2004, pp. 1134-1138

- [29] G. Witz, X.-D. Su, K. Kwanitza, R. Flükiger, AC losses in Bi,Pb(2 2 2 3) multifilamentary wires with square cross-section, *Physica C*, Vol. 384, 2003, pp. 334-344
- [30] Received from N. Magnusson
- [31] E-mail correspondence between G. Grasso of Columbus Superconductors Spa and N. Magnusson at Sintef Energy Research on 28.02.07, received from N. Magnusson.
- [32] E-mail correspondence between Matt Rindfleisch at Hyper Tech Research, Inc. and N. Magnusson at Sintef Energy Research on 25.01.07, received from N. Magnusson.
- [33] E-mail correspondence with O. Darell at SINTEF Materials and chemistry, section Energy conversion and materials on 12.02.07.
- [34] H. Kang, J.H. Kim, H. Hwangbo, J. Joo, W. Nah, M. Jang, H.M. Kim, Y.S. Yoon, S.S. Oh, K.S. Ryu, T.K. Ko, The experimental study of AC loss dependency on joint method in BSCCO-2223 tape, *IEEE transactions on applied superconductivity*, Vol. 11, no 1, 2001, pp. 2216-2219

Bibliography

- A.M Campbell, AC Losses in High Tc Superconductors, *IEEE transactions on applied superconductivity*, vol.5, no 2, 1995, pp 682-687
- C.H. Cheng, Y. Zhao Self-heating and ac losses in superconductors, *Physica C*, Vol. 386, 2003, pp 31-34
- F. Darmann, R. Zhao, G. McCaughey, M. Apperley, T.P.Beales, C. Friend, AC Losses of Filamentary HTS Twisted Filament Round Wires and Flat Tapes, *IEEE Transactions on applied superconductivity*, Vol. 9, no 2, June 1999, pp 789-792
- S. Ginocchio, E. Perini, R. Jakomin, F. Fontana, S. Zannella, L. Martini, AC losses in first and second generation high Tc tapes and MgB₂ tapes, *IEEE Transactions on applied superconductivity*, Vol. 15, no 2, 2005
- B.A Glowaki, M. Majoros, M. Eisterer, S. Toenies, H.W. Weber, M. Fukutomi, K. Komori, K. Togano, MgB₂ superconductors for applications, *Physica C* Vol. 387, 2003, pp 153-161
- R. Inada, H. Kimura, K. Tatemaya, Y. Nakamura, A. Oota, P.X. Zhang, Total AC losses in AG-sheathed Bi₂223 taped with different filament arrangements in AC longitudinal magnetic field, *Physica C*, Vol. 426-431, 2005, pp 1322-1327
- A. Kilic, S. Okur, N. Güclü, U. Kölemen, O. Uzun, L. Özyüzer, A. Gencer, Structural and low-field magnetic characterization of superconducting MgB₂ wires, *Physica C*, Vol. 415, 2004, pp 51-56
- P. Kovac, I. Husek, T. Melisek, M. Ahoranta, J. Souc, J. Lehtonen, F. Gömöry, Magnetic interaction of an iron sheath with a superconductor, *Superconductor Science and Technology*, Vol. 16, 2003, pp 1195-1201
- K.Kwasnitza, St. Clerc, AC losses of superconducting high-Tc multifilament Bi-2223/Ag sheathed tapes in perpendicular magnetic fields, *Physica C*, Vol. 233, 1994, pp 423-435
- M. Majoros, B.A. Glowaki, A.M. Campbell, Magnetic screening as a possible way to decrease transport AC losses in multifilamentary superconductors – basic theoretical considerations, *Physica C*, Vol. 334, 2000, pp 129-140
- S. Murase, T. Ohzawa, T. Harada, N. Nanato, S.B. Kim, Y. Yamada, K. Tachikawa, Self-field loss in AC transport current of Ni-sheathed MgB₂ superconducting tapes, *IEEE transactions on applied superconductivity*, Vol. 16, no 2, 2006
- Ogawa, J., Nakayama, H., Odaka, S., Tsukamoto, O., AC loss characteristics of YBCO coated conductors with Ag protection layer, *Physica C*, Vol. 412-414, 2004, pp 1021-1025
- M. Polak, F. Hanic, I. Hlasnik, M. Majoros, F. Chovanec, I. Horvath, L. Krempsky, P. Kottman, M. Kedrova, L. Galikova, Critical current density, magnetization and ac losses in the YBa₂Cu₃O_{6.5+x} superconductor, *Physica C*, Vol. 156, 1988, pp 79-89

A.A Polyanskii, A. Gurevich, J. Jiang, D.C Larbalestier, S.L. Bud'ko, D.K. Finnemore, G. Lapertot, P.C Canfield, Magneto-optical studies of the uniform critical state in bulk MgB₂, *Supercond. Sci. Technol*, Vol. 14, 2001, pp. 811-815

R.V Sarmago, M.P. Olbinado, AC loss intrinsic to MgB₂ at low magnetic fields, *Superconductor Science and Technology*, Vol. 18, 2005, pp 307-310

S. Stavrev, B. Dutoit, P. Lombard AC Losses of Multifilamentary Bi-2223/Ag Conductors with Different Geometry and Filaments Arrangement, *IEEE Transactions on applied superconductivity*, Vol. 13, no 2 2003

H. Suzuki, J. Ogawa, M. Ciszek, O. Tsukamoto, AC losses in multifilamentary Bi-2223/Ag tapes subjected to bending strains, *Physica C*, Vol. 426-431, 2005, pp 1333-1338

G. Witz, X.-D. Su, K. Kwanitza, M. Dhallé, C. Beneduce, R. Passerini, E. Gianni, R. Flükiger, Reduction of AC losses in Bi,Pb(2223) tapes by the introduction of barriers and the use of new wire configuration, *Physica C*, Vol. 372-376, 2002, pp 1814-1817

D. Zola, F. Gömöry, M. Polichetti, F. Strycek, J. Souc, P. Kovac, S. Pace, Analysis of Coupling Losses in Multifilamentary Unteiced BSCCO/Ag Tapes Through a.c. Susceptibility Measurements, *IEEE transactions on applied superconductivity*, Vol. 15, no 2, 2005

Appendix

Appendix 1	Resistance ratio table.....	i
Appendix 2	Resistance ratio versus linear resistivity equations.....	ii
Appendix 3	Critical current in the superconductors used in the experiments	iv
Appendix 4	Heat treatment of Hyper Tech superconductor	vi
Appendix 5	Equipment list	viii
Appendix 6	Tables of thermo element voltage versus temperature.....	ix
Appendix 7	Calibration graphs	x
Appendix 8	Thermo element and copper wire temperatures	xiii
Appendix 9	Temperature increase during AC loss measurements	xvi
Appendix 10	Curve fitting to tape shape equations, 30 Kelvin	xix
Appendix 11	Soldering of BSCCO tapes.....	xx

Appendix 1 Resistance ratio table

Table A 1 Resistance ratio versus temperature for copper resistance thermometer [30]

Temperature [K]	R/R ₀	Temperature [K]	R/R ₀
4.2	0.01118	64	0.08686
19	0.011753	68	0.10137
20	0.011918	72	0.11626
21	0.012116	76	0.13239
22	0.012352	80	0.14854
23	0.012621	85	0.16975
24	0.012919	90	0.19145
25	0.013268	95	0.21348
26	0.013675	100	0.23582
27	0.014128	110	0.28105
28	0.014642	120	0.32649
29	0.015201	130	0.37192
30	0.015827	140	0.41723
31	0.01651	150	0.46233
32	0.01727	160	0.50705
33	0.01812	170	0.55169
34	0.01903	180	0.59603
35	0.02004	190	0.64002
36	0.02113	200	0.68387
38	0.02355	210	0.7275
40	0.02621	220	0.77098
42	0.02927	230	0.81429
44	0.03274	240	0.8575
46	0.03671	250	0.90051
48	0.04089	260	0.94358
50	0.04547	270	0.98653
52	0.05039	280	1.0293
54	0.05563	290	1.07218
56	0.0613	300	1.11504

Appendix 2 Resistance ratio versus linear resistivity equations

Figure A 1 is a plot of the resistance ratios versus temperature found in Appendix 1 and the linear resistivity equation (13) found in Chapter 4: $\rho_{\Theta} = \rho_{20^{\circ}}(1 + \alpha(\Theta - 20^{\circ}))$ [Ωm] with $\alpha=4 \cdot 10^{-3} K^{-1}$. In the plot, the curve based on the equation is called formula. Figure A 2 is a close-up of where the two mentioned curves separate and Figure A 3 is a close-up of the resistance ratio at the temperatures used in the measurements.

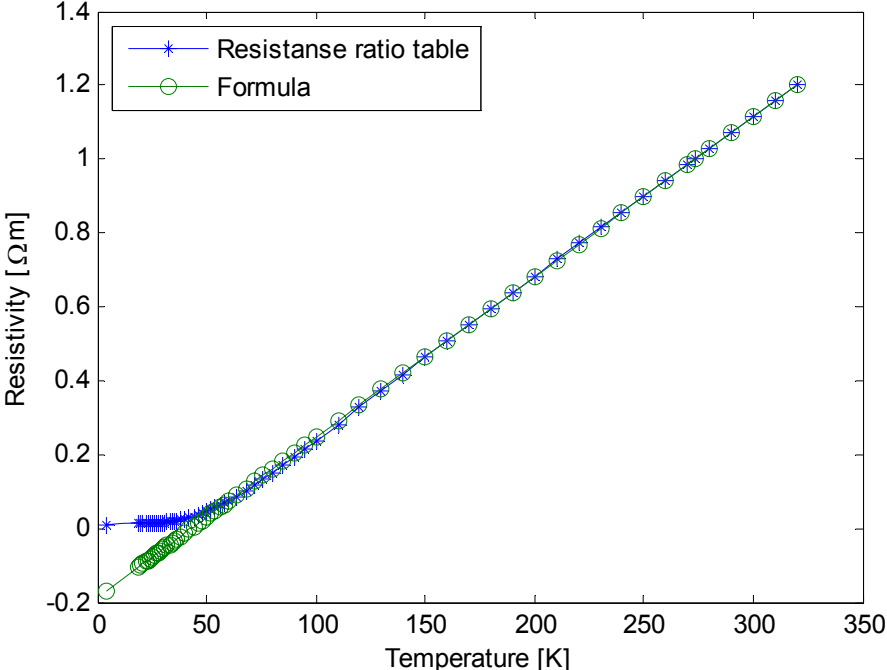


Figure A 1 Resistivity against temperature from resistance ratio versus temperature table compared with linear equations

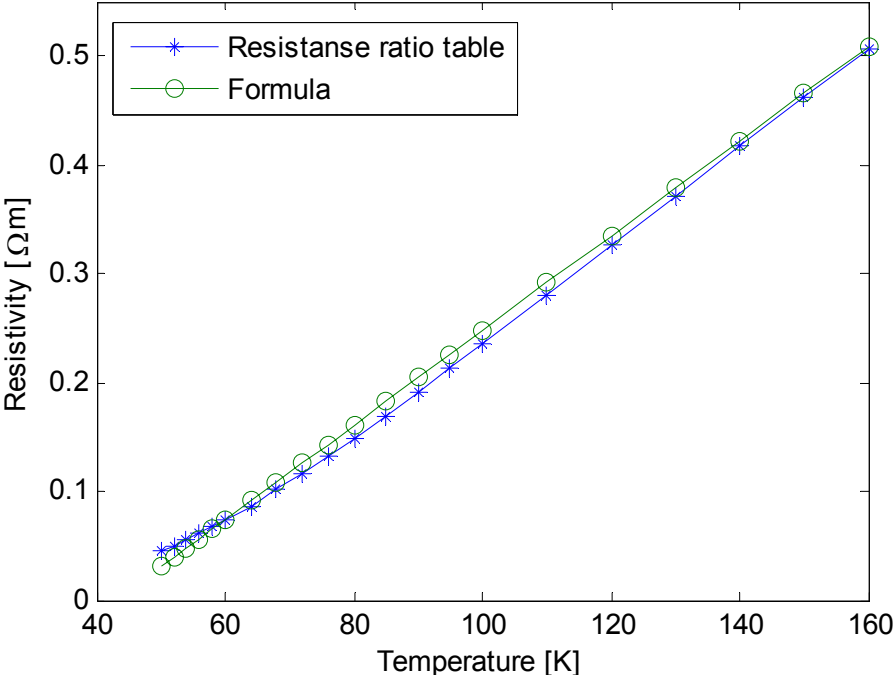


Figure A 2 Close up of a smaller temperature area, the two graphs separate at the highest temperatures shown in the figure

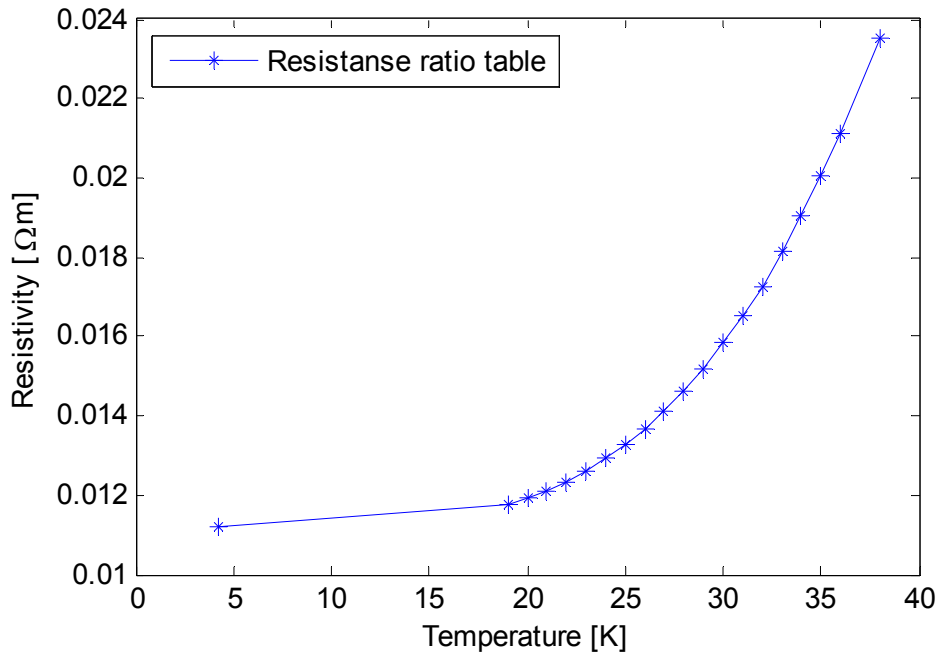


Figure A 3 Resistane ratio around the temperatures used in the study

Figure A 4 is an example of using the resistivity rate of change at 25 K to draw a line of the same slope to compare the resistivity changes for a given temperature rise.

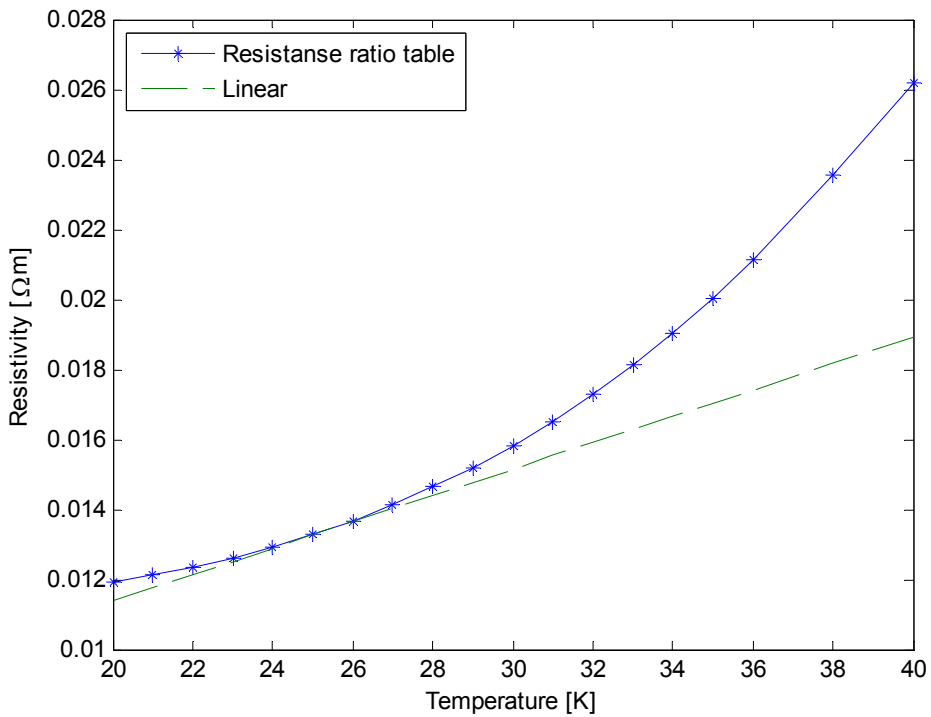


Figure A 4 Comparison between the real resistivity at 25 K, and a linear approximation

Appendix 3 Critical current in the superconductors used in the experiments

Critical current at 20 K

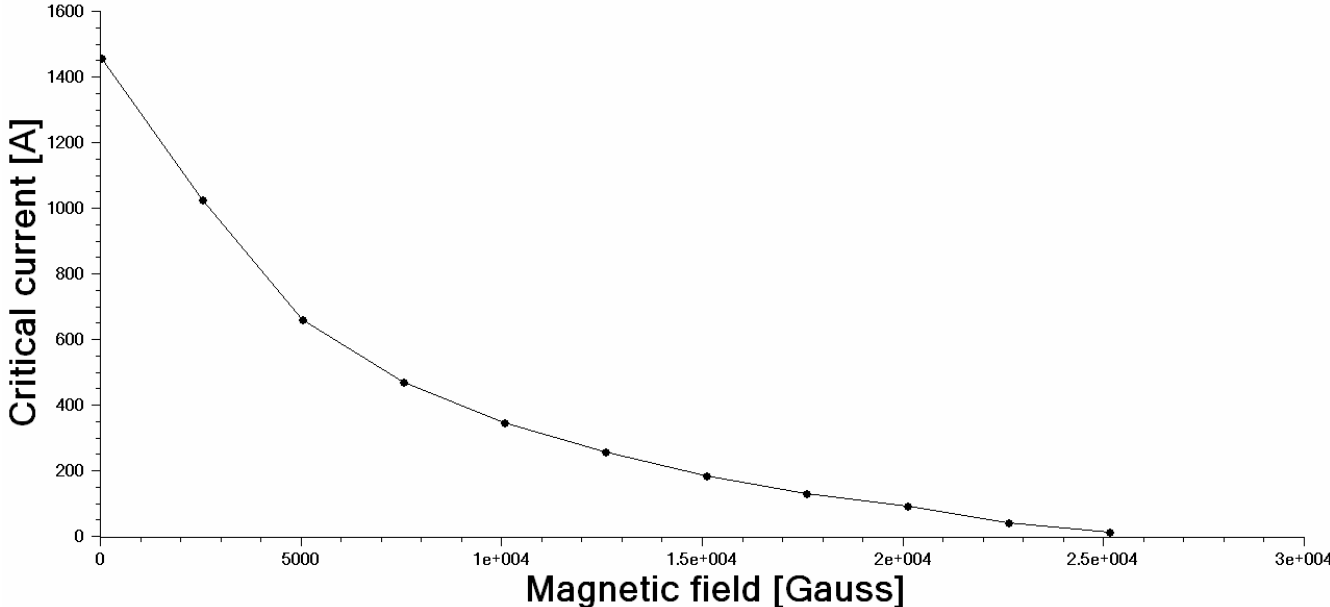


Figure A 5 The critical current in the Columbus superconductor at 20 K versus magnetic field. [31]

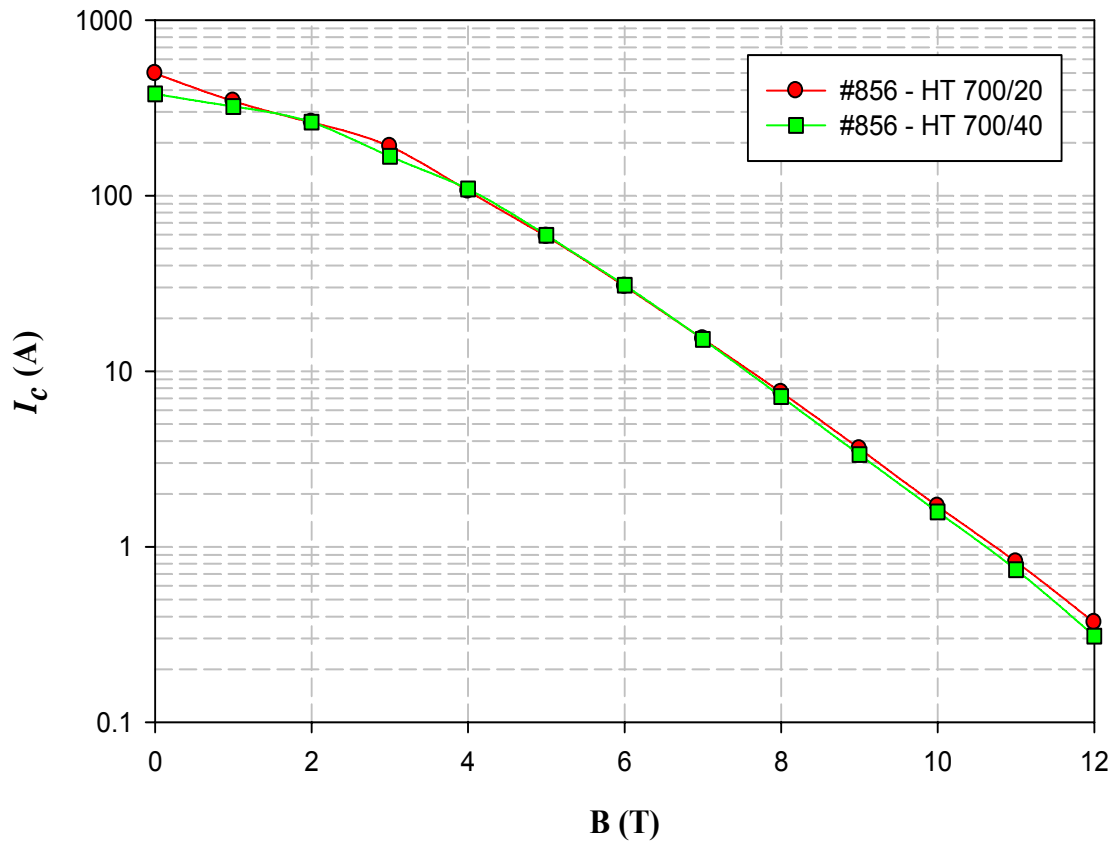


Figure A 6 Critical current in an analogous superconductor as the Hyper Tech sample. The two were produced from the same monofilament stock. The temperature is 4.2 K, the sample length 1 m and the two curves correspond to two different heat treatments. [32]

Appendix 4 Heat treatment of Hyper Tech superconductor

The Hyper Tech superconductor went through a heat treatment after being received. Instructions were given by Hyper Tech, and were as exemplified in Figure A 7. The time above 600 °C should be 40 minutes, 20 of them at 700 °C. The treatment was to be done in argon gas.

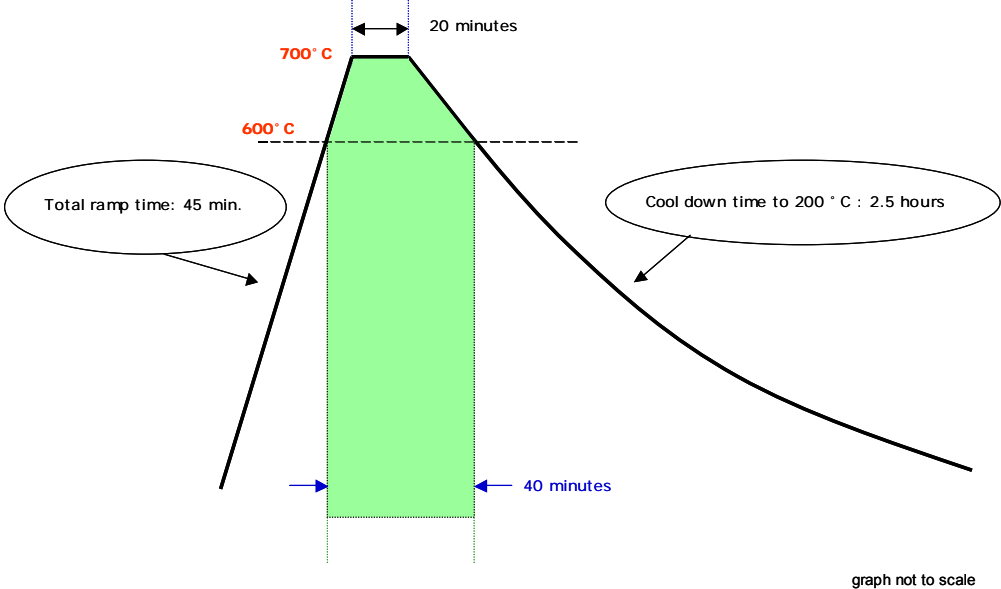


Figure A 7 Recommended heat treatment profile of Hyper Tech superconductor [32]

The actual heat treatment is summarized in Figure A 8 and Figure A 9. It was performed at SINTEF Materials and chemistry, section Energy conversion and materials. The ramp time was to be 45 minutes, but was a little over an hour. By looking at Figure A 9 it is found that the time at 700 °C is about 20 minutes, as is was supposed to, but the time above 600 °C was over an hour. This was supposed to be 40 minutes. The cool down time should be 2.5 hours, but was much longer than this, see Figure A 8. The treatment was performed in argon, but as the oven walls could contain other gases, it was flushed and evacuated three times before the treatment. The superconductor surface was shiny prior to the treatment, but blackish afterwards.

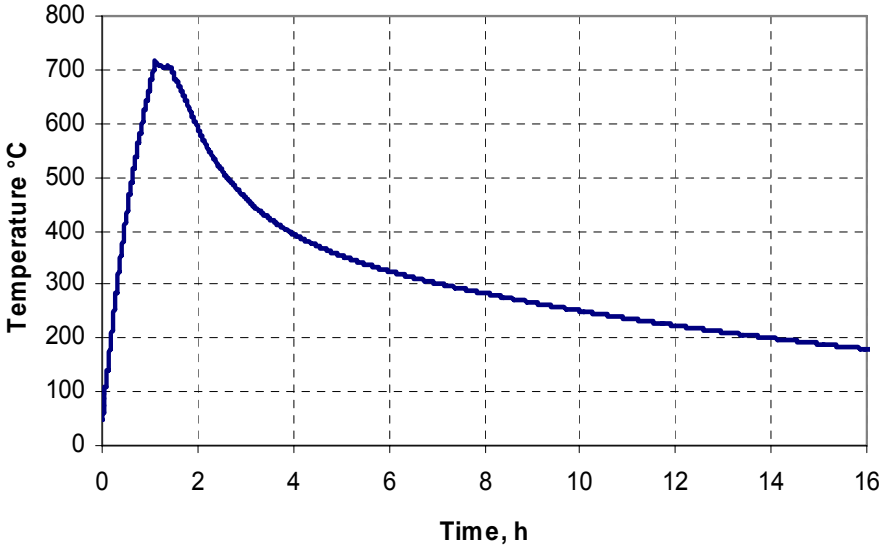


Figure A 8 Actual heat treatment profile [33]

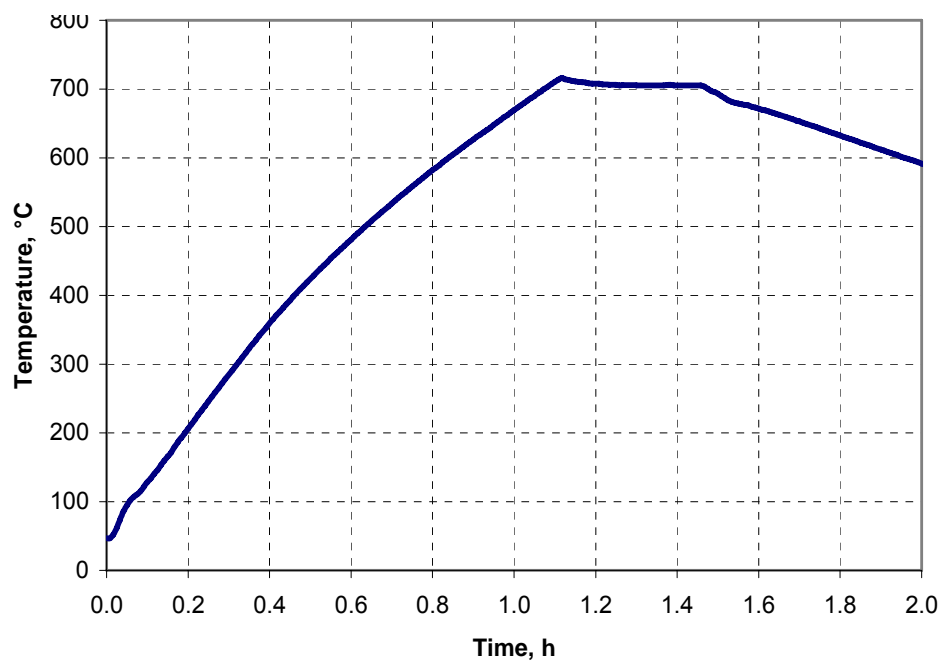


Figure A 9 Close-up of the first two hours [33]

Appendix 5 Equipment list

Table A 2 List of equipment used, together with Id and some additional comments

Type of equipment	Id	Additional information
Capacitor bank	-	
Clip-on ammeter	I04-0409	
Cold pump	P05-0058	
Contactator	-	
Data acquisition unit	G05-0102	
Manometer	-	
Oscilloscope	G04.0225	
PC	P07-0739	
Power sources	B02-0430	Connected to copper wire
	B02-0256	Heater switch; base settings
	B02-0062	Heater switch; calibration settings
	B02-0211	Connected to H3+/H3-
Switch	-	
Transformer	B01-0393	
Vacuum pump	P05-0060	Alcatel
Variac	B01-0601	
20 channel multiplexer	G05-0139-01	Used for copper wire and heater

Appendix 6 Tables of thermo element voltage versus temperature

Table A 3 Corrected voltage against temperature for thermo elements [30]

Temperature [K]	Voltage, corrected [μ V]
3	-1116
13	-1078
23	-999
33	-885
43	-736
53	-555
63	-344
73	-106
83	158
93	446
103	756
113	1087
123	1440
133	1812
143	2203
153	2612
163	3038
173	3482
183	3942
193	4417
203	4908
213	5413
223	5932
233	6464
243	7010
253	7567
263	8137
273	8719
283	9310
293	9911
303	10520

Appendix 7 Calibration graphs

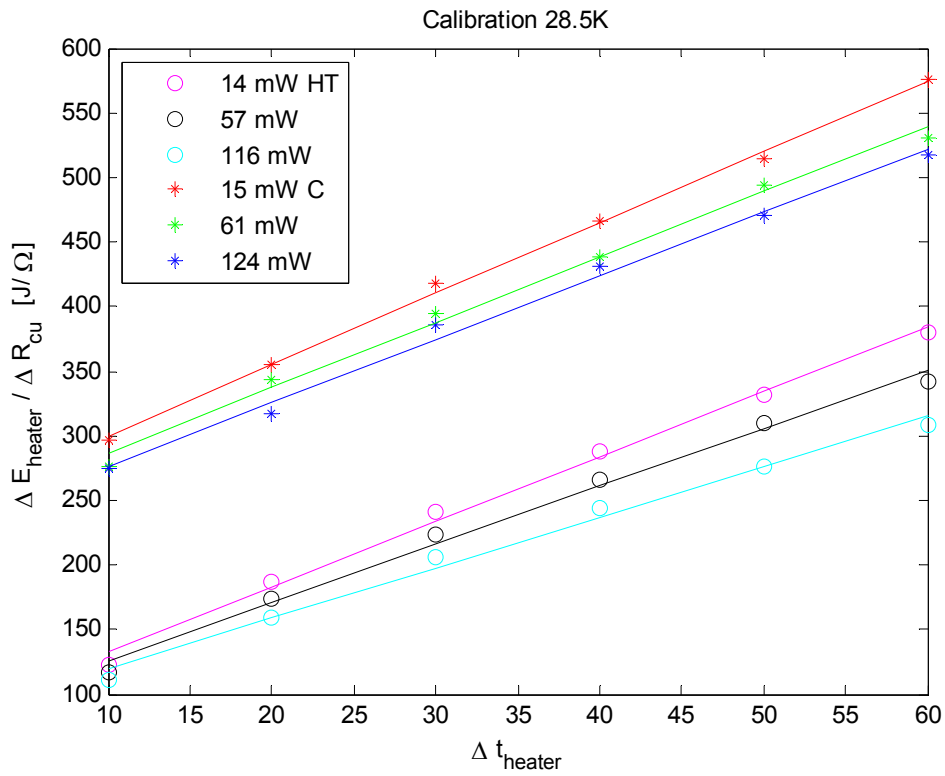


Figure A 10 Calibration results for 28.5 K. The powers listed in the legend are heater powers and the lines are regression lines given by the results.

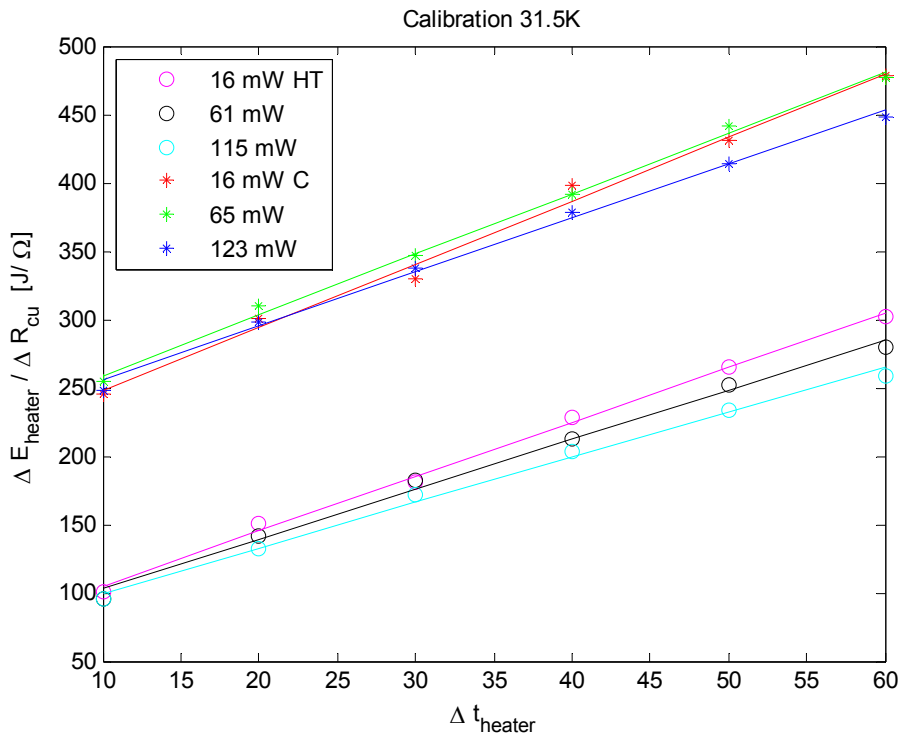


Figure A 11 Calibration results for 31.5 K. The powers listed in the legend are heater powers and the lines are regression lines given by the results.

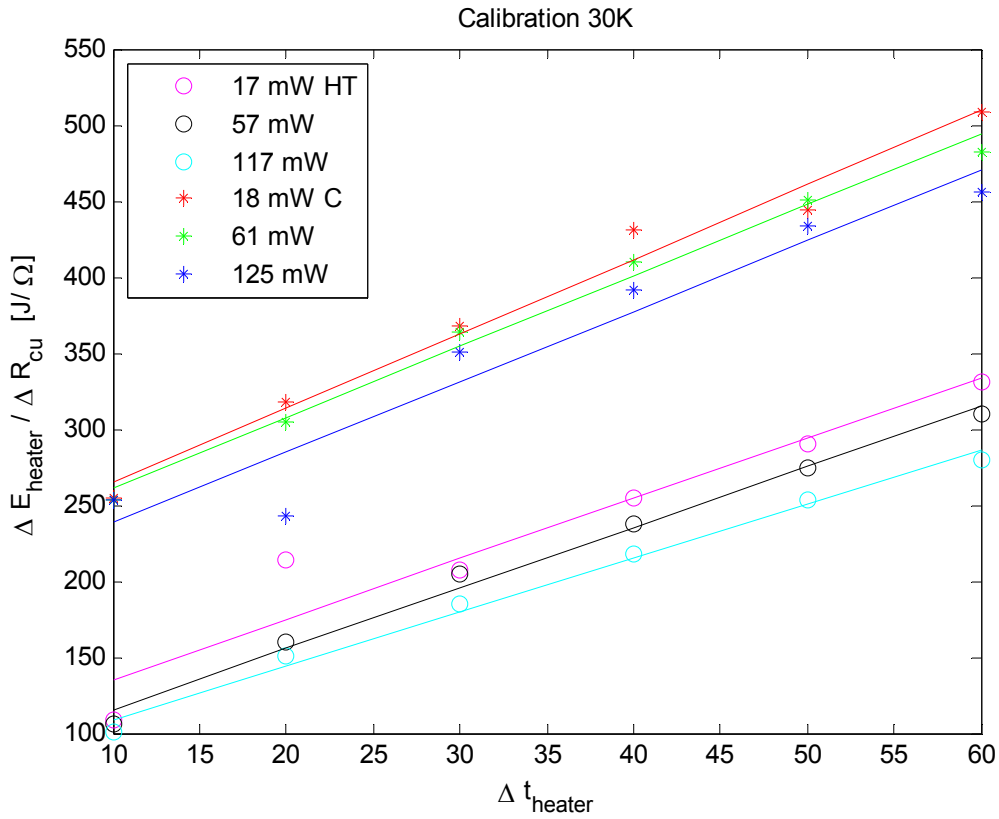


Figure A 12 Calibration results for 30 K, first series. The powers listed in the legend are heater powers and the lines are regression lines given by the results.

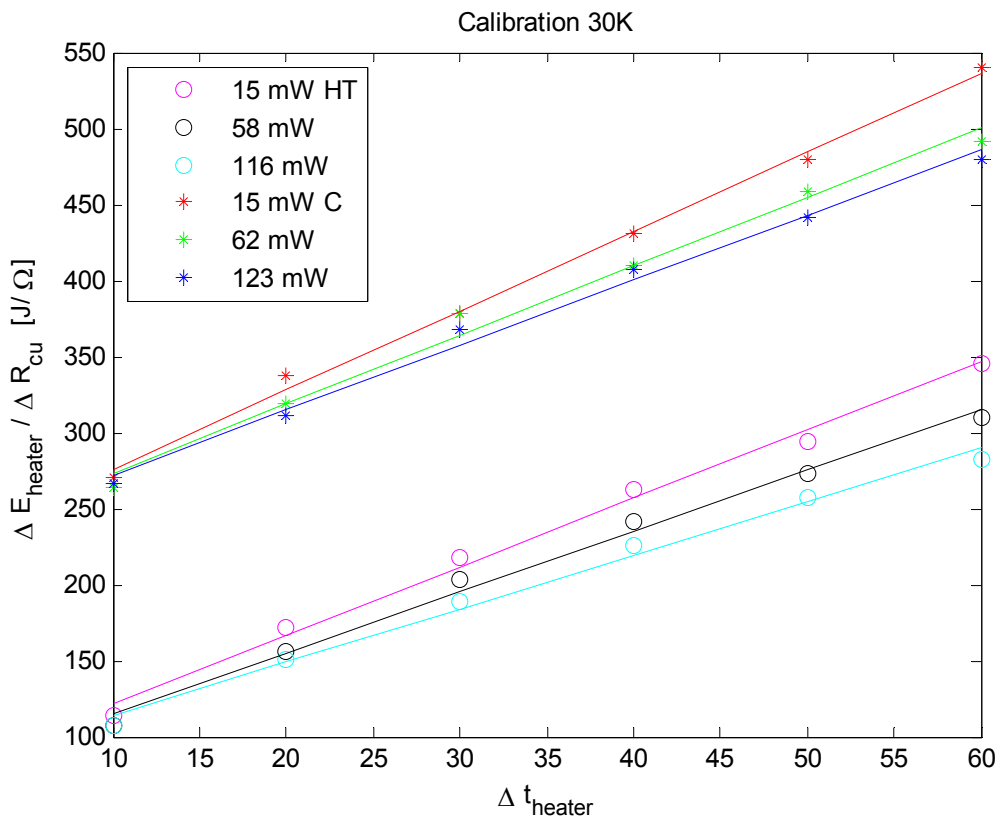


Figure A 13 Calibration results for 30 K, second series. The powers listed in the legend are heater powers and the lines are regression lines given by the results.

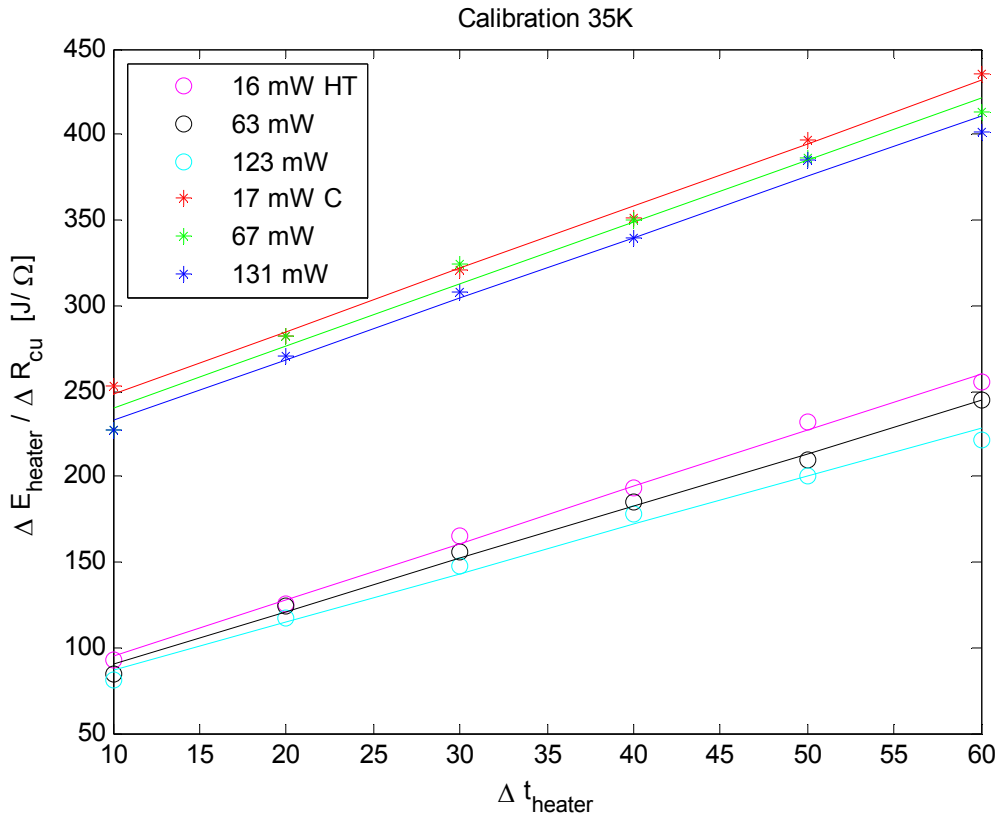


Figure A 14 Calibration results for 35 K. The powers listed in the legend are heater powers and the lines are regression lines given by the results.

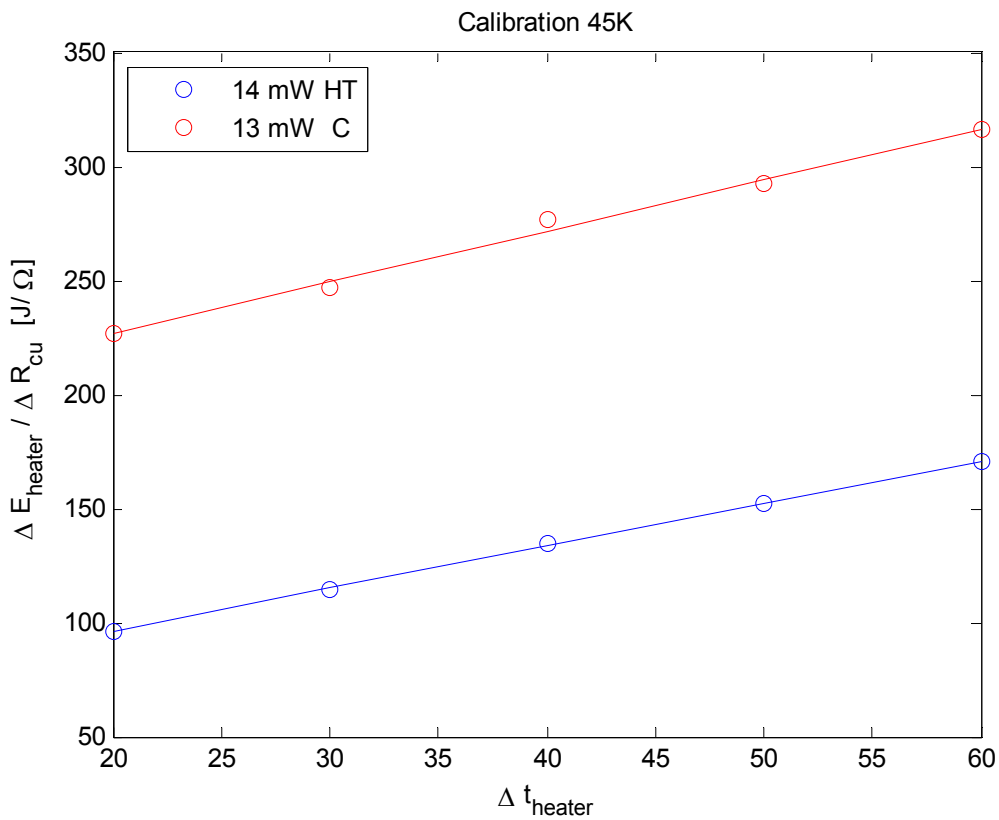


Figure A 15 Calibration results for 45 K. The powers listed in the legend are heater powers and the lines are regression lines given by the results.

Appendix 8 Thermo element and copper wire temperatures

Table A 4 Initial thermo element and copper wire readings, 25K. The actual copper temperature when the measurements were done was somewhat higher

Thermo element, Columbus	Temperature [K]	Thermo element Hyper Tech	Temperature [K]
6	27.8187	9	28.3886
30	28.2332	2	28.4404
7	29.2694	3	26.5751
18	28.2850	Average	27.80
16	29.2176	Copper wire	24.90
11	28.0259		
17	29.1140		
20	29.1658		
22	28.0259		
12	29.5803		
14	28.3368		
Average	28.64		
Copper wire	22.49		

Table A 5 Initial thermo element and copper wire readings, 30 K, first series

Thermo element, Columbus	Temperature [K]	Thermo element Hyper Tech	Temperature [K]
6	32.7927	9	33.8808
30	32.6373	2	35.0207
7	33.8725	3	30.5168
18	32.5973	Average	33.14
11	31.9933	Copper wire	32.54
17	34.6107		
20	33.4027		
22	31.7919		
12	34.9463		
14	31.3893		
Average	33.00		
Copper wire	30.68		

Table A 6 Initial thermo element and copper wire readings, 30 K, second series

Thermo element, Columbus	Temperature [K]	Thermo element Hyper Tech	Temperature [K]
6	30.5855	9	31.3161
30	29.7668	2	31.2850
7	31.8549	3	27.8083
18	30.0363	Average	30.14
11	29.4249	Copper wire	32.91
17	32.5026		
20	31.6891		
22	30.1140		
12	31.1503		
14	30.3523		
Average	30.75		
Copper wire	30.26		

Table A 7 Initial thermo element and copper wire readings, 31.5 K

Thermo element, Columbus	Temperature [K]	Thermo element Hyper Tech	Temperature [K]
6	36.0403	9	36.7584
30	33.5101	2	38.2081
7	36.0671	3	30.9866
18	33.7517	Average	35.32
11	32.5436	Copper wire	34.61
17	38.0470		
20	35.3020		
22	33.3758		
12	35.9128		
14	24.7383		
Average	33.93		
Copper wire	31.86		

Table A 8 Initial thermo element and copper wire readings, 35 K

Thermo element, Columbus	Temperature [K]	Thermo element Hyper Tech	Temperature [K]
6	36.8255	9	40.0470
30	36.2215	2	42.7315
7	37.4295	3	35.0805
18	36.2215	Average	39.29
11	35.7517	Copper wire	37.98
17	39.3758		
20	37.1611		
22	35.6846		
12	39.7114		
14	34.5436		
Average	36.89		
Copper wire	35.01		

Appendix 9 Temperature increase during AC loss measurements

The orders of the temperature increases are with rising applied field magnitude. T is copper wire temperature and ΔT the temperature increase from the initial temperature.

Table A 9 Temperature increase during alternating field measurements at 25 K

T Hyper Tech parallel field [K]	ΔT [K]	T Columbus parallel field [K]	ΔT [K]	T Hyper Tech perpendicular field [K]	ΔT [K]	T Columbus perpendicular field [K]	ΔT [K]
27.3186	0	25.2000	0	27.3186	0	25.2000	0
27.4397	0.1210	25.7128	0.5128	27.3736	0.0550	25.3282	0.1282
27.5607	0.2420	26.2026	1.0027	27.4287	0.1100	25.5333	0.3333
27.7312	0.4125	27.2109	2.0109	27.4837	0.1650	25.6807	0.4807
27.8687	0.5500	27.7692	2.5692	27.5112	0.1925	25.8666	0.6666
28.0310	0.7124	28.1144	2.9145	27.7037	0.3850	26.3466	1.1467
28.1069	0.7882	28.3711	3.1712	27.7862	0.4675	26.6058	1.4058
28.2839	0.9652	28.7678	3.5679	27.8907	0.5721	26.8649	1.6650
28.3345	1.0158	28.3478	3.1478	28.0816	0.7629	27.1601	1.9602
28.6885	1.3699	28.9078	3.7079	28.0310	0.7124	27.0078	1.8079
29.1283	1.8097	28.8612	3.6612	28.2839	0.9652	27.6169	2.4170
28.9920	1.6733	29.2094	4.0095	28.4103	1.0917	28.0211	2.8211
29.1283	1.8097	28.7678	3.5679	28.9920	1.6733	29.1261	3.9261
29.4896	2.1710	29.2094	4.0095	28.9414	1.6227	28.4878	3.2878
30.2359	2.9173	29.7095	4.5096	29.4445	2.1258	28.9545	3.7545
30.6499	3.3312	31.6470	6.4471	29.3541	2.0355	29.1261	3.9261

Table A 10 Temperature increase during alternating field measurements at 30 K, first series

T Hyper Tech parallel field [K]	ΔT	T Columbus parallel field [K]	ΔT	T Hyper Tech perpendicular field [K]	ΔT	T Columbus perpendicular field [K]	ΔT
32.5375	0	30.5359	0	32.5375	0	30.5359	0
32.5741	0.0366	30.6123	0.0764	32.6772	0.1397	31.0463	0.5104
32.6539	0.1164	30.7574	0.2215	32.797	0.2594	31.6642	1.1283
32.7205	0.1829	30.9331	0.3972	32.9034	0.3659	32.1755	1.6396
32.8502	0.3127	31.4754	0.9395	33.0154	0.4779	32.6972	2.1614
32.9500	0.4124	32.1141	1.5782	33.1583	0.6208	32.8814	2.3455
33.0185	0.4810	32.3289	1.7931	33.3447	0.8072	33.0039	2.468
33.1117	0.5742	32.4517	1.9158	33.1894	0.6519	32.2982	1.7624
33.1117	0.5742	32.1755	1.6396	33.3292	0.7917	32.421	1.8851
33.1583	0.6208	32.5131	1.9772	33.702	1.1645	32.7893	2.2534
33.2205	0.6829	32.2369	1.7010	33.5001	0.9626	32.5745	2.0386
33.0341	0.4965	31.647	1.1112	33.6554	1.1179	32.4210	1.8851
33.8108	1.2732	32.2676	1.7317	33.5001	0.9626	32.4517	1.9158
33.1428	0.6053	32.0067	1.4708	33.3913	0.8538	32.5131	1.9772
33.3758	0.8383	32.3289	1.7931	33.469	0.9315	32.4824	1.9465
33.6088	1.0713	32.0834	1.5475	33.469	0.9315	32.4517	1.9158

Table A 11 Temperature increase during alternating field measurements at 30 K, second series

T Hyper Tech parallel field [K]	ΔT	T Columbus parallel field [K]	ΔT	T Hyper Tech perpendicular field [K]	ΔT	T Columbus perpendicular field [K]	ΔT
32.7038	0	30.0890	0	32.7038	0	30.0890	0
32.7105	0.0067	30.1249	0.0359	32.7112	0.0073	30.1073	0.0183
32.7158	0.0120	30.1463	0.0573	32.7165	0.0126	30.1257	0.0367
32.7158	0.0120	30.1501	0.0611	32.7155	0.0116	30.1272	0.0382
32.7178	0.0140	30.2055	0.1165	32.7178	0.0140	30.1310	0.0420
32.7654	0.0615	30.3067	0.2177	32.7175	0.0136	30.1348	0.0458
32.7770	0.0732	30.4098	0.3209	32.7364	0.0326	30.1807	0.0917
33.2018	0.4980	32.5223	2.4333	32.9101	0.2062	30.8338	0.7448
33.6244	0.9205	32.7678	2.6789	33.2360	0.5322	32.3688	2.2799
33.7797	1.0759	32.4916	2.4026	33.5622	0.8584	32.6451	2.5561
33.9040	1.2001	32.5530	2.4640	33.6244	0.9205	32.1233	2.0343

Table A 12 Temperature increase during alternating field measurements at 31.5 K

T Hyper Tech parallel field [K]	ΔT	T Columbus parallel field [K]	ΔT
34.6894	0	31.9209	0
34.6908	0.0014	31.9346	0.0137
34.6950	0.0056	31.9525	0.0316
34.6941	0.0048	31.9649	0.0440
34.7062	0.0168	32.0153	0.0944
34.7146	0.0252	32.0645	0.1436
34.7314	0.0420	32.1320	0.2112
34.7594	0.0701	32.3840	0.4631
34.8967	0.2074	33.2913	1.3704
34.9528	0.2634	33.4635	1.5426
35.0393	0.3500	33.5496	1.6287
35.1016	0.4123	33.4635	1.5426
35.0964	0.4071	33.1765	1.2556
35.1665	0.4772	33.3200	1.3991
35.2315	0.5421	33.4061	1.4852
35.2704	0.5810	33.3200	1.3991
35.3743	0.6849	33.6070	1.6861
35.2834	0.5940	33.3487	1.4278
35.3223	0.6330	33.4635	1.5426
35.2444	0.5551	33.2052	1.2843
35.1795	0.4902	33.0186	1.0978

Table A 13 Temperature increase during alternating field measurements at 35 K

T Hyper Tech parallel field [K]	ΔT	T Columbus parallel field [K]	ΔT	T Hyper Tech perpendicular field [K]	ΔT	T Columbus perpendicular field [K]	ΔT
37.9308	0	34.8667	0	37.9308	0	34.8667	0
37.9448	0.014	35.1063	0.2396	37.9331	0.0023	35.135	0.2683
37.9576	0.0269	35.1876	0.3209	37.9354	0.0047	35.1781	0.3114
37.9541	0.0234	35.1828	0.3161	37.9775	0.0467	35.2355	0.3688
37.9623	0.0315	35.1781	0.3114	37.9775	0.0467	35.1637	0.297
37.9693	0.0386	35.2259	0.3592	37.9775	0.0467	35.135	0.2683
37.9693	0.0386	35.2594	0.3927	37.9635	0.0327	35.044	0.1773
37.9752	0.0444	35.1637	0.297	37.9635	0.0327	35.0584	0.1917
37.9583	0.0276	35.1302	0.2635	37.9728	0.0421	35.0871	0.2204
37.9705	0.0397	35.1039	0.2372	37.9822	0.0514	35.1063	0.2396
37.9623	0.0315	35.1063	0.2396	37.9985	0.0678	35.1254	0.2587
37.9693	0.0386	35.0153	0.1486	37.9939	0.0631	35.1254	0.2587
37.9845	0.0537	35.1398	0.2731	38.0305	0.0998	35.1924	0.3257
37.9658	0.035	35.0967	0.2300				
38.0093	0.0785	35.2235	0.3568				

Appendix 10 Curve fitting to tape shape equations, 30 Kelvin

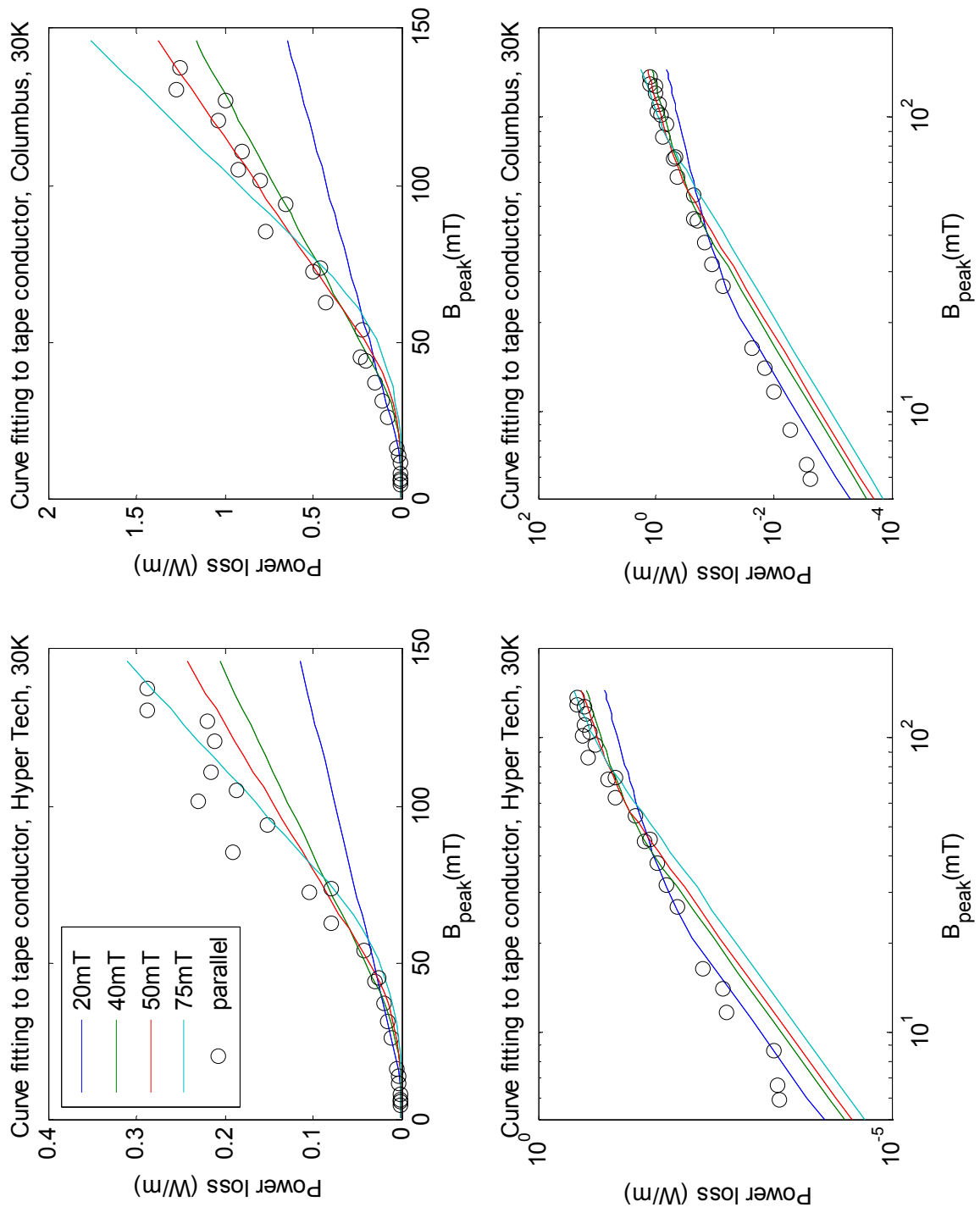


Figure A 16 Tape shape equations as basis for curve fitting to measured AC losses. The field magnitudes in the legend are the various penetration fields.

Appendix 11 Soldering of BSCCO tapes

In the preparations leading to critical current density experiments it was necessary to optimize the soldering technique used on BSCCO tapes. This is used as the HTS which carries current between the copper bushings and the MgB_2 superconductor. The following procedure gave good results:

- remove insulation with a scalpel, the leftover glue is washed off with acetone
- sand down the surface a bit and wash with acetone
- use plenty of soldering paste/flux, and make sure all of the surface is moistened by it at all times when soldering
- set the soldering iron at 180 °C and use low temperature tin solder, one drop is enough
- place the soldering iron onto the tape and leave it still for the tape to heat up. Remember to keep the tape moistened with flux
- carefully nudge the soldering iron at an angle back and forth to drag the tin solder out, be cautious not to do it too fast – the tape needs to heat during the soldering
- when the entire surface is covered with tin solder, removing surplus tin solder may be done by holding the tape perpendicular to the table and drag the soldering iron along the surface towards the table

The joint resistance in several soldered joints, using the procedure above, were measured and the results are listed in Table A 14. The circuit used is sketched in Figure A 17. The voltage measurement across the joint was done by a multiplexer in a data acquisition unit. The shunt and voltmeter in the outer circuit is for measuring the current flowing in the circuit. A 300 A current was measured as 50 mV voltage. For the double joint, each soldering resistance was measured, but not the separate currents, only the outer circuit current. Here, the end with two tapes coming out of the soldering was also soldered together for the current to divide between them. In the resistance calculations it was assumed the current split evenly between the two superconductors.

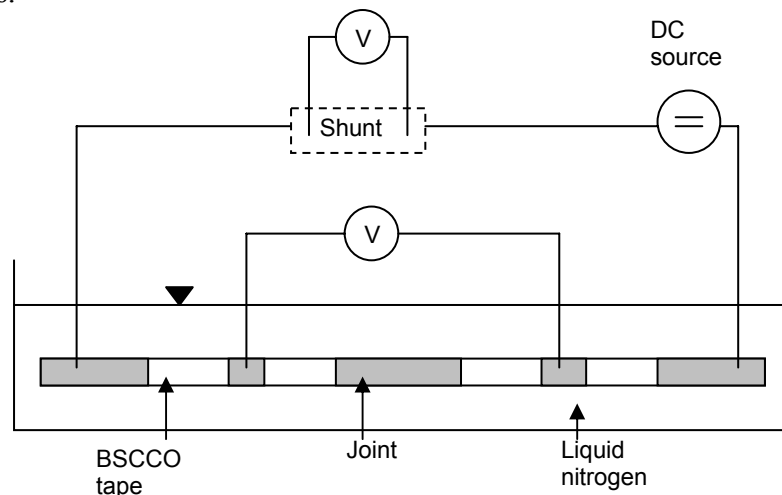


Figure A 17 Soldered joint testing setup

Table A 14 Soldered joint resistance values measured

Current [A]	Measured resistance [$\mu\Omega/cm$]				
	Single joint, assumed good	Single joint, assumed less good	Single joint, assumed good	Double joint, assumed good	
	4.6 cm	4.5 cm	10 cm	4.5 cm	
10.8	0.1791	0.1626	0.0204	0.0864	0.0576
15.0	0.1797	0.1674	0.0233	0.0919	0.0593
21.0	0.1812	0.1661	0.0257	0.0952	0.0741
25.2	0.1768	0.1684	0.0266	0.0970	0.0794
31.2	0.1798	0.1724	0.0279	0.1011	0.0755
36.0	0.1781	0.1704	0.0281 (36.6)	0.1025	0.0852
41.4	0.1801 (40.8)	0.1712	0.0285	0.1084	0.0891

The numbers in parenthesis in Table A 14 are current values differing from the ones listed in the first column. Both the short, single joints - independent on the expected quality of the soldering – were worse than the longest and the double joint. A fair expectation is halving the resistance when doubling the soldering length. However, the resistances in the shorter joints are 6.5 to 7 times higher than the long joint. The double joint soldering is also better than the short, single ones. It is unknown why there are such large differences between the joints, and there are no visible differences when soldering. For comparison to a study done on joints in BSCCO-2223 tape see [34]. The obtained results for soldered joints in the article are $1.8 \cdot 10^{-8}$ and $7.3 \cdot 10^{-8} \Omega$.

Soldering for use in cryostat

The soldered joints needed for use in the cryostat when measuring critical current is four copper – BSCCO joints per current bushing, four BSCCO – BSCCO joints for reducing the number of BSCCO tapes inside the cryostat and four BSCCO – MgB_2 joints. A bushing with BSCCO tapes is shown in Figure A 18.

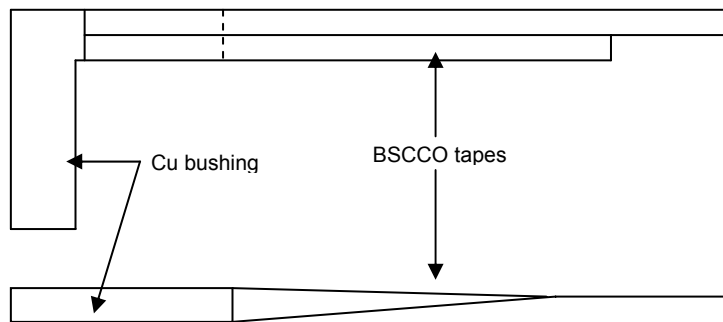


Figure A 18 Sketches of the cu bushing and BSCCO tapes, the upper sketch is from the side, the lower from above

Experience gained from preparations prior to measuring critical current gave some ideas on how to improve the end result. The current bushings were placed in a hot cabinet at $160 \text{ }^\circ\text{C}$, tin solder was then put on them. The BSCCO tapes (also with soldering tin) were then pressed against the bushings and placed in the hot cabinet for them to fasten. It seemed as if it was harder to spread tin solder on the BSCCO surface after having been heated. A suggestion is therefore to only heat the bushings to quite a high temperature, take them out of the cabinet and to place the superconductors onto the bushings right away, while putting pressure on the joints. The procedure for BSCCO jointing described in the previous section should then work better.